



UNIVERSITY OF LEEDS

This is a repository copy of *Virtual high throughput screening of natural peptides against ErbB1 and ErbB2 to identify potential inhibitors for cancer chemotherapy.*

White Rose Research Online URL for this paper:

<https://eprints.whiterose.ac.uk/202272/>

Version: Accepted Version

---

**Article:**

Patnaik, S.K., Ayyamperumal, S., Jade, D. et al. (7 more authors) (2023) Virtual high throughput screening of natural peptides against ErbB1 and ErbB2 to identify potential inhibitors for cancer chemotherapy. *Journal of Biomolecular Structure and Dynamics*. ISSN 0739-1102

<https://doi.org/10.1080/07391102.2023.2226744>

---

**Reuse**

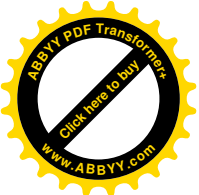
This article is distributed under the terms of the Creative Commons Attribution-NonCommercial-NoDerivs (CC BY-NC-ND) licence. This licence only allows you to download this work and share it with others as long as you credit the authors, but you can't change the article in any way or use it commercially. More information and the full terms of the licence here: <https://creativecommons.org/licenses/>

**Takedown**

If you consider content in White Rose Research Online to be in breach of UK law, please notify us by emailing [eprints@whiterose.ac.uk](mailto:eprints@whiterose.ac.uk) including the URL of the record and the reason for the withdrawal request.



[eprints@whiterose.ac.uk](mailto:eprints@whiterose.ac.uk)  
<https://eprints.whiterose.ac.uk/>



## Virtual high throughput screening of natural peptides against ErbB1 and ErbB2 to identify potential inhibitors for cancer chemotherapy

Sunil Kumar Patnaik<sup>1</sup>, Selvaraj Ayyamperumal<sup>1,7</sup>, Dhananjay Jade<sup>2</sup>, Nagarjuna Palathoti<sup>1</sup>,  
Krishna Swaroop Akey<sup>1</sup>, Srikanth Jupudi<sup>1</sup>, Michael A. Harrison<sup>2</sup>, Sreenivasan  
Ponnambalam<sup>3</sup>, MJ Nanjan<sup>5,6</sup>, MJN Chandrasekar<sup>\*1,4</sup>

<sup>1</sup>Department of Pharmaceutical Chemistry, JSS College of Pharmacy, JSS Academy of Higher Education and Research, Ooty, 643001, Tamilnadu, India.

<sup>2</sup>School of Biomedical Sciences, University of Leeds, Leeds LS2 9JT, UK.

<sup>3</sup>School of Molecular & Cellular Biology, University of Leeds, UK

<sup>4</sup>School of Life Sciences, JSS Academy of Higher Education & Research (Ooty Campus), Longwood, Mysuru Road, Ooty-643001, Tamilnadu, India

<sup>5</sup>Research Director, JSS College of Pharmacy, JSS Academy of Higher Education and Research, Ooty, 643001, Tamilnadu, India.

<sup>6</sup>Present Address: Masi Educational Consultants, 128, Vijayanagar Palace Road, Ooty-643001, The Nilgiris, Tamilnadu, India

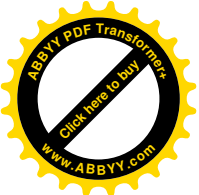
<sup>7</sup>Present Address: IMol Polish Academy of Sciences, M. Flisa 6, 02-247 Warsaw, Poland

### Corresponding Authors:

Prof. MJN Chandrasekar, Ph.D

Email: [ncsekar@jssuni.edu.in](mailto:ncsekar@jssuni.edu.in)

ORCID ID- 0000-0001-6420-9119

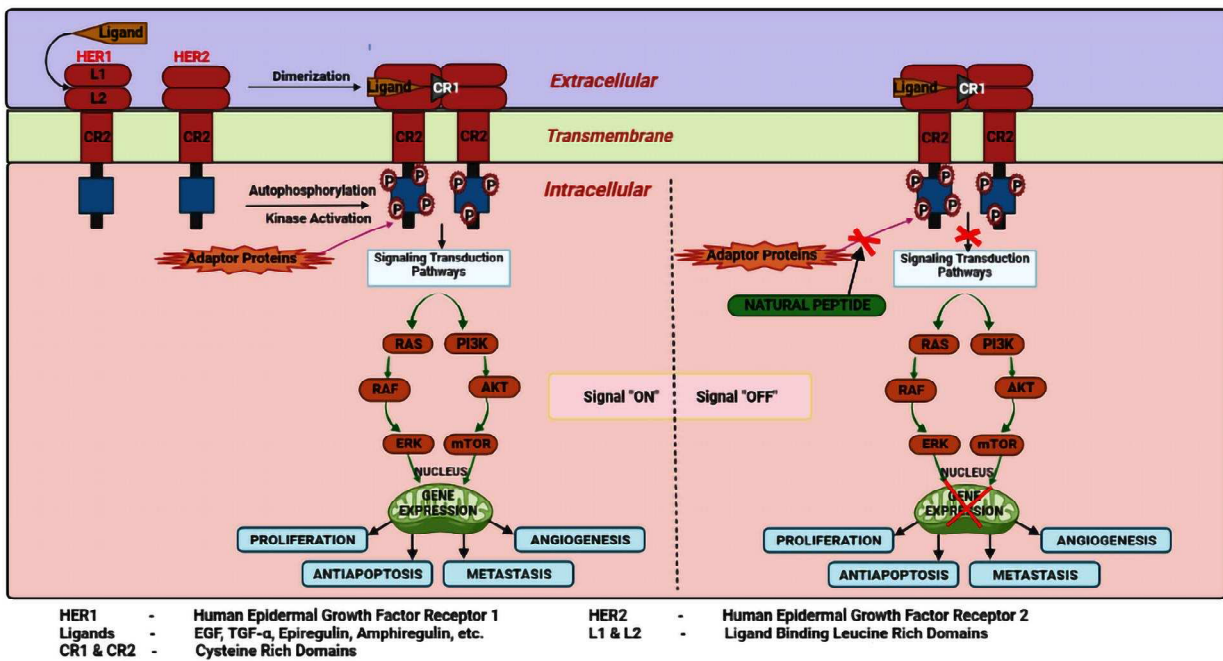


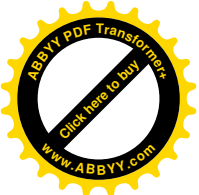
## Abstract

Human epidermal growth factor receptors (EGFR), namely ErbB1/HER1, ErbB2/HER2/neu, ErbB3/HER3, and ErbB4/HER4, the trans-membrane family of tyrosine kinase receptors, are overexpressed in many types of cancers. These receptors play an important role in cell proliferation, differentiation, invasion, metastasis and angiogenesis including unregulated activation of cancer cells. Overexpression of ErbB1 and ErbB2 that occurs in several types of cancers is associated with poor prognosis leading to resistance to ErbB1-directed therapies. In this connection, promising strategy to overcome the disadvantages of the existing chemotherapeutic drugs is the use of short peptides as anticancer agents. In the present study, we have performed virtual high throughput screening of natural peptides against ErbB1 and ErbB2 to identify potential dual inhibitors and identified five inhibitors based on their binding affinities, ADMET analysis, MD simulation studies and calculation of free energy of binding. These natural peptides could be further exploited for developing drugs for treating cancer.

**Keywords:** Drug Discovery, Anticancer peptides, Dual targeting, vHTS, ADME TOPKAT, MM-PBSA, Peptide therapeutics.

# Graphical abstract

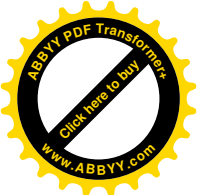




## Abbreviations:

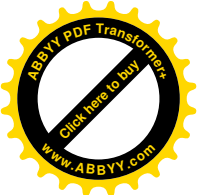
<b>3D</b>	Three dimensional
<b>ErbB</b>	Erythroblastic Leukemia Viral Oncogene
<b>EGFR</b>	Epidermal growth factor receptor
<b>HER</b>	Human epidermal growth factor receptor
<b>ATP</b>	Adenosine triphosphate
<b>EGF</b>	Epidermal growth factor
<b>TGF-<math>\alpha</math></b>	Transforming growth factor
<b>EGFR-TK</b>	Epidermal growth factor receptor-tyrosine kinase
<b>RTK</b>	Receptor tyrosine kinase
<b>SH2</b>	Src Homology 2
<b>PTB</b>	Phosphotyrosine binding
<b>ERK</b>	Extracellular signal regulated kinases
<b>MAPK</b>	Mitogen-activated protein kinases
<b>PI3K</b>	Phosphatidylinositol 3-kinases
<b>mTOR</b>	Mechanistic target of rapamycin
<b>SDF</b>	Structure Data File
<b>BE</b>	Binding Energy
<b>BFE</b>	Binding free energy
<b>nm</b>	nanometer
<b>ns</b>	nanoseconds
<b>ps</b>	picoseconds
<b>PDB</b>	Protein Data Bank
<b>RMSD</b>	Root Mean Square Deviation
<b>RMSF</b>	Root Mean Square Fluctuation
<b>Rg</b>	Radius of gyration
<b>MD</b>	Molecular Dynamics
<b>MM-PBSA</b>	Molecular Mechanics Poisson-Boltzmann Surface Area
<b>ADMET</b>	Absorption, Distribution, Metabolism, Excretion, Toxicity
<b>TOPKAT</b>	Toxicity Prediction by Komputer Assisted Technology

## 1. Introduction



Cancer is the leading cause of death worldwide accounting for nearly 10 million deaths in 2020. The impact of cancer on populations throughout the world has been devastating [1]. Despite the advancements in cancer treatments, the death rate due to cancer is increasing and causing millions of people to die even after treatment [2,3]. Conventional methods used to treat cancer includes surgery, radiotherapy, chemotherapy, biological and hormonal therapy, which focus mainly on the killing cancer cells. Among all the strategies chemotherapy is still the major approach for treating cancer. The main drawback with this approach, however, is their low bioavailability, increased chances of resistance and recurrence of the disease. The chemotherapeutic drugs kill normal cells along with the tumor cells resulting in the occurrence of severe toxicities. There is an urgent need, therefore, to develop newer drugs to fight this deadly disease [4–6].

The ErbB receptor family members, EGFR (HER1, ErbB1), HER2 (ErbB2, HER2/Neu), HER3 (ErbB3) and HER4 (ErbB4), are important in cell proliferation, survival, migration, adhesion and differentiation in cancer cells [7]. The EGFR is a 170kDa transmembrane glycoprotein, primarily synthesized as a 1210 residue precursor, which is cleaved at the N-terminal. This results in the formation of matured 1186 residue receptor, EGFR [8]. From the N-terminal to C-terminal, all EGFRs contain similar protein structures with (i) an extracellular ligand binding and dimerization arm (exons 1-16) (ii) a hydrophobic transmembrane domain (exon 17) and (iii) an intracellular tyrosine kinase and C-terminal tail domains (exons 18-28) [9]. The tyrosine kinase domain is divided into N-lobe ( $\alpha$ -sheet) and C-lobe ( $\alpha$ -helical) with an ATP-binding site located between the two lobes [10]. The first step in the receptor tyrosine kinase activation is the ligand induced receptor dimerization. The activation ligands like EGF, TGF- $\alpha$ , Epiregulin, Amphiregulin, etc., bind to the extracellular EGFR domain. EGFR/ErbB1 heterodimerization with ErbB2/HER2 is a potent activator of Epidermal Growth Factor Receptor-Tyrosine kinase (EGFR-TK) complex than EGFR alone. The dimerization leads to the stimulation of the intracellular kinase domain and tyrosine autophosphorylation in transmembrane domain. Trans autophosphorylation of various tyrosine residues depends on the interaction of the N-lobe of one receptor with the C-lobe of the other. The lysine residues in the kinase domain are primary sites for the receptor ubiquitination. This leads to the phosphorylation of tyrosine residues in the juxtamembrane part and the C-terminal of ErbB monomer. The phosphorylated tyrosine kinases serve as docking sites for downstream signaling molecules with residues like SH2 (Src-homology 2) and PTB (phosphotyrosine-binding) domains of cytoplasmic signaling proteins. The cascade



of downstream pro-oncogenic signaling pathways, RAS-RAF-MEK-ERK MAPK and AKT-PI3K-mTOR, then get over activated [8,11–14].

EGFRs downregulation signaling is the reason benefiting cancer cells for increased proliferation, chronic initiation and progression through cell cycle, decreased apoptosis and enhanced cell motility, adhesion and metastasis and angiogenesis [8,11–15]. The available tyrosine kinase inhibitors (TKIs) have succeeded in inhibiting EGFR directed pathways but acquire resistance which remains a significant clinical issue. They also show poor therapeutic activity [16]. Out of all the four family members of ErbBs, ErbB1 and ErbB2 are attractive targets as they are involved in the development and metastasis of different human cancers [14,17]. Targeting these two oncogenes is, therefore, a promising therapeutic strategy for anticancer chemotherapy. As already mentioned, ErbB1 plays an important role in cancer cells for attaining the hallmarks of cancer. ErbB2 is an important biomarker in cancer. It does not, however, contain a ligand-binding domain and so far no direct ligand has been identified. It depends on dimerization for its activation. ErbB2 appears to be the preferred binding partner to other family members of HER [18,19]. ErbB2 overexpression accompanied by ErbB1 expression is associated with increased cancer metastasis and poor cancer prognosis. Conversely, increased ErbB2 expression causes resistance to ErbB1 directed therapies [20–22].

ErbB1 and ErbB2 share a high sequence homology and structural conservation. They associate distinctly with different types of cancer. ErbB1 is a well-established target for lung cancer and drugs such as gefitinib and erlotinib have been approved by the US FDA to treat non-small-cell lung cancers (NSCLC). ErbB2 has been a biomarker and prominent therapeutic target for breast cancer [23]. The dual inhibitor, Lapatinib, for ErbB1 and ErbB2, approved by FDA is being used clinically [24]. However, resistance develops against this drug by the escape route signaling. Small molecules can target proteins with established binding pockets but proteins in shallow and undefined pockets are not easily available and remain unaffected. Large sized and high molecular weight monoclonal antibodies (mAbs) have limitations in permeability into solid tumors. In addition mAbs have expensive manufacturing procedures and variability with manufactured batches [25].

Peptides are short chain amino acid monomers linked by peptide bonds. They are small in size, easy to synthesize, have the ability to penetrate easily through cell membrane and have high activity, specificity and affinity, with minimal drug interactions and biological and



chemical diversity [26]. Further, peptides from natural and synthetic sources can specifically bind to cancer cells thus causing less toxicity to normal cells. Small peptides (<30 amino acids) are often cationic in nature and have emerged as prominent anticancer agents [27–31]. The tumor specificity and anticancer ability of peptides are based on the amino acid residues containing structures of glycine, leucine, arginine and lysine [6,32]. With anionic charged components of the cancer cell membrane, these cationic charged amino acids form hydrogen bonds, indicating that the presence of these amino acids is the main reason for the tumor specificity of the peptides. Besides selectivity, small peptides have low molecular weight and good cellular uptake. Compared to the normal cells, high membrane fluidity and high cell-surface area of cancer cells lead to enhanced binding and lytic activity of peptides. Peptides induce apoptosis in cancer cells by disrupting their mitochondrial membrane [6,33,34]. Peptides also play an important role in early diagnosis and prognostic predictors in the treatment of cancer patients [35]. Peptides can serve as inhibitors of protein–protein interactions (PPIs) and their potential as drugs has been widely demonstrated. Peptides normally interact with the target protein having well-structured domains, which form clefts or pockets ideal for recognition. Their affinity towards cancer targets, however, is less explored [36]. The present work is focused on virtual high throughput screening of short peptides to target ErbB1 and ErbB2 dual inhibition.

## **2. Materials and Methods**

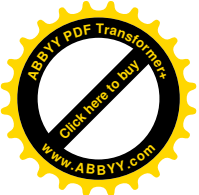
### **2.1. Preparation of the protein structures**

The protein structure of the Epidermal growth factor receptors, ErbB1 (PDB ID: 1XKK) and ErbB2 (PDB ID: 3PP0), were retrieved from the protein data bank [37,38]. The ligand molecules, ions and water molecules were removed from the crystal structures. The protein structures were prepared by adding hydrogen atoms and subjected to energy minimization using Discovery Studio 4.1 (DS 4.1). The missing amino acids and loops were built using the SEQRES module. Energy minimization was performed using CHARMM minimization. The protein structures were then protonated and the protocol parameter value was set to protein dielectric constant of 10, protonation pH of 7.4, ionic strength of 0.145 and energy cut off of 0.9. The CHARMM forcefield was used to prepare the protein structures [39].

### **2.2. Analysis of ErbB1 and ErbB2 receptors**

The ErbB1 and ErbB2 structures were thoroughly analyzed to understand their folding states and binding pockets. The physicochemical properties of ErbB1 and ErbB2 were calculated





using Expasy's ProtParam (<https://web.expasy.org/protparam/>). These include the extinction coefficient, molecular weight (MW), theoretical isoelectric point (pI), aliphatic index (AI), instability index, the total number of positive and negative residues and the grand average hydropathy (GRAVY). The proteins folding state were also checked using the FoldIndex program [40]. The proteins health report, hydrophobicity plot and Ramachandran plot were generated using DS 4.1 to analyze the quality of the protein structures.

### 2.3. Prediction of the active site

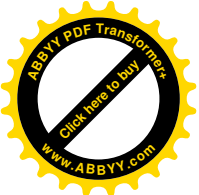
The PDB structure ErbB1 is bound to GW572016 (Lapatinib) and ErbB2 is bound to TAK285 [38]. The binding sites of these ligands were, therefore, selected for our study. The ligand-binding residues involved in the binding regions and binding pockets were predicted through DS 4.1 and used for molecular docking. The ErbB1 binding site grid box centre is X=16.51, Y=39.9, Z=40.33 with threshold value 2.5, the grid spacing is X=0.5, Y=0.5, Z=0.5, the grid angle is X=90, Y=90, Z=90, the radius of the grid box is 20.75 and the total point count is 3022. The ErbB2 binding site grid box centre is X=17.36, Y=17.32, Z=26.94, the grid spacing is X=0.5, Y=0.5, Z=0.5, the grid angle is X=90, Y=90, Z=90, the radius of the grid box is 11.9 and the total point count is 2967.

### 2.4. Peptide data collection and preparation

Natural peptides with <15 residues were downloaded from different databases namely DRAMP, CancerPPD, BiopepUWM, Strapep, Tumorhope, SATPDb and cell penetrating peptides. The detailed database descriptions are as follows;

**DRAMP** (Data repository of antimicrobial peptides) contains diverse antimicrobial peptides (AMPs) [41]. **CancerPPD** is a repository of experimentally verified anticancer peptides (ACPs) [42]. **BiopepUWM** consists of the integrated fundamental parts of sequence databases of proteins, bioactive peptides, allergenic proteins with their epitopes and sensory peptides including single amino acid residues [43]. **Strapep** is a structure database of bioactive peptides [44]. **TumorHoPe** database contains experimentally characterized tumor homing peptides [45]. **SATPDb** is a database of structurally annotated therapeutic peptides [46]. **Cell Penetrating peptides** is a database containing around 1700 unique cell penetrating peptides (CPPs) along with their secondary and tertiary structures [47,48].

The peptides, downloaded in 2D, PDB and SDF format, were converted to 3D and mol2 format using the molconvert tool of InstJChem, ChemAxon software



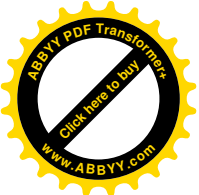
(<http://www.chemaxon.com>) [49,50] and hydrogen atoms were added through ChemAxon command line. The peptide structures were prepared using the D.S 4.1 prepare ligand command. The following parameters were used to run the protocol; change ionization, generate tautomers and generate isomers are set as false because the natural peptide structures have already been reported with their ionization, tautomers and isomers. The fix bad valencies parameters are set as true to check each peptide atom and their angles along with their valencies and the final prepared structure was generated with 3D coordinates. The duplicate structures of the peptides were removed by the 'prepare ligand protocol'.

## **2.5. Virtual high throughput docking of the peptide libraries**

The selected peptide libraries were subjected to vHTS docking using Libdock [51]. Dock Ligand (Libdock) is a high-throughput algorithm used for docking ligands to the receptor's active site. The structure minimization was performed using CHARMM forcefield [39]. The HotSpot of the protein site feature was calculated using Prepare Ligand module. HotSpot consists of a polar and an apolar HotSpot. Apolar HotSpot is preferred by an apolar ligand atom (Carbon atom), and polar HotSpot is preferred by a polar ligand atom (hydrogen bond acceptor and donor). The active site was validated using root mean square deviation (RMSD), which was set to 1Å. The following parameters were used to perform libdock; the input site sphere was set with cocrystal binding sphere, the number of hotspots was 100 with docking tolerance 0.25, the docking preferences were set to high quality with BEST conformation method, the minimization algorithm was steepest descent with RMSD cut off 1.0. Libdock score was calculated by Libdock module and used for further study. The libdock scoring function resembles a piecewise linear potential (PLP) summed over interacting atoms in the protein-ligand complex. The atoms were divided into four types, namely apolar, acceptor, donor, and donor/acceptor and the score between interacting atoms was scored using either the hydrogen bonding potential or the steric potential. Relative and absolute energies were the conformational scores of a particular pose.

## **2.6. ADME and TOPKAT prediction**

The screened virtual hit peptides were subjected to artificial intelligence based ADMET prediction for calculating absorption, distribution, metabolism, excretion, and toxicity using DS.4.1[52]. This model predicts human intestinal absorption after oral administration. The intestinal absorption model includes and reside within the ellipse regions of 95% and 99% confidence level in the ADMET PSA 2D and AlogP98 plane [53]. The aqueous solubility was



predicted using linear regression model that predicts the solubility of each peptide in water at 25°C [54]. The cytochrome P450 2D6 (CYP2D6) model was used to predict CYP2D6 enzyme inhibition using 2D chemical structure. CYP2D6 is involved in the metabolism of a wide range of substrates in the liver and its inhibition by a drug constitutes a majority case of drug-drug interaction [55]. The hepatotoxicity model predicts potential organ toxicity for a wide range of structurally diverse peptides using leave-one-out cross validation method [56]. The plasma protein binding model predicts whether a compound is likely to be highly bound ( $\geq 90\%$  bound) to the carrier protein in the blood. Plasma protein binding of drug molecules can affect the efficiency of a drug because the bound fraction is temporarily shielded from metabolism. Only the unbound fraction exhibits pharmacological effects [57]. TOPKAT was used to predict the ames mutagenicity, rodent carcinogenicity, rate lethal dose (LD50) and the development of toxicity potential of all the peptides.

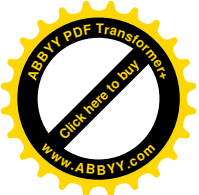
## **2.7. Calculation of physicochemical properties of peptides for drug-likeness**

To check the drug-likeness of the peptides, Lipinski's Rule of 5 [58] and Veber's Rule of 3 [59] were used to determine the physicochemical parameters of the peptides. This property of space filtering is based on certain threshold physicochemical parameters of the peptides, namely Molecular weight (MW), ALogP, Hydrogen Bond Acceptors (HBA), Hydrogen Bond Donors (HBD), Molecular Polar Surface Area (MPSA) and Rotatable bonds. The parameters for Lipinski's drug-likeness were set as hydrogen bond donors 5, hydrogen bond acceptors 10, molecular weight 500, AlogP 5 and the number of violations allowed was 1. The parameters for Veber's drug-likeness were set as rotatable bonds 10, polar surface area 140 and hydrogen bond donors and acceptors 12. The drug-likeness properties were calculated using the DS 4.1.

## **2.8. Multiple molecular docking and interaction study**

The selected top peptides were subjected to molecular dynamics based docking, CDOCKER and Autodock. CDOCKER uses a CHARMM-based molecular dynamics (MD) scheme to dock ligands into a receptor binding site. Random ligand conformations were generated using high-temperature MD. The conformations were then translated into the binding site. Candidate poses were then created using random rigid-body rotations followed by simulated annealing. A final minimization was then used to refine the ligand poses.

A detailed CDOCKER protocol with the following parameters was used for redocking the peptides; a total of 10 conformations/top hits were generated for each screened peptide. The dynamics steps parameter was 1000 and dynamics target temperature was 1000. The

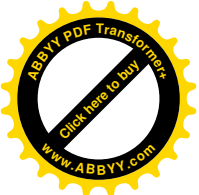


electrostatic interactions were included for calculations. The other parameters considered for calculations include orientations to refine 10, maximum bad orientations 800, and orientation vdW energy threshold 300. The simulated annealing was set as true with heating step 2000, heating target temperature 700, cooling step 5000 and cooling target temperature 300. The CDOCKER dockings were performed with CHARMM forcefield with final minimization as full potential. The CDOCKER results were selected based on top poses with negative cdocker energy and negative cdocker interaction energy. CHARMM energy and the top scoring (most negative favorable to binding) poses were retained. The interactions were analyzed using the view interactions module in DS4.1. Each peptide and protein nonbond interactions were analyzed and top poses were taken for binding energy calculation.

The lowest binding energy (BE) conformation and molecular interaction between the receptors and the ligands were determined. *In situ* ligand minimization method with smart minimizer was used for BE calculations with the minimization maximum step of 500. Additionally, the following parameters were used for BE calculations; the ligand conformational entropy was set as true with the distance-dependent dielectrics implicit solvent model, the non-bond list radius was  $14\text{\AA}$ , non-bond higher cut off distance was  $12\text{\AA}$  and the non-bond lower cut off distance was  $10\text{\AA}$ . The electrostatic energies were generated using Particle Mesh Ewald method. The BE and the complex energy were analyzed for the top poses of the peptide-ErbB1 and peptide-ErbB2 complexes. The same complexes were taken for the molecular dynamics (MD) simulation study.

## 2.9. Molecular dynamic simulation

MD simulation was performed using GROMACS-4.6.5 [60] and the protein topology was generated using GROMOS 54A7 force field [61] The topologies for the ligands were created using PRODRG server [62]. The protein-ligand complex was put in a triclinic box. The complex structure was solved with simple point charge (spc216) water and  $\text{Cl}^-$  &  $\text{Na}^+$  ions were added to neutralize the system. The system was relaxed using an energy minimization process. Electrostatic interactions were estimated using the PME algorithm. MD simulations with reasonable initial velocity follow the steepest descent path on the potential energy surface to a local minimum. The temperature and pressure equilibrium step of 1ns was performed before 100ns production simulation [63–66]. After successful completion of MD simulation, MD trajectories were subjected to calculate root mean square deviation (RMSD), root mean square fluctuation (RMSF), Radius of gyration (Rg) using `g_rms`, `g_rmsf`, and



g\_gyrate. Hydrogen bond formation between the protein and the ligands were determined and the change in the secondary structure of the free protein and the protein-ligand complexes were checked with time using the do\_dssp program. Principal component analysis (PCS) was then carried out.

## 2.10. MM-PBSA calculation of binding free energy

After the completion of MD simulation, the trajectories were subjected to MM-PBSA calculation for determining the binding free energy (BFE). The BFE of the protein-ligand complexes were estimated using Molecular Mechanics energies combined with Poisson-Boltzmann (MM-PBSA) [67]. Stable interval snapshots were taken from 100ns MD trajectory to calculate MM-PBSA using g\_mmpbsa Tool40 [68] and the equation,

$$\Delta G_{\text{bind}} = \langle \text{GPL} \rangle - \langle \text{GP} \rangle - \langle \text{GL} \rangle$$

$$G = \Delta G_{\text{bind}} + \Delta E_{\text{vdW}} + \Delta E_{\text{ele}} + \Delta G_{\text{pol}} + \Delta G_{\text{nonpol}} - T\Delta S,$$

where  $\Delta G_{\text{bind}}$  is the binding free energy, GPL is the free energy of protein-ligand complex, GP and GL represent the free energy of protein and ligand, respectively.  $\Delta E_{\text{ele}}$  and  $\Delta E_{\text{vdW}}$  are electrostatic and van der Waals components, respectively and  $\Delta G_{\text{pol}}$  and  $\Delta G_{\text{nonpol}}$  are polar and non-polar components, respectively.  $T\Delta S$  is the temperature and entropic contribution towards BFE. BFE plays a significant role in drug discovery, giving a quantitative estimation of the ligand's binding efficacy to the protein. Dissociation constant ( $K_d$ ) values were also considered where the complex with less ( $<10 \mu\text{M}$ ) dissociation constant shows good binding affinity [69].

## 2.11. Analysis tools used for data analysis

The protein-ligand complex interaction analysis and visualization were carried out using DS 4.1, AutoDock ADT and PyMOL. Docking conformation results were generated using PyMOL. 2D graphs of RMSD, RMSF, Rg, hydrogen bonds and the protein-ligand secondary structure plot were generated using D.S 4.1, Xmgrace. The MD simulation for protein-Apo enzyme was performed using Desmond Maestro v11.3 (Schrodinger, 2019) simulation package from Schrodinger [70].

## 3. Results and Discussion

### 3.1. Preparation of the protein structure

The 3D crystal structure of ErbB1 has an  $\alpha$ -helix,  $\beta$ -sheet and a loop. Energy minimization was carried out using the CHARMM force field. The 3D protein structure of ErbB1 was analyzed using PDB Sum tool which revealed two  $\beta$ -sheets, four  $\beta$ -hairpins, four  $\beta$ -bulges, eight strands, sixteen heli-helix interacts, twenty five  $\beta$ -turns, two  $\gamma$ -turns and fifteen helices (**Figure 1a**). The 3D crystal structure of ErbB2 contains four  $\beta$ -sheets, five  $\beta$ -hairpins, five  $\beta$ -bulges, eleven strands, seventeen helix-helix interacts, nineteen  $\beta$ -turns, four  $\gamma$ -turns and fifteen helices (**Figure 1b**).

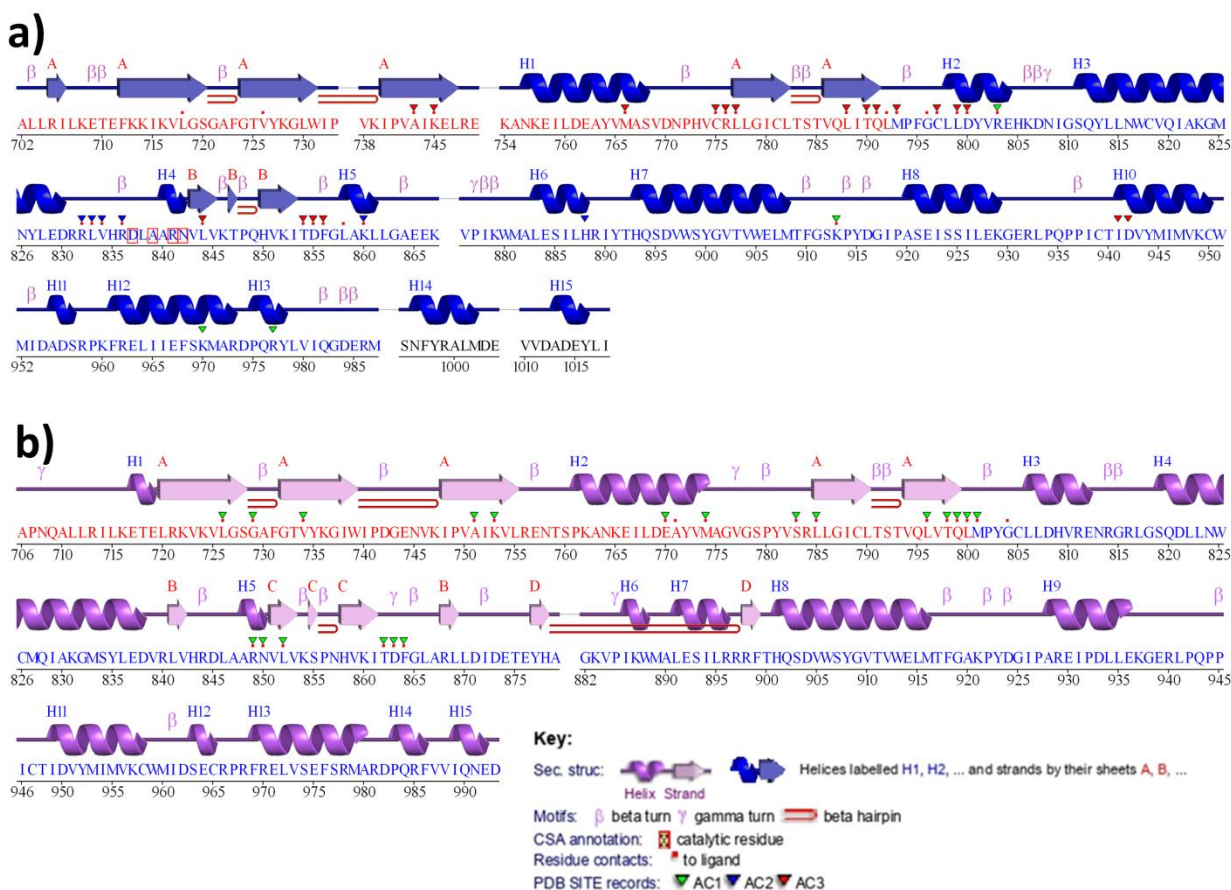


**Figure 1:** Topology diagram of the ErbB1 crystal structure: (1a) The ErbB1 3D structure, (1b) ErbB2 3D structure

### 3.2. Analysis of ErbB1 and ErbB2 receptors

The validation of the protein structures were performed using Ramachandran Plot (**Figure 2**). In the ErbB1 structure AA residues are in 92.9% allowed region, 4.6% marginal region and 2.5% disallowed region. In the ErbB2 structure AA residues are in 97.6% allowed region, 2.4% marginal region, 0% disallowed region. Hydrophobicity map (**Figure 3**) of ErbB1 and ErbB2 shows the folding state of the structures. FoldIndex program was used to predict the folding state of the proteins. The ErbB1 protein sequence revealed an unfolding ability in the

sequence of 0.235 (Charge: 0.000, Phobic: 0.498). The ErbB2 protein sequence revealed an unfolding ability in the sequence of 0.161 (Charge: 0.018, Phobic: 0.477). **Figure 4** shows the positive and negative numbers representing the ordered or folded (Green) and disordered or unfolded (Red) protein. Amino acids that are ordered are shown in green and the disordered in red (**Figure 4**). No disordered region was found in ErbB1 structure (**Figure 4a**). One disordered region was found in the ErbB2 structure between 284-338 amino acid sequence region (**Figure 4b**).

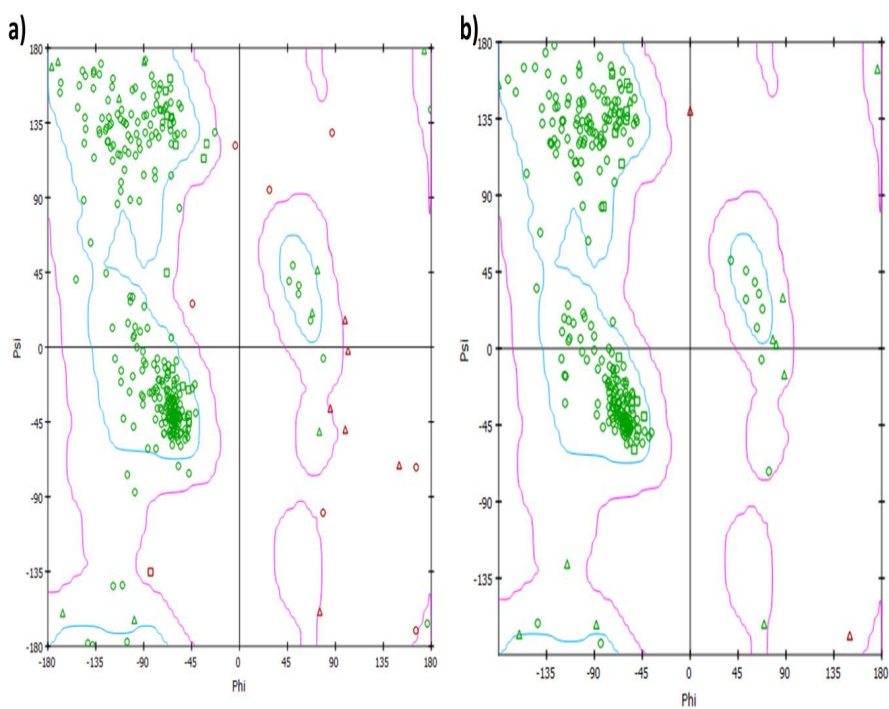


**Figure 2:** Ramachandran plot: (2a) ErbB1 and (2b) ErbB2

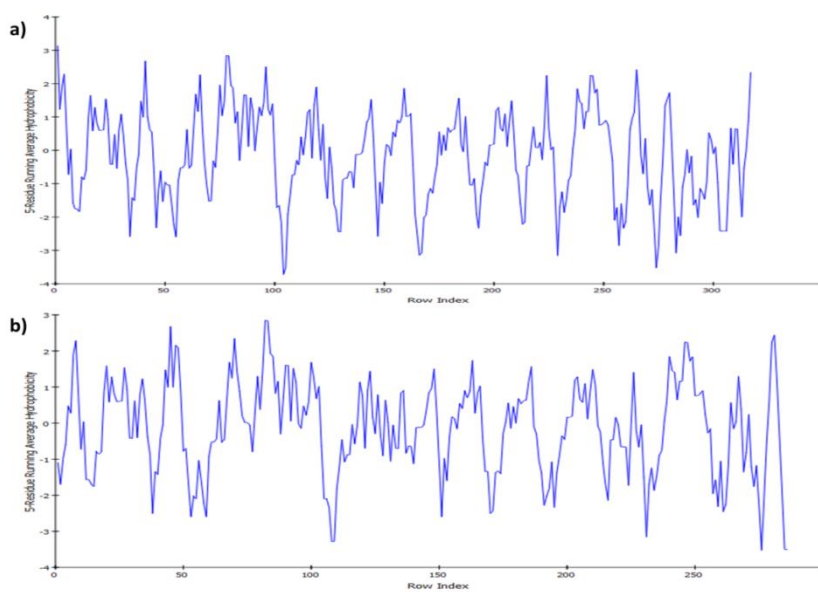


**Figure 3:** Hydrophobicity map: (3a) ErbB1 and (3b) ErbB2

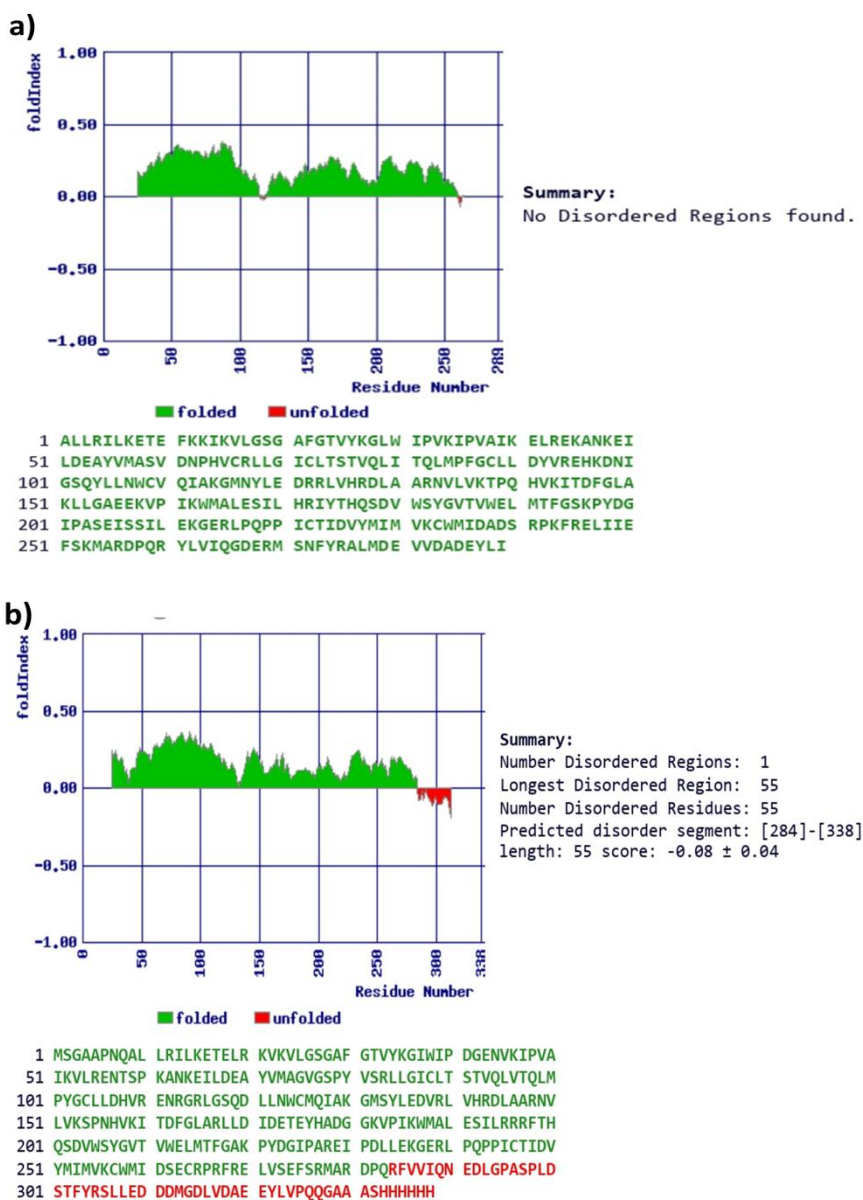
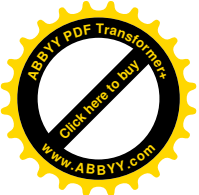


**Figure 4:** FoldIndex plot: **(4a)** ErbB1 and **(4b)** ErbB2.

The y-axis represents the positive and negative values, the ordered and disordered regions, respectively.

ErbB1 revealed 352 amino acids with an average MW of 40269.43 Daltons, 50 negatively charged residues (Aspartic acid + Glutamic acid) and 41 positively charged residues (Arginine + Lysine). The theoretical pI of ErbB1 is 5.88. Based on the instability index, ExPasy's ProtParam classified the optimized protein as stable with an instability index of 42.52. The Instability index is a measure of the protein, namely whether it will be stable in a test tube. The protein's aliphatic index is 91.11 and the grand average of hydropathicity (GRAVY) is -0.315.





The calculated physicochemical properties of ErbB2 revealed 338 amino acids with an average MW of 38179.02 Daltons, 45 negatively charged residues (Aspartic acid + Glutamic acid) and 39 positively charged residues (Arginine + Lysine). The theoretical pI of ErbB2 is 6.02. Based on the instability index, ExPASy's ProtParam classified the optimized protein as unstable with an instability index of 48.10. Again the instability index is a measure of protein, namely whether it will be stable in a test tube. The protein's aliphatic index is 95.15 and the grand average of hydropathicity (GRAVY) is -0.203.

### 3.3. Predicting the active binding sites

The active binding site of ErbB1 was selected based on the known ligand, GW572016, which shows strong binding to the protein (**Figure 5a**). Similarly, the active binding site of the ErbB2 was selected based on the known ligand, ChEMBL1614726, which shows strong binding to the protein (**Figure 5b**). Based on the evidence of strong binding with antagonist action of the binding site, the same sites were used for the docking study. DS4.1 binding site prediction tool was used to find the binding pocket. The amino acids for ErbB1 binding site mentioned in literature and also predicted by DS 4.1 are ARG977, VAL834, ALA743, LYS745, MET766, CYS775, ARG776, LEU777, LEU788, THR790, GLN791, MET793, CYS797, LEU799, ASP800, ARG803, ARG832, LEU833, ARG836, LEU844, LYS860, THR854, ASP855, PHE856, HIS888, LYS913, ILE941, ASP942, LYS970 and ARG977. The amino acids for ErbB2 binding site mentioned in literature and also predicted by DS 4.1 are LEU726, GLY729, VAL734, ALA751, LYS753, GLU770, MET774, SER783, LEU785, LEU796, THR798, GLN799, LEU800, MET801, ARG849, ASN850, LEU852, THR862, ASP863 and PHE864. The superimposition of ErbB1 and ErbB2 structures are shown in **Figure 5c** and the allied sequence of both the proteins are shown in **Figure 5d**.

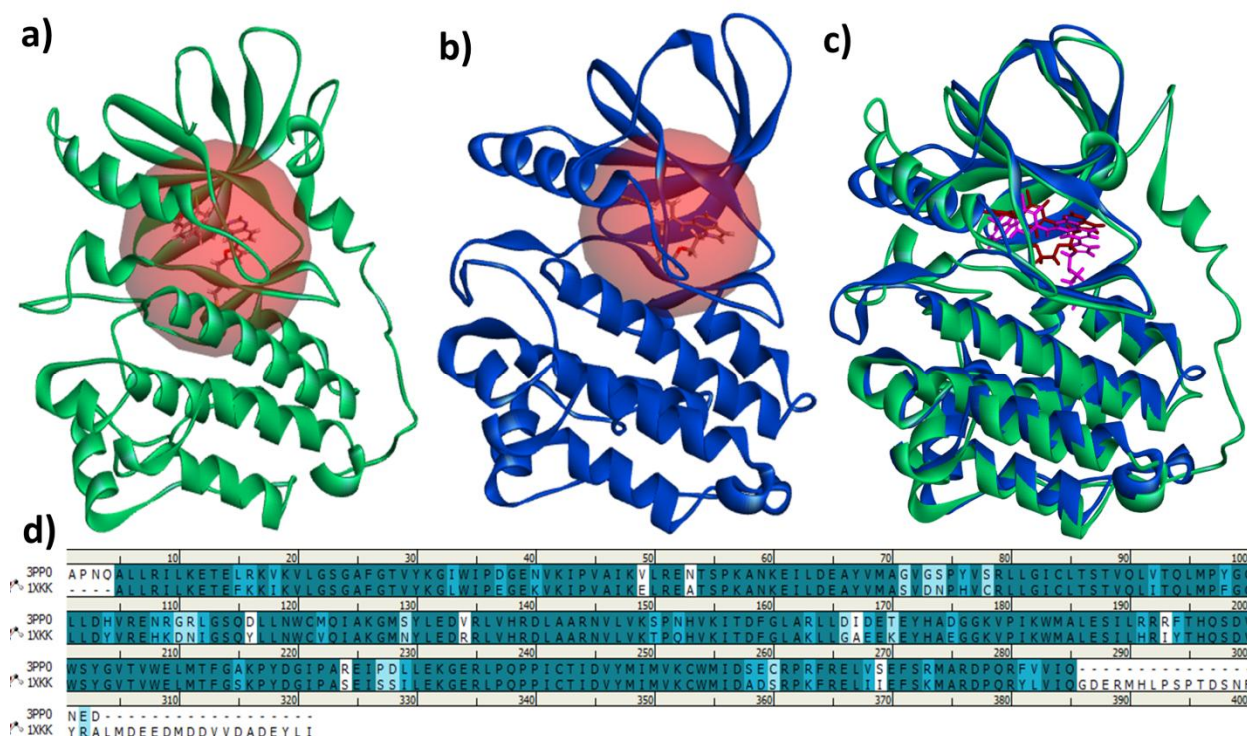


**Figure 5:** ErbB1 and ErbB2 receptor binding pockets: (**5a**) Surface ErbB1 structure, which shows the binding pocket with Lapatinib binding, (**5b**) Surface ErbB2 structure, which shows the binding pocket with CHEMBL1614726 binding, (**5c**) Super imposition of the ErbB1 and ErbB2 structures and (**5d**) The aligned sequence of ErbB1 and ErbB2.

### 3.4. Peptide data collection and preparation

Natural peptides containing below 15 amino acid sequence have been shown to possess high therapeutic potential [27–29,71,72]. We, therefore, selected natural peptides with amino acid sequence below 15 for the present investigation. A total of seven peptide databases were used and 8950 peptides below 15 amino acid sequence were downloaded for the preparation of ligands. The duplicate peptides were rejected by ligand preparation by DS 4.1. A total of 5465 natural peptides from different databases were used for vHTS by libdock (**Table 1**).

**Table 1: Natural peptides collected from different databases**

S. No	Database	Prepared	Accepted	Rejected
-------	----------	----------	----------	----------

		Ligands	Ligands	Ligands (Reason)
1	DRAMP	17	17	-
2	Cancer PPD			
	Below 5	18	5	Duplicate
	05 to 10	220	38	Duplicate
	11 to 15	973	182	Duplicate
	Natural cyclic	93	54	Duplicate
	Natural modified	316	316	-
	Natural linear	1525	1511	Duplicate
3	BiopepUWM	846	846	
4	Strapep			
	Strapep data structures	3883	1721	Duplicate
	AMP	13	13	-
	Hormones	15	14	Duplicate
	Toxins & venoms	36	33	Duplicate
5	SATP Db	644	432	Duplicate
6	Tumorhoep	293	270	Duplicate
7	Cell penetrating peptides	58	13	Duplicate
	<b>Total</b>	<b>8950</b>	<b>5465</b>	

### 3.5. Virtual high throughput docking

Virtual high throughput docking (vHTD) using Libdock docking, was applied for the selected peptides with ErbB1 and ErbB2. Lapatinib was used as the standard as there is no other peptide standard available till date. Lapatinib extracted from the ErbB1 crystal structure showed an absolute energy of 83.30, relative energy of 11.17 and libdock score of 165.603. A total of 295 natural peptides were found to bind to the ErbB1 binding pocket with absolute energy between 0.129 and 189.888, relative energy between 0.04 and 19.99, and libdock score between 7.308 and 214.517 (**Figure 6**). The higher libdock score indicates that the peptides bind well to the ErbB1 binding pocket. All these 295 natural peptides were then docked with ErbB2 structure. The cocrystal ligand of ErbB2 showed an absolute energy of 139.17, relative energy of 14.33 and libdock score of 158.112. The known dual inhibitor, Lapatinib, showed an absolute energy of 94.25, relative energy of 9.37 and libdock score of



109.273 towards ErbB2 binding. A total of 132 natural peptides were binding to the ErbB2 binding pocket with an absolute energy between 0.272 and 139.17, relative energy between 0.204 and 19.26, and libdock score between 62.96 and 199.599 (**Figure 6**). These 132 natural peptides, the dual binding peptides with ErbB1 and ErbB2, were, therefore, taken for studying ADME and TOPKAT prediction.

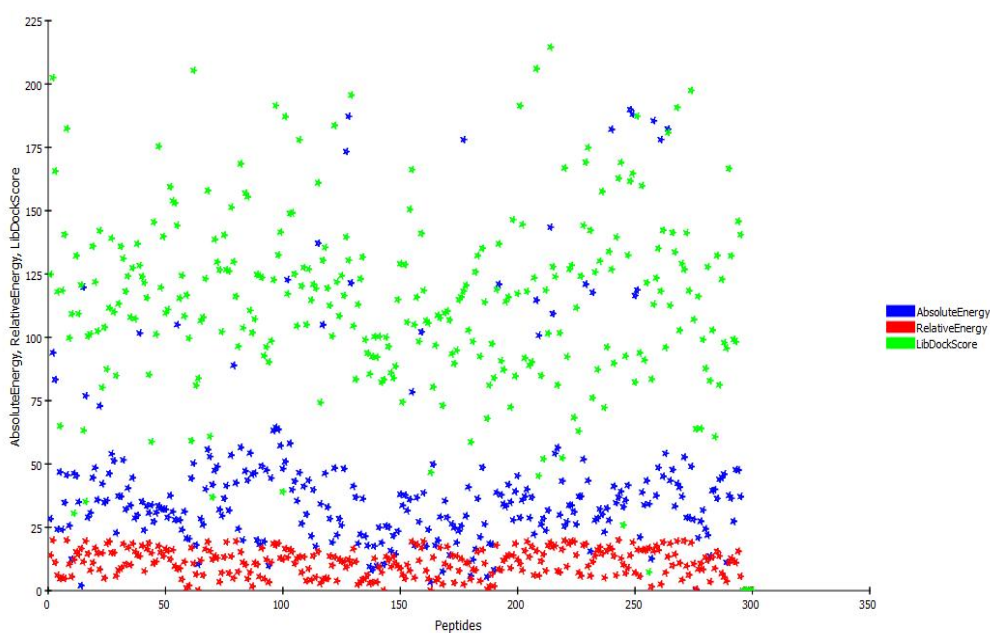


**Figure 6a**

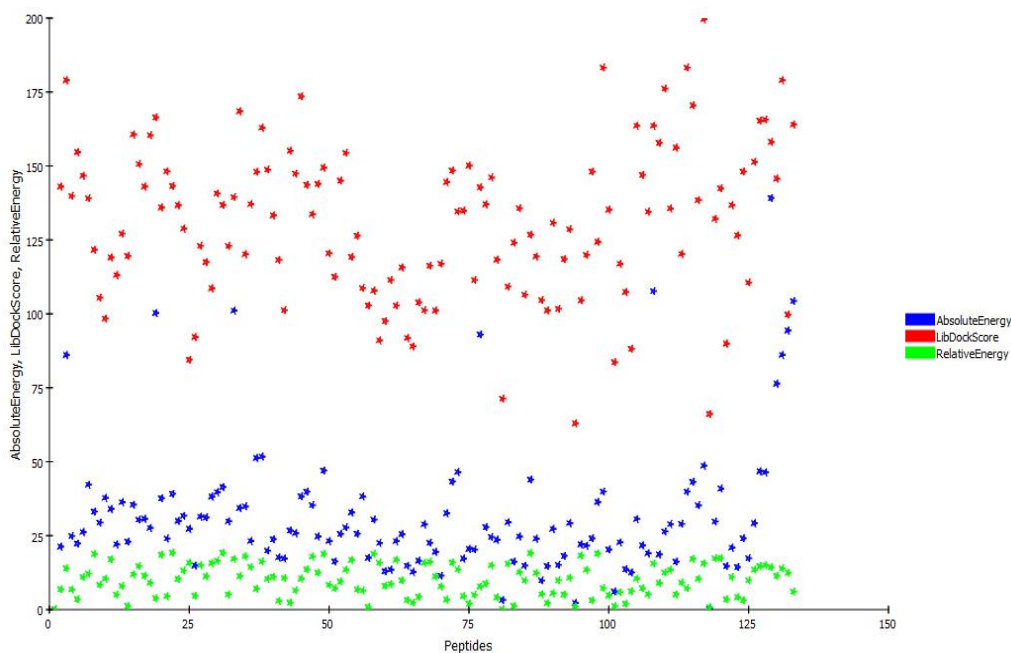


**Figure 6b**

**Figure 6:** Libdock Docking scores.

(6a) The natural peptides binding with ErbB1, (6b) The natural peptides binding with ErbB2  
 Absolute energy (Blue colour), Relative energy (Green colour), and Libdock Score (Red colour).

### 3.6. ADME and TOPKAT prediction

The selected 132 peptides were further analyzed for ADMET descriptors using DS 4.1. The peptides fell within a 95% confidence interval in the human intestinal absorption (HIA) level and were excluded from an ellipse on a 99% confidence interval in the blood-brain barrier penetration. Plasma protein binding, cytochrome P450 2D6 inhibition and hepatotoxicity were calculated. Out of the 132 peptides, 25 peptides that fell in an eclipse and passed the ADMET properties were selected for further study (**Figure 7** and **Supplementary Table.1**).

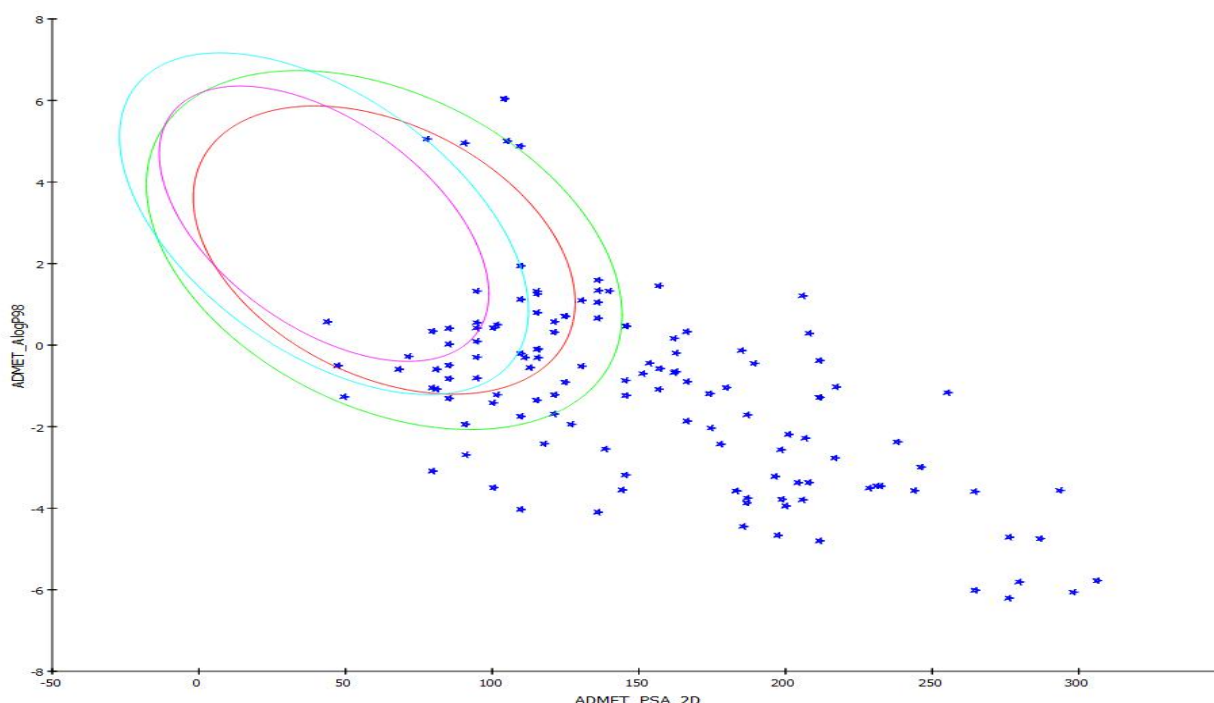


**Figure 7:** The plot of ADMET\_PSA\_2D vs. ADMET\_AlogP98 (the 95 and 99% confidence limit ellipses corresponding to the BBB and HIA models for ligands).

TOPKAT accurately and rapidly assesses the toxicity of chemicals based solely on their 2D molecular structure. TOPKAT uses a range of robust, cross-validated, Quantitative Structure-Toxicity Relationship (QSTR) model for assessing specific toxicological end points. These methods were used to predict the toxicity of the natural peptides. We predicted the Ames mutagenicity, rodent carcinogenicity, Rat lethal dose (LD50) and Developmental Toxicity Potential (DTP) of the peptides. We found 23 peptides were non-mutagenic, non-

carcinogenic and non-toxic and hence selected them for further screening (**Supplementary Table 2**).

### 3.7. Physicochemical properties of the natural peptides

The physicochemical property of a drug candidate is very important for the drug's therapeutic potential. Based on Rule of 5 and Rule of 3 threshold parameters, namely Molecular Weight (between 150-400), SlogP (between -3 to 4), Hydrogen Bond Acceptors ( $\leq 7$ ), Hydrogen Bond Donors ( $\leq 4$ ), Topological Polar Surface Area ( $\leq 160$ ), Rotatable Bonds ( $\leq 9$ ) and Aromatic Rings ( $\leq 4$ ), (**Figure 8**) 23 peptides were selected for our study.

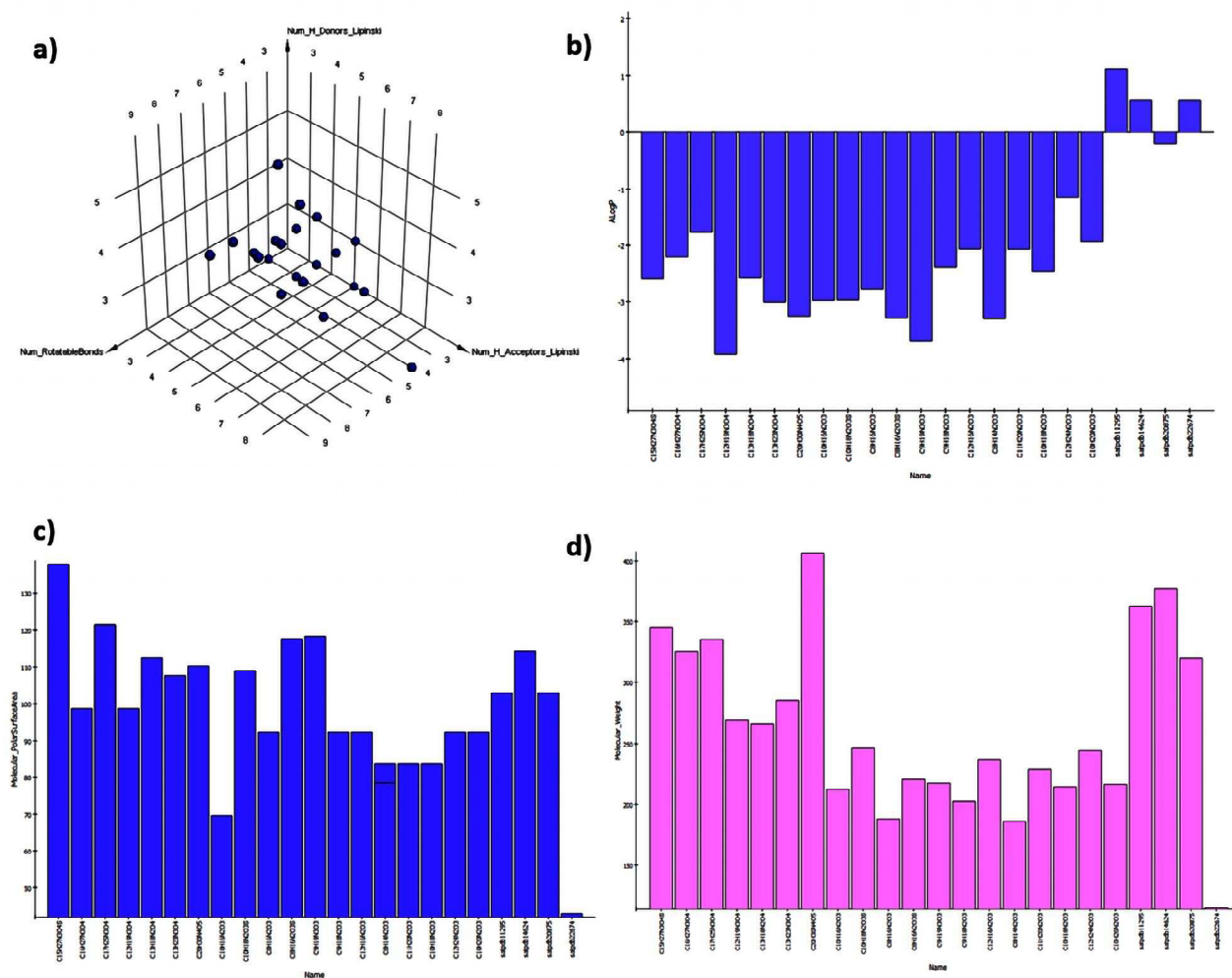


**Figure 8.** Physicochemical properties of the natural peptides:

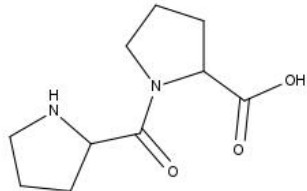
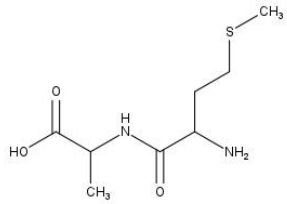
Plot showing (**8a**) hydrogen bond acceptors, hydrogen bond donors and rotatable bonds  
**(8b)** S logP **(8c)** topological polar surface area **(8d)** molecular weight

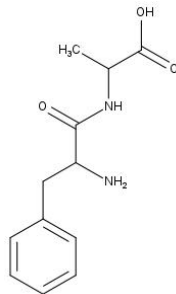
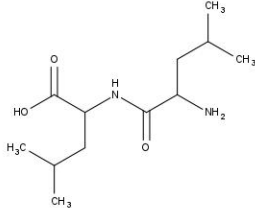
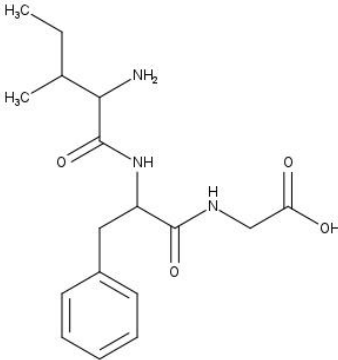
Based on the above studies, the general description like aminoacid sequence, pI, MW, pH, TM index, melting temperature and structures of the top 5 peptides were selected for further study (**Table 2** and **Table 3**).

**Table 2: TOPKAT results of top 5 potential peptides**

Peptides	Mouse Female/Male	Rat / Male	Rat / Female	Carcinogenic TD50 Mouse mg/kg_body_weight/day	Carcinogenic TD50 Rat mg/kg_body_weight/day	DTP
C10H16N2O3	Non-Carcinogen	Non-Carcinogen	Non-Carcinogen	86.1911	0.902526	Non-Toxic
C8H16N2O3S	Non-Carcinogen	Non-Carcinogen	Non-Carcinogen	120.123	1.9077	Non-Toxic
C12H16N2O3	Non-Carcinogen	Non-Carcinogen	Non-Carcinogen	300.373	49.1748	Non-Toxic
C12H24N2O3	Non-Carcinogen	Non-Carcinogen	Carcinogen	82.5517	7.60163	Non-Toxic
satpdb20875	Non-Carcinogen	Non-Carcinogen	Non-Carcinogen	142.385	111.145	Non-Toxic

**Table 3: General description of the selected top 5 natural peptides**

Peptide Formula	Aminoacid sequence	pI	MW	pH	TM Index	Melting Tem.	Source	Structure
C10H16N2O3	PP (Proline-Proline)	5.50	212.248	7.0	-6.08	Below 55	Trypanosoma brucei	
C8H16N2O3S	MA (Methionine-Alanine)	5.50	220.28	7.0	-2.88	Below 55	Trypanosoma brucei	

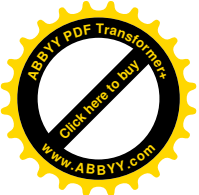
<b>C12H16 N2O3</b>	FA (Phenylal- anine- Alanine)	5. 50	236.6 7	7.0	- 10.98	Below 55	Trypanosoma brucei	
<b>C12H24 N2O3</b>	LL (Leucine- Leucine)	5. 50	244.3 3	7.0	-6.78	Below 55	Trypanosoma brucei	
<b>C17H25 N3O4 (satpdb2 0875)</b>	IFG (Isoleucin e- Phenylala- nine- Glycine)	5. 50	335.4 0	7.0	- 18.30	Below 55	Tuna muscles	

### 3.8. Multiple docking and Interaction analysis

Multiple docking was performed to confirm the binding potential of the peptides with ErbB1 and ErbB2. Docking was carried out for the selected top 5 peptides that passed the drug likeness and ADMET properties. The peptides that bind to the selected pocket is shown in **Table 3, Figure 9a** and **9b**. The five peptides that bind with ErbB1 and ErbB2 were screened by both libdock, CDOCKER and Autodock. These top 5 peptides were also subjected to detailed interaction studies, binding energy (BE), ligand energy, protein energy, complex energy, entropic energy, hydrophobic interactions and hydrogen bond interactions (**Table 4** and **Supplementary Table 3**).

The PP molecule was found to interact with ErbB1 via hydrogen bond interactions with THR854, ASP855, PHE856, and ASP855, and hydrophobic bond interactions with LYS745, and LEU788. Also, PP bind with ErbB2 binding pocket residues, SER783, THR798,





ASP863, SER783 and ASP863 via hydrogen bonding and MET774, LEU785, LEU796 and PHE864 via hydrophobic interactions. The peptide MA interact with ErbB1 via hydrogen bond interactions with LEU777, THR790, ASP855, CYS775, ARG776, and ASP855 via hydrogen bond interactions and via hydrophobic interactions with ALA743, VAL726 and LYS745 via hydrophobic interactions. Also, MA binds efficiently with ErbB2 binding pocket with LYS753, SER783, ASP863 and ARG784 via hydrogen bond interactions and with LEU796 via hydrophobic interactions. The peptide FA is found to interact with ErbB1 binding pocket with PHE856, ASP855, CYS775, ASP855 and THR854 via hydrogen bond interactions and with LYS745 and LEU788 via hydrophobic interactions. Also, FA binds with ErbB1 amino acid residues, THR862 and ASP863 via hydrogen bond interactions and with VAL734, ALA751 and LYS753 via hydrophobic interactions. The peptide LL binds with ErbB1 amino acid residues, THR854, ASP855 and THR790 via hydrogen bond interactions and with ALA743, MET766, LEU777, CYS775, LEU777, VAL726, LEU844, LYS745 and PHE856 via hydrophobic interactions. The peptide IFG forms hydrogen bond interactions with ErbB1 amino acid residues, MET793, THR854, ARG841, ASP855, LEU793, ASN842 and ASP855 and forms hydrophobic interactions with VAL726, ARG841, ALA743, LYS745 and LEU788. Also, IFG interacts strongly with ErbB2 via hydrogen bond interactions with ASP863, MET801, THR862, THR862, ASP863, ASN850, ARG849, ARG849, ASN850, ASP863 and ASP863, and via hydrophobic interactions with LEU726, VAL734, LYS753 and LEU796. The standard compound, Lapatinib, forms hydrogen bond interactions with ErbB1 amino acids residues, THR798, SER728, LEU845 and THR862, and hydrophobic interactions with VAL726, ALA743, LYS745, LEU718, ALA743, LEU844, ALA743, LEU844, LEU718, CYS797 and LEU1001. Also, Lapatinib interacts with ErbB2 amino acid residues, THR798, SER728, LEU845 and THR862 via hydrogen bond interactions and with VAL734, LYS753, LEU726, CYS805, LEU852, LEU726, VAL734, ALA751, LEU852 and CYS805 via hydrophobic interactions. Detailed bond interactions are given along with bond angles and the type of the interactions in the **Supplementary Table 4** and **5**.

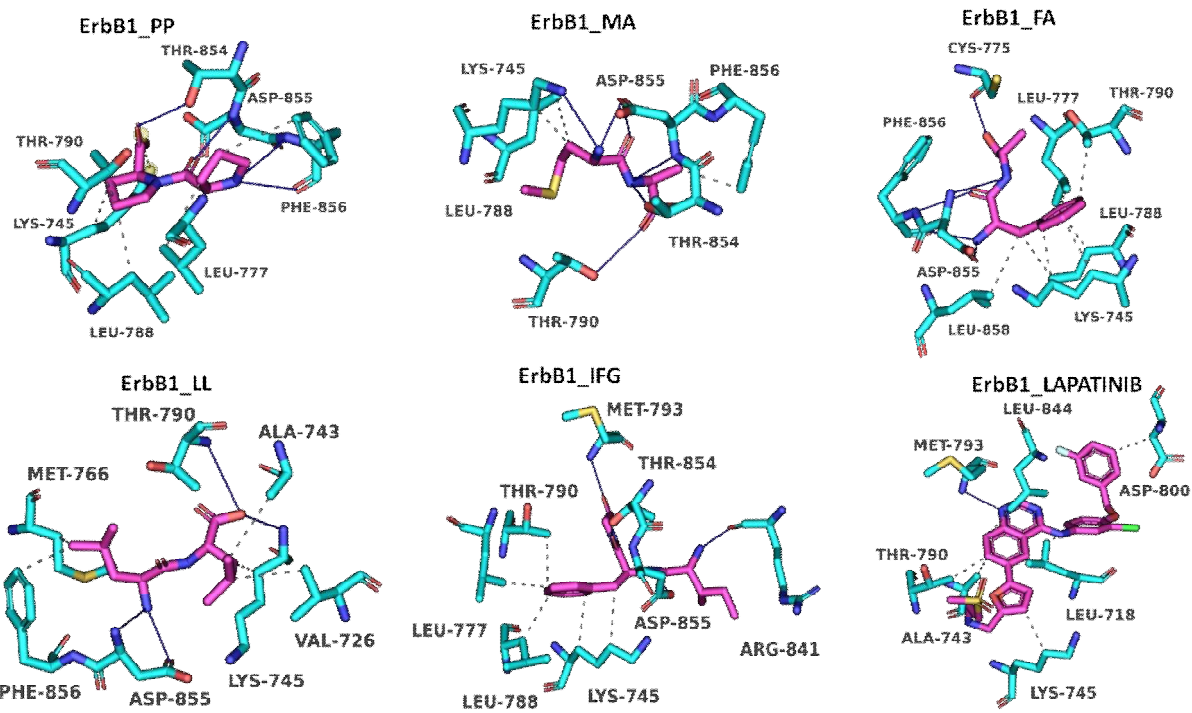


**Figure 9a**

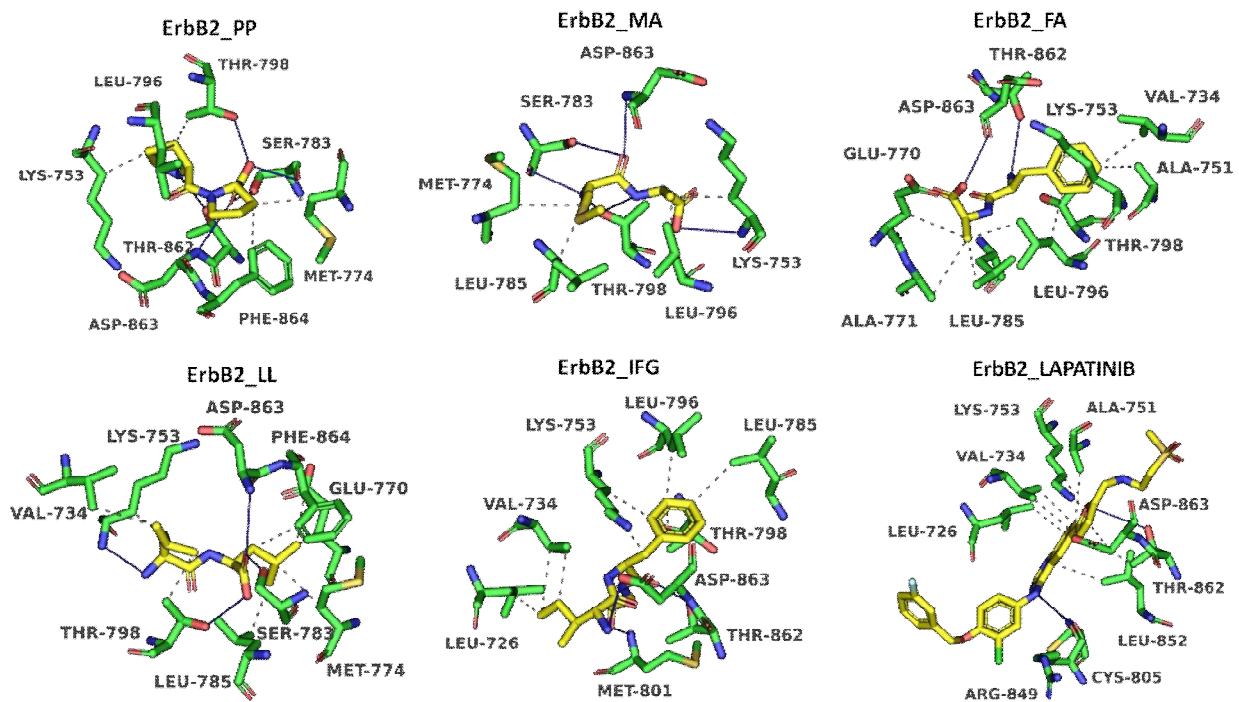


**Figure 9b**

**Figure 9:** The best conformation extracted for the peptides based on BE. The dark blue line shows hydrogen bonds, and the gray (discontinuous) line shows hydrophobic interactions.

(9a) ErbB1, (9b) ErbB2

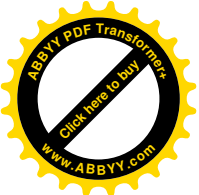
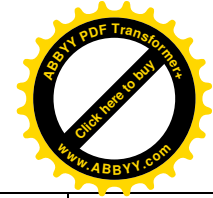
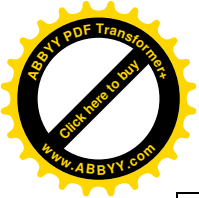


**Table 4.** Docking scores, hydrogen bond and hydrophobic interactions for the selected peptides.

Ligand Name	Target	Binding Energy (kcal/mol)	Ligand Energy (kcal/mol)	Protein Energy (kcal/mol)	Complex Energy (kcal/mol)	Entropic Energy (kcal/mol)	Hydrogen Bonds	Hydrophobic and Other bonds
<b>PP</b>	ErbB1	-58.5824	-24.9838	-9855.9455	-9889.5441	18.3657	THR854, ASP855, PHE856, ASP855	LYS745, LEU788
	ErbB2	-60.5368	-20.3193	-10831.807	-10872.024	18.3656	SER783,T HR798,A SP863,SE R783, ASP863	MET774, LEU785, LEU796, PHE864
<b>MA</b>	ErbB1	-80.3692	-34.6355	-9855.9455	-9970.9501	18.5754	LEU777, THR790, ASP855, CYS775, ARG776, ASP855	ALA743, VAL726, LYS745
	ErbB2	-66.3845	-33.7443	-10831.807	-10931.936	18.6084	LYS753, SER783, ASP863, ARG784	LEU796
<b>FA</b>	ErbB1	-71.8276	-34.8633	-9855.9455	-9962.6365	18.7745	PHE856, ASP855, PHE856, CYS775, ASP855, THR854	LYS745, LEU788
	ErbB2	-61.943	-30.3809	-10831.807	-10924.131	18.811	THR862, ASP863	VAL734, ALA751, LYS753
	ErbB1	-83.3466	-29.7436	-9855.9455	-9969.0357	18.8921	THR854, ASP855, THR790	ALA743, MET766, LEU777, CYS775, LEU777,



<b>LL</b>								VAL726, LEU844, LYS745, PHE856
	ErbB2	-56.4563	-27.7286	-10831.807	-10915.992	18.9649	SER783, THR798, ASP863, ALA751, THR798, LEU796	ALA751, VAL734, MET774, LEU785, MET774, PHE864
<b>IFG</b>	ErbB1	-66.5795	-56.0951	-9855.9455	-9978.6201	19.64	MET793, THR854, ARG841, ASP855, LEU793, ASN842, ASP855	VAL726, ARG841, ALA743, LYS745, LEU788
	ErbB2	-89.0453	-45.1388	-10831.807	-10965.991	19.7002	ASP863, MET801, THR862, THR862, ASP863, ASN850, ARG849, ARG849, ASN850, ASP863, ASP863	LEU726, VAL734, LYS753,L EU796
<b>Lapatinib</b>	ErbB1	-54.9033	-42.7946	-9855.9455	-9868.0541	21.4965	MET793, ASP855, PHE856, THR854, MET793	VAL726, ALA743, LYS745, LEU718, ALA743, LEU844, ALA743, LEU844, LEU718, CYS797, LEU1001
	ErbB2	-51.7079	-42.4279	-10831.807	-10841.087	21.3102	THR798,	VAL734,

							SER728, LEU845, THR862	LYS753, LEU726, CYS805, LEU852, LEU726, VAL734, ALA751, LEU852, CYS805
--	--	--	--	--	--	--	------------------------------	--

### 3.9. Binding energy

The top 5 peptides showing high drug-likeness potential were taken for binding energy calculations. The binding energy is calculated for all the selected five peptides with ErbB1 and ErbB2 complexes. DS 4.1 was used to perform binding energy calculations. The results, reveal that LL-ErbB1 complex has a highest BE of -83.34 kcal/mol. Complexes ErbB1-PP, ErbB1-MA, ErbB1-FA, ErbB1-IFG show BE of -58.58, -80.36, -71.82 and -66.57 kcal/mol, respectively. The standard inhibitor, ErbB1-Lapatinib shows a BE of -54.90 kcal/mol. In the ErbB2-peptide complex, the ErbB2-IFG complex shows the highest BE of -89.04 kcal/mol. Complexes, ErbB2-PP, ErbB2-MA, ErbB2-FA, and ErbB2-LL show BE of -60.53, -66.38, -61.94, -56.45 kcal/mol, respectively. The standard inhibitor, ErbB2-Lapatinib shows a BE of -51.70 kcal/mol. The BE calculation results suggest that the selected peptides bind better than the known dual inhibitor, lapatinib. The other calculated energies like negative Cdocker energy, negative Cdocker interaction energy, ligand energy, protein energy, complex energy, and entropic energy are given in **Table 4** and **Supplementary Table 3**.

### 3.10. Molecular dynamic simulation analysis

The structural stability and the dynamic behavior of the ligand-ErbB1 and ligand-ErbB2 complexes were analyzed by calculating the RMSD, RMSF, Rg, checking hydrogen bond interactions, 2D projection of trajectory, free energy surface, gibbs energy landscape and residual components.

#### 3.10.1. Root mean square deviation (RMSD)

RMSD of all the protein-ligand complexes were calculated to analyze the deviation of compounds for 100 ns trajectory period (**Figure 10**). The RMSD of the five protein-ligand complexes, namely ErbB1-PP, ErbB1-MA, ErbB1-FA, ErbB1-LL and ErbB1-IFG (**Figure 10a**) and ErbB2-PP, ErbB2-MA, ErbB2-FA, ErbB2-LL and ErbB2-IFG (**Figure 10b**) reveal

their stability. The average value of RMSD for ErbB1-PP, ErbB1-MA, ErbB1-FA, ErbB1-LL and ErbB1-IFG complexes is 0.354 nm, 0.306 nm, 0.4815 nm, 0.283 nm, and 0.3775 nm, respectively which are comparable to the standard and Apo protein, ErbB1-Lapatinib complex which shows an RMSD of 0.304 nm. The pattern of deviation of ErbB1-MA and ErbB1-LL are almost similar to that of ErbB1-Lapatinib throughout the 100 ns trajectory period. ErbB1-PP shows deviation from the standard from 60 ns trajectory period, ErbB1-IFG shows deviation from 55 ns trajectory period. The RMSD values of the Apo protein fluctuate between 0.2 nm and 0.4 nm, with a slight fluctuation range from 0 to 100 ns. This suggests that the protein structure is relatively stable over time in the absence of a bound ligand or cofactor (**Figure. 10a**), while the ErbB1-ligand complexes shows structural stability over the 100 ns trajectory period. The ligand binding induces specific conformational changes in the ErbB1 protein structure, which vary depending on the specific ligand and binding mode, while the Apo protein does not have any ligand-induced changes in structure.

The average value of RMSD for ErbB2-PP, ErbB2-MA, ErbB2-FA, ErbB2-LL and ErbB2-IFG complexes is 0.3325 nm, 0.4675 nm, 0.461 nm, 0.4295 nm, and 0.4805 nm, respectively which are comparable to the standard, ErbB2-Lapatinib complex which shows an RMSD of 0.3755 nm. The pattern of deviation of ErbB2-PP and ErbB2-LL were similar throughout the 100ns trajectory period whereas the remaining complexes show fluctuations that are comparable to the standard, ErbB2-Lapatinib complex. The Apo protein has little fluctuations and is completely stable from 45-100 ns (**Figure. 10b**). This suggests that, the Apo protein is more stable than the ErbB2-ligand complexes.

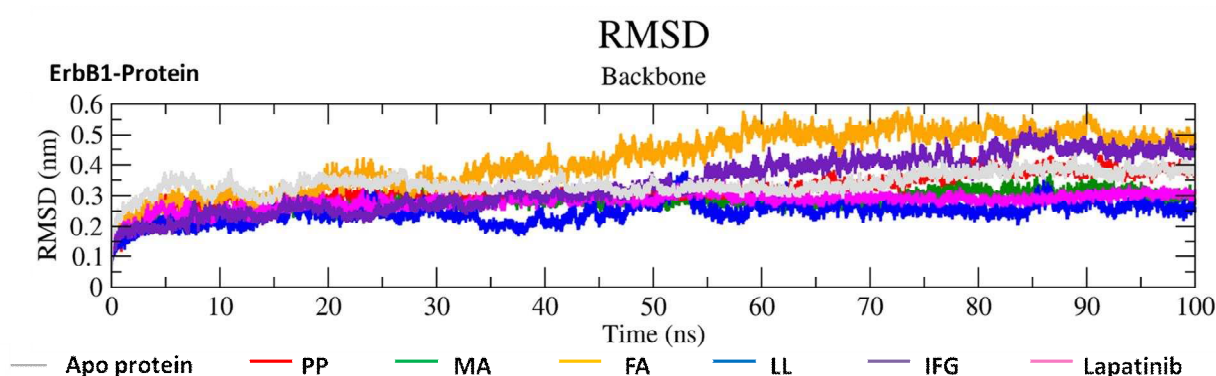


**Figure 10a**

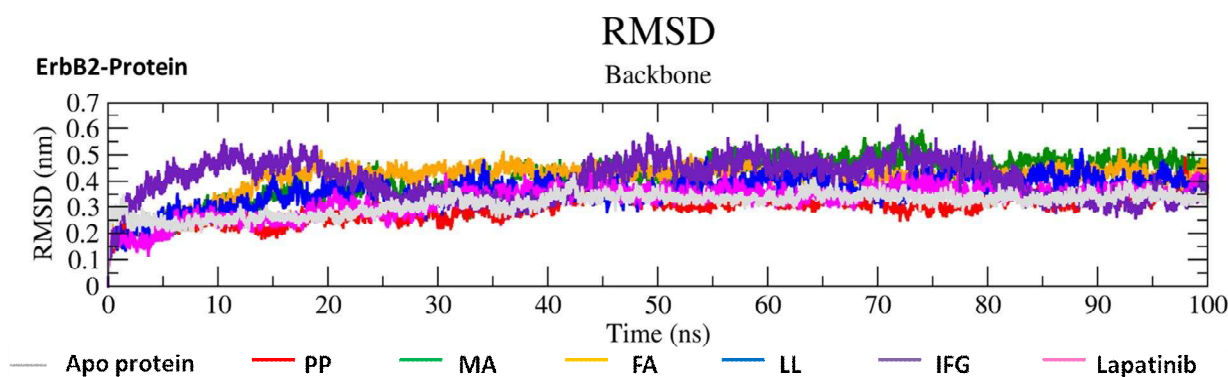


**Figure 10b**

**Figure 10:** Root Mean Square Deviation of protein-ligand complexes

(10a) ErbB1 (10b) ErbB2

### 3.10.2. Root mean square fluctuation (RMSF)

The local changes of compounds as well as the protein chain residues were analyzed using RMSF measurement at a particular temperature and pressure. There were very few variations in the constituent residues of ErbB1 and ErbB2 during the 100 ns trajectory period. All the protein-ligand complexes were plotted to compare the flexibility of each residue in the protein and the complex (**Figure 11**). **Figure 11a** shows the fluctuations of all ErbB1-ligand complexes are under 0.82 nm. ErbB1-IFG complex shows a fluctuation of 0.81 nm at 870 residue, ErbB1-FA shows a fluctuation of 0.79 nm at 920 residue. From 860-900 residues all the complexes show fluctuations. However, no active amino acid residues fall in this region. ErbB1-PP and ErbB1-LL complexes show fluctuation in residues that are significantly similar and comparable to the reference, ErbB1-Lapatinib thus revealing less fluctuation and good stability. On the other hand, the Apo protein has a RMSF value ranging from 0.1 to 0.4 nm. Additionally, the fluctuations of the Apo protein occur over the period of a 100ns trajectory period (**Figure. 11a**), while the fluctuations of the ErbB1-ligand complexes are measured at specific residues same as Apo protein. Overall, the ErbB1-ligand complexes appear to be relatively stable..

**Figure. 11b** shows the fluctuations of all ErbB2-ligand complexes are under 0.61 nm. ErbB2-MA complex shows a fluctuation of 0.56 nm at 760 residue, 0.46 nm at 880 residue and 0.61 nm at 928 residue. ErbB2-PP complex shows a slight fluctuation of 0.3 nm at 867 residue, the remaining complexes show significantly similar fluctuation in residue comparable to the reference, ErbB2-Lapatinib reveal less fluctuations and good stability. The

Apo protein exhibits higher RMSF values ranging from 0.1 to 0.3 nm, and the fluctuations occur over the period of a 100ns trajectory period (**Figure. 11b**), while the fluctuations of the ErbB2-ligand complexes are measured at specific residues same as Apo protein. Overall, the ErbB2-ligand complexes exhibit relatively low fluctuations and good stability.

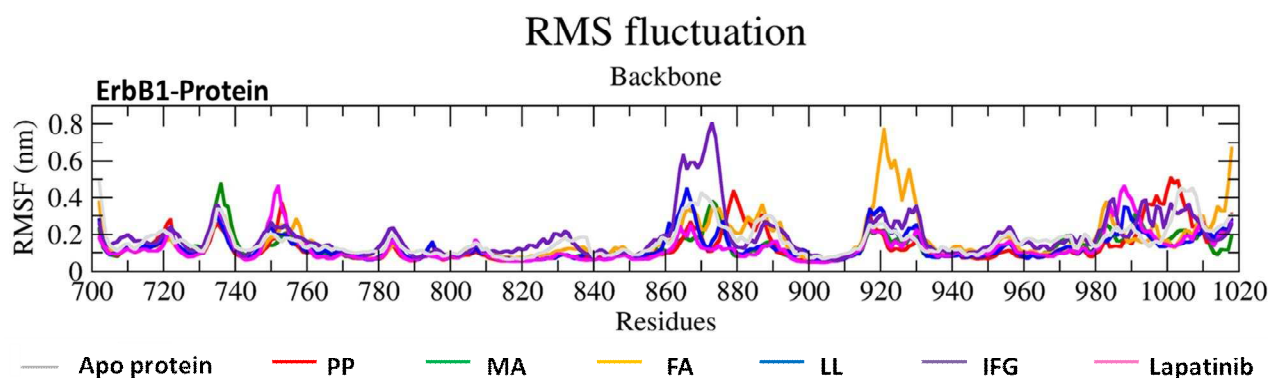


**Figure 11a**

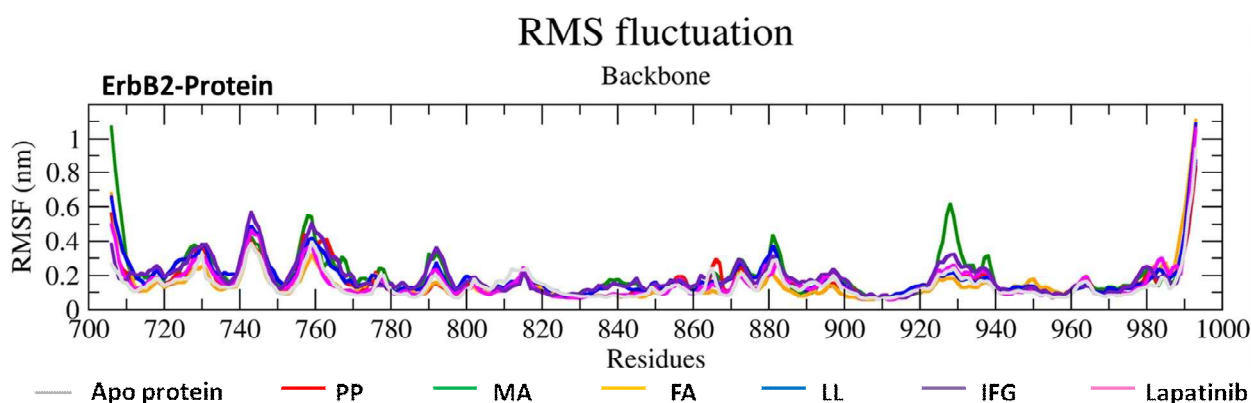


**Figure 11b**

**Figure 11:** Root Mean Square Fluctuation of protein-ligand complexes

(11a) ErbB1 (11b) ErbB2

### 3.10.3. Radius of gyration (Rg)

The Rg analysis was carried out to assess the stability of protein-ligand systems by calculating the structural compactness along the MD trajectories. Rg was calculated for the stably folded or unfolded protein and the ligand-protein complexes. We used 100 ns trajectories for the Rg analysis. The plot of Rg as a function of time for ErbB1-ligand and ErbB2-ligand complexes are shown in **Figure 12a** and **12b**, respectively. The data reveal that the average Rg value of ErbB1-PP, ErbB1-MA, ErbB1-FA, ErbB1-LL and ErbB1-IFG is



2.0585 nm, 2.084 nm, 2.0755 nm, 2.077 nm and 2.114 nm, respectively which are comparable to the standard, ErbB1-Lapatinib that shows an Rg value of 2.0855 nm. All the complexes show a similar pattern throughout the trajectory period except for ErbB1-PP, ErbB1-MA and ErbB1-IFG. The average Rg value of ErbB2-PP, ErbB2-MA, ErbB2-FA, ErbB2-LL and ErbB2-IFG is 2.0525 nm, 2.065 nm, 2.053 nm, 2.097 nm and 2.0845 nm, respectively which are comparable to the standard, ErbB2-Lapatinib that shows Rg value of 2.032 nm. Up to 40 ns all the complexes show a pattern similar to the standard protein-Lapatinib complex. From 40 ns to 100 ns there is a variation of 0.02 to 0.08 nm in all the complexes compared to the standard protein-Lapatinib complex. The Rg value of the Apo protein is 2.08 nm and 2.02 nm respectively for ErbB1 and ErbB2, suggesting that the protein structure is relatively stable over time in the absence of a bound ligand or cofactor (**Figure 12a & 12b**), while the ErbB1-ligand complexes shows structural stability over the 100 ns trajectory period. The ligand binding induces specific conformational changes in the ErbB1 protein structure, which vary depending on the specific ligand and binding mode, while the Apo protein does not have any ligand-induced changes in structure.

### Radius of gyration

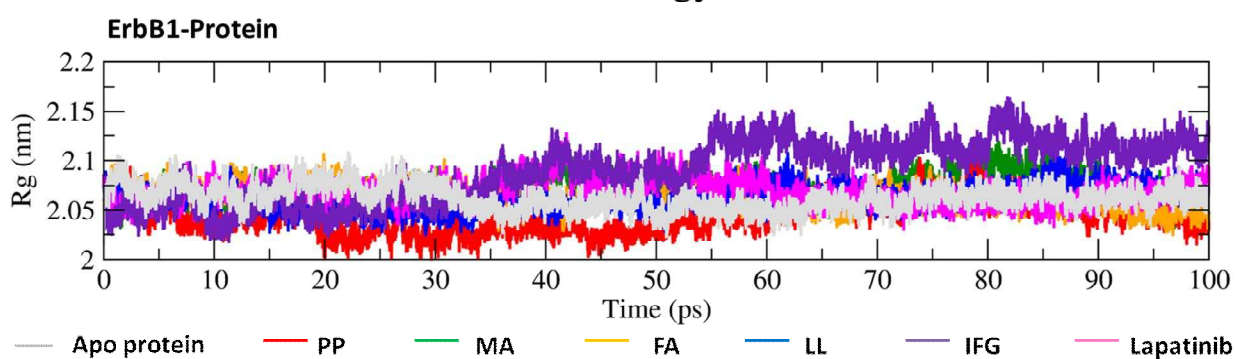


**Figure 12a**

### Radius of gyration

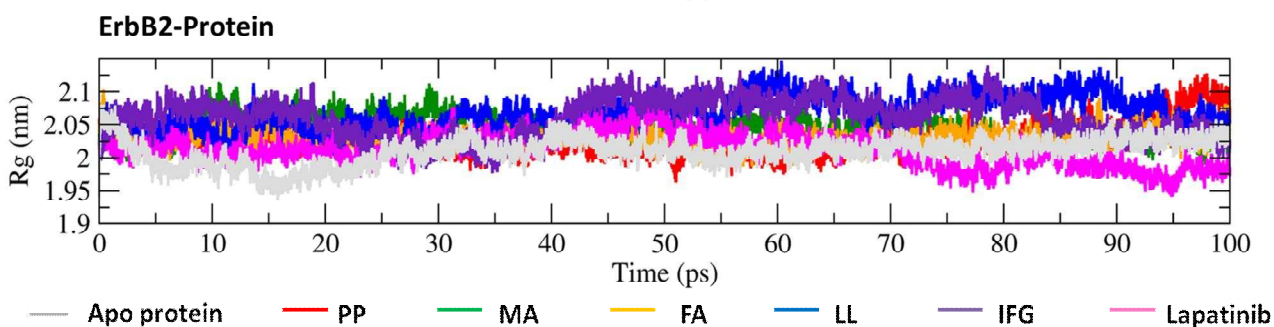


**Figure 12b**

**Figure 12:** Radius of gyration of protein-ligand complexes  
(12a) ErbB1 (12b) ErbB2

### 3.10.4. Hydrogen bond analysis

Hydrogen bond is essential in ligand binding to receptors because it affects drug specificity, metabolization and adsorption. Hydrogen bonding between a protein and the ligand provides a directionality and specificity of interaction which is an important aspect for molecular recognition. During the 100 ns simulation phase, the total number of hydrogen bonds that are present in the ErbB1-ligand and ErbB2-ligand complexes were estimated. Around 1 to 4 hydrogen bonds are observed in the reference complex, ErbB1-Lapatinib, while in complexes, ErbB1-PP, ErbB1-MA, ErbB1-FA, ErbB1-LL and ErbB1-IFG, 5, 1, 5, 6 & 6, respectively, hydrogen bonds are observed (**Figure 13a**). Around 1 to 5 hydrogen bonds are observed in the reference complex, ErbB2-Lapatinib, while in complexes, ErbB2-PP, ErbB2-MA, ErbB2-FA, ErbB2-LL and ErbB2-IFG, 7, 1, 6, 4 & 4, respectively, hydrogen bonds are observed (**Figure 13b**).

In order to validate the stability of the docked complexes, the hydrogen bonds paired between proteins and the ligands were calculated in the solvent environment and during the MD simulations. Throughout the 100 ns simulation phase, all the protein-ligand complexes show strong hydrogen bonds to the active pockets of ErbB1 and ErbB2 with least fluctuations (**Figure 13c and 13d**).

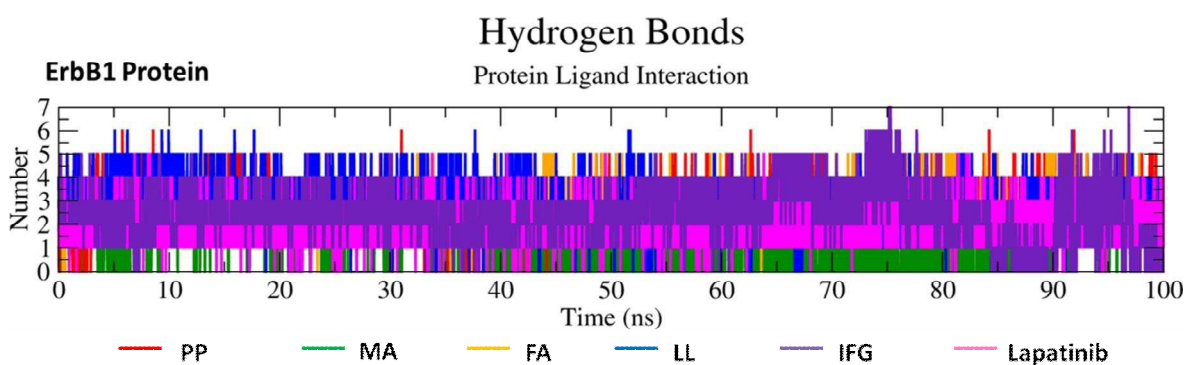


**Figure 13a**

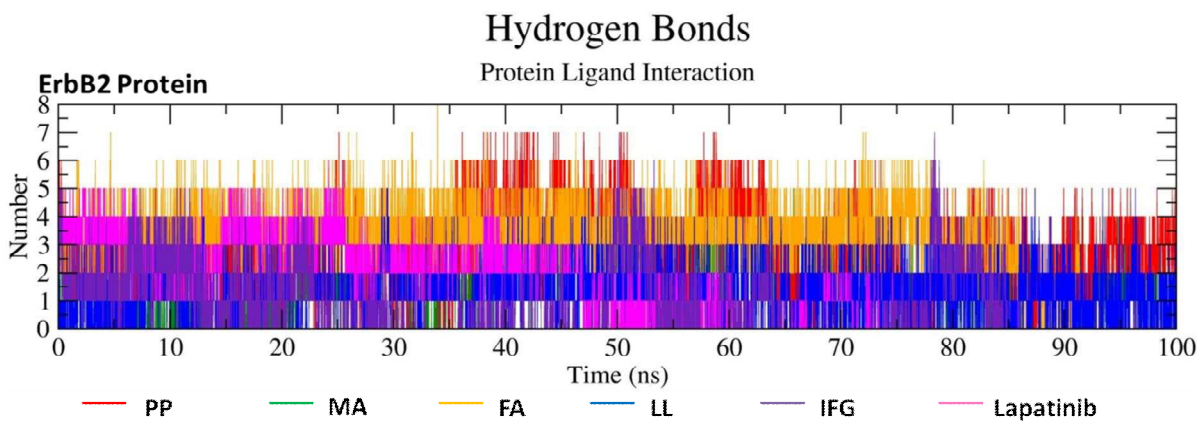


**Figure 13b**

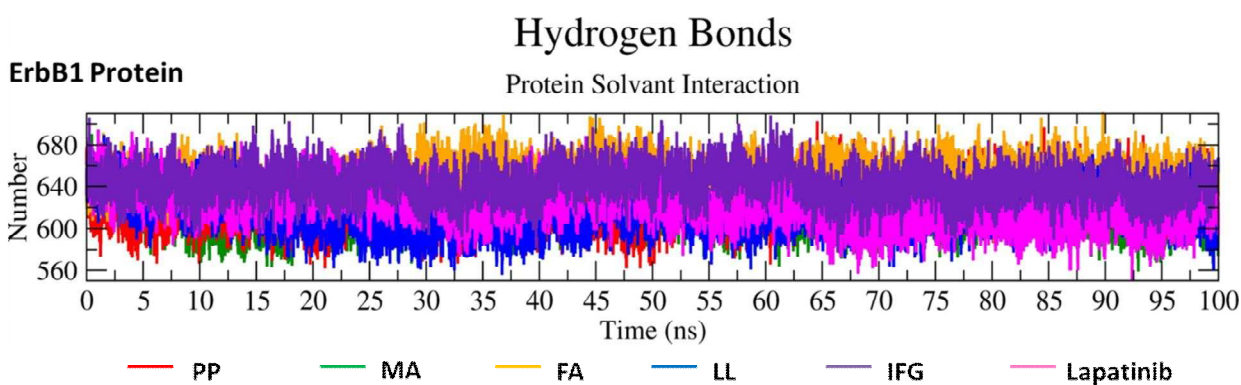


**Figure 13c**

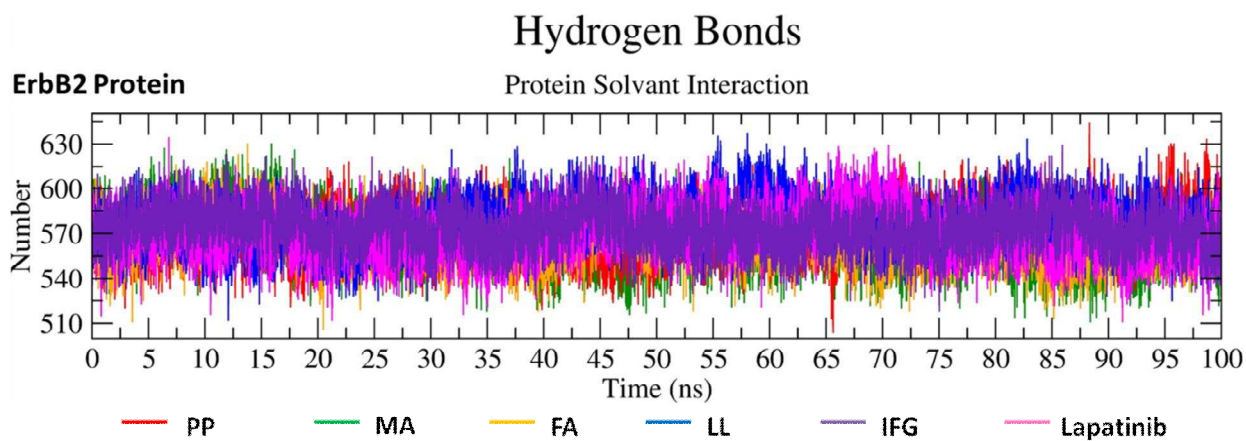


**Figure 13d**

**Figure 13:** Hydrogen bond analysis of protein-ligand complexes

(13a) Protein-ligand interaction of ErbB1-peptide complexes

(13b) Protein-ligand interaction of ErbB2-peptide complexes

(13c) Protein-solvent interaction of ErbB1-peptide complexes

### (13d) Protein-solvent interaction of ErbB2-peptide complexes

#### 3.10.5. Principal component analysis (PCA) / 2D projection of trajectory

We generated 2D projection plots to analyze the dynamics of protein-ligand complexes via principal component analysis (PCA). We used the first two principal components, PC1 and PC2, for analysis of motions. **Figure 14a** and **14b** display the projection of eigenvectors for the reference compound as well as the hit compounds for ErbB1-ligand and ErbB2-ligand complexes, respectively. In the 2D projection plot, the stable cluster is represented by the complex that occupies more space. The plot reveals that the complexes, ErbB1-PP, ErbB1-MA, and ErbB1-LL, occupy the same space, comparable to the reference, ErbB1-Lapatinib and Apo protein. Non-stable clusters of ErbB1-FA and ErbB1-IFG are seen to occupy more space. Complexes ErbB2-PP, ErbB2-MA, ErbB2-FA, ErbB2-LL and ErbB2-IFG occupy the same space, comparable to the reference, ErbB2-Lapatinib.

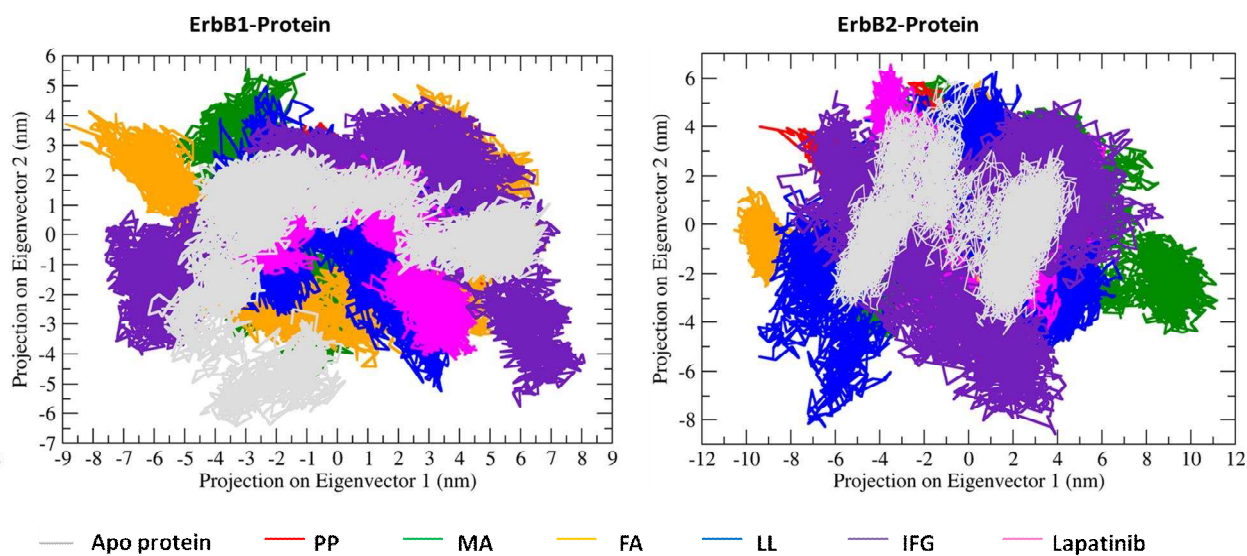


**Figure 14a**

**Figure 14b**

**Figure 14:** 2D Projection of trajectory of protein-ligand complexes

(14a) ErbB1 (14b) ErbB2

#### 3.10.6. Free energy surface / landscape

We studied the free energy surface and Gibbs free energy landscape (FEL) against the first two principal components, PC1 (Rg) and PC2 (RMSD) to visualize the energy minima

landscape of the unbound ligands to proteins (**Figure 15**). The  $\Delta G$  values are at a range above 10 kcal/mol for ErbB1 (**Figure 15a**) and ErbB2 (**Figure 15b**) protein-ligand complexes with peptides PP, MA, FA, LL, IFG, standard Lapatanib and Apo protein at RMSD ranging from 0.1 to 0.6 nm and Rg ranging from 2 to 2.16 nm. The shape and size of the minimal energy area indicate the stability of the protein and protein-ligand complexes.

The projection of their own first (PC1) and second (PC2) eigenvectors were used to examine the Gibbs energy landscape (**Figure 15**). Gibbs free energy landscape examines the path of fluctuation in the two structures for all C $\alpha$  atoms of the free ErbB1-Lapatinib, ErbB1-PP, ErbB1-MA, ErbB1-FA, ErbB1-LL and ErbB1-IFG, (**Figure 15c**) and ErbB2-Lapatinib, ErbB2-PP, ErbB2-MA, ErbB2-FA, ErbB2-LL and ErbB2-IFG, (**Figure 15d**). A  $\Delta G$  value of 13, 13.4, 13.2, 15, 14, 14.4 & 14.2 kJ/mol was obtained for ErbB1-PP, ErbB1-MA, ErbB1-FA, ErbB1-LL, ErbB1-IFG, ErbB1-Lapatinib and ErbB1-Apo protein respectively. A  $\Delta G$  value of 14.5, 13, 12.5, 13.1, 13, 13.7 & 13.7 kJ/mol was obtained for ErbB2-PP, ErbB2-MA, ErbB2-FA, ErbB2-LL, ErbB2-IFG, ErbB2-Lapatinib and ErbB2-Apo protein respectively. Lower energy is shown by a deeper blue colour in the free energy plot.

**Figure 15c** indicates ErbB1-FA and ErbB1-LL are more stable than the remaining complexes when compared to the standard, ErbB1-Lapatinib. **Figure 15d** indicates ErbB2-FA, ErbB2-LL and ErbB2-MA are more stable than the other complexes when compared to the standard, ErbB2-Lapatinib. The peptides, FA, LL, MA thus have the potential to induce ErbB1 and ErbB2 protein to enter the local energy minimal state.

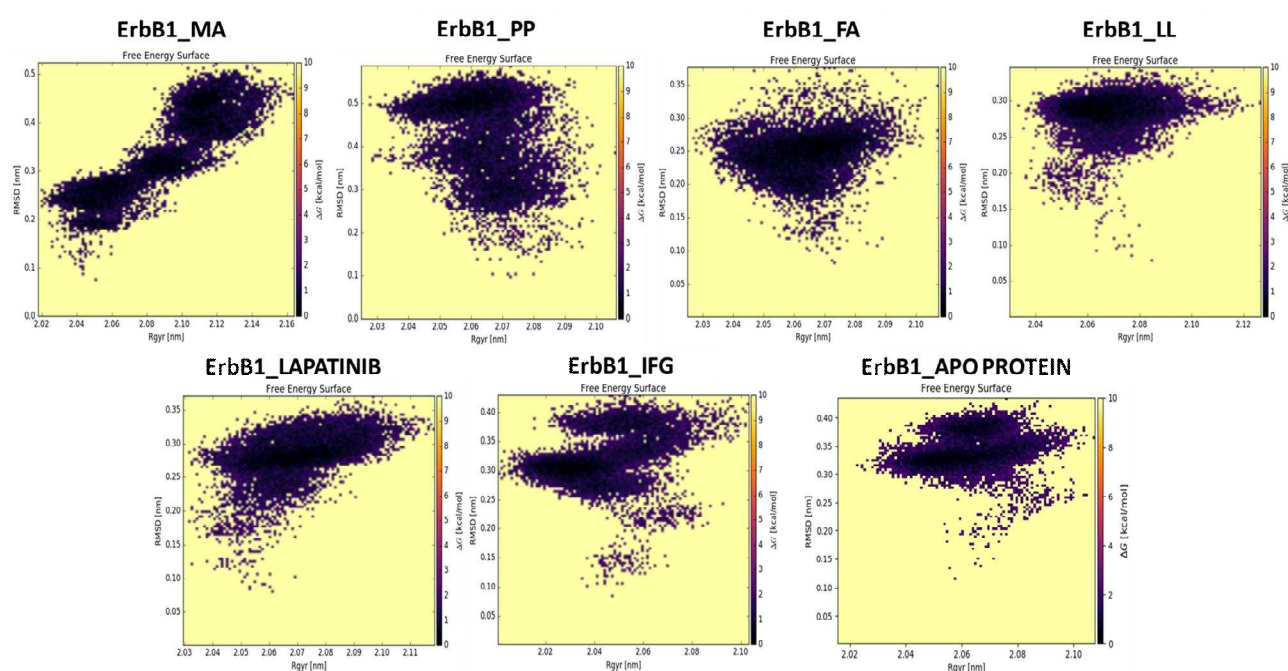


Figure 15a

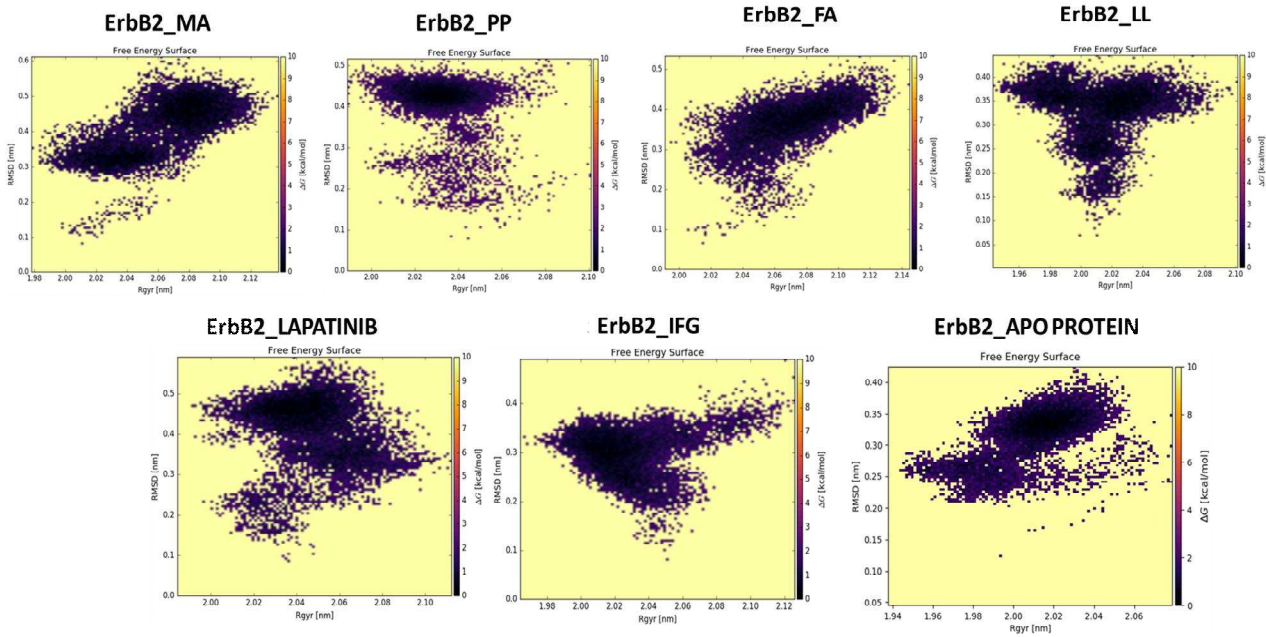


Figure 15b

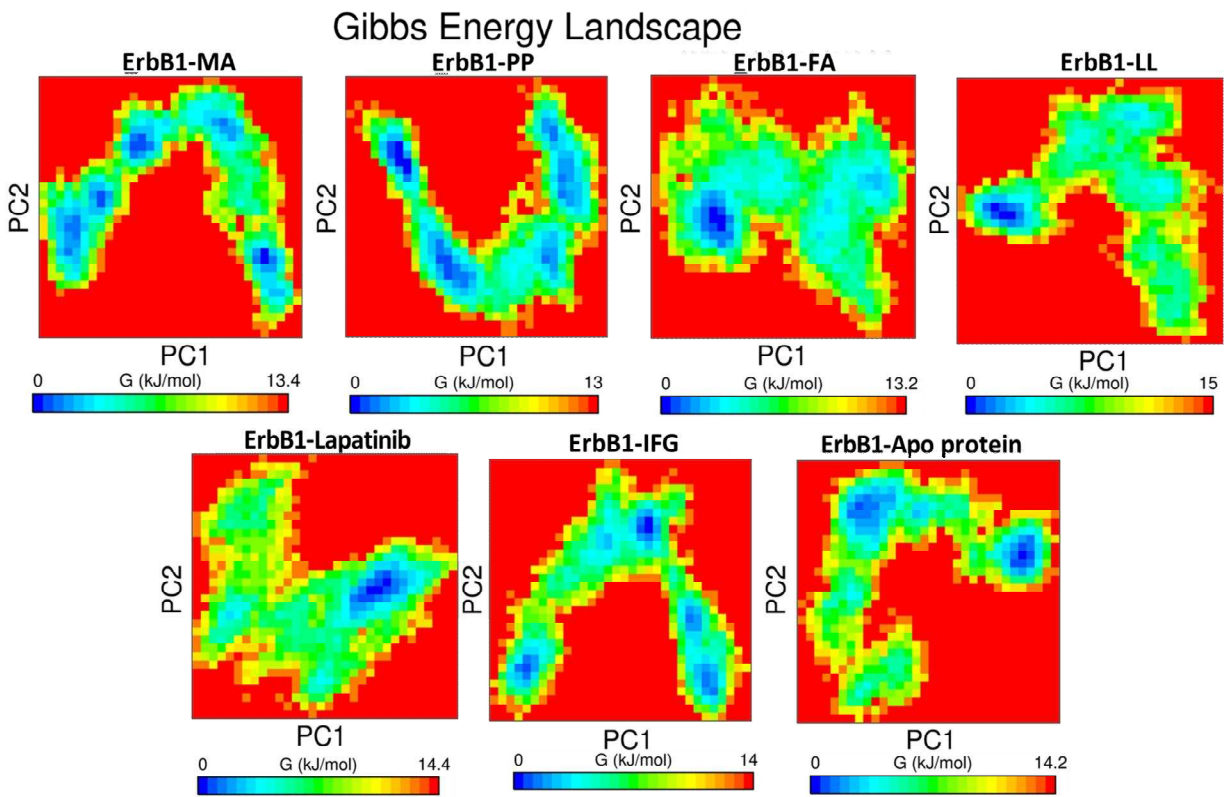
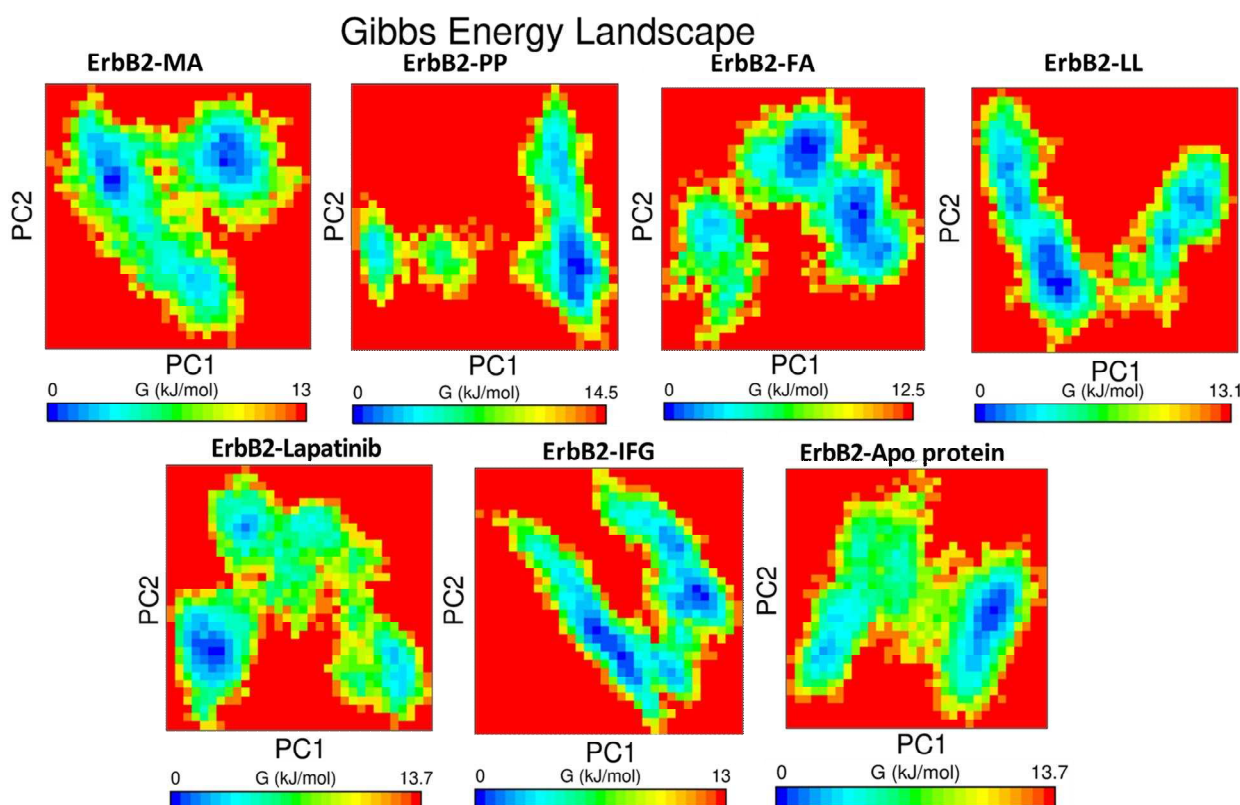


Figure 15c



**Figure 15d**

**Figure 15:** Free Energy analysis of protein-ligand complexes

(15a) Free Energy Surface analysis of ErbB1-peptide complexes

(15b) Free Energy Surface analysis of ErbB2-peptide complexes

(15c) Gibbs Free Energy Landscape analysis of ErbB1-peptide complexes

(15d) Gibbs Free Energy Landscape analysis of ErbB2-peptide complexes

### 3.10.7. Residue / secondary structure changes upon ligand binding

The secondary structure content of the protein as a function of time was also measured. The secondary structure assignments in the protein such as the  $\alpha$ -helix,  $\beta$ -sheet, turn, coil, bend,  $\beta$ -bridge and 3-helix were found to be fragmented into individual residues for each time step for 100 ns. **Figure 16** shows the secondary structures of the dimer system are mostly composed of  $\alpha$ -helix conformations from residues 50 to 300, followed by  $\beta$ -sheet, coil, turn, bend,  $\beta$ -bridge and 3-helix for all the ErbB1-ligand (**Figure 16a**) and ErbB2-ligand (**Figure 16b**) complexes.

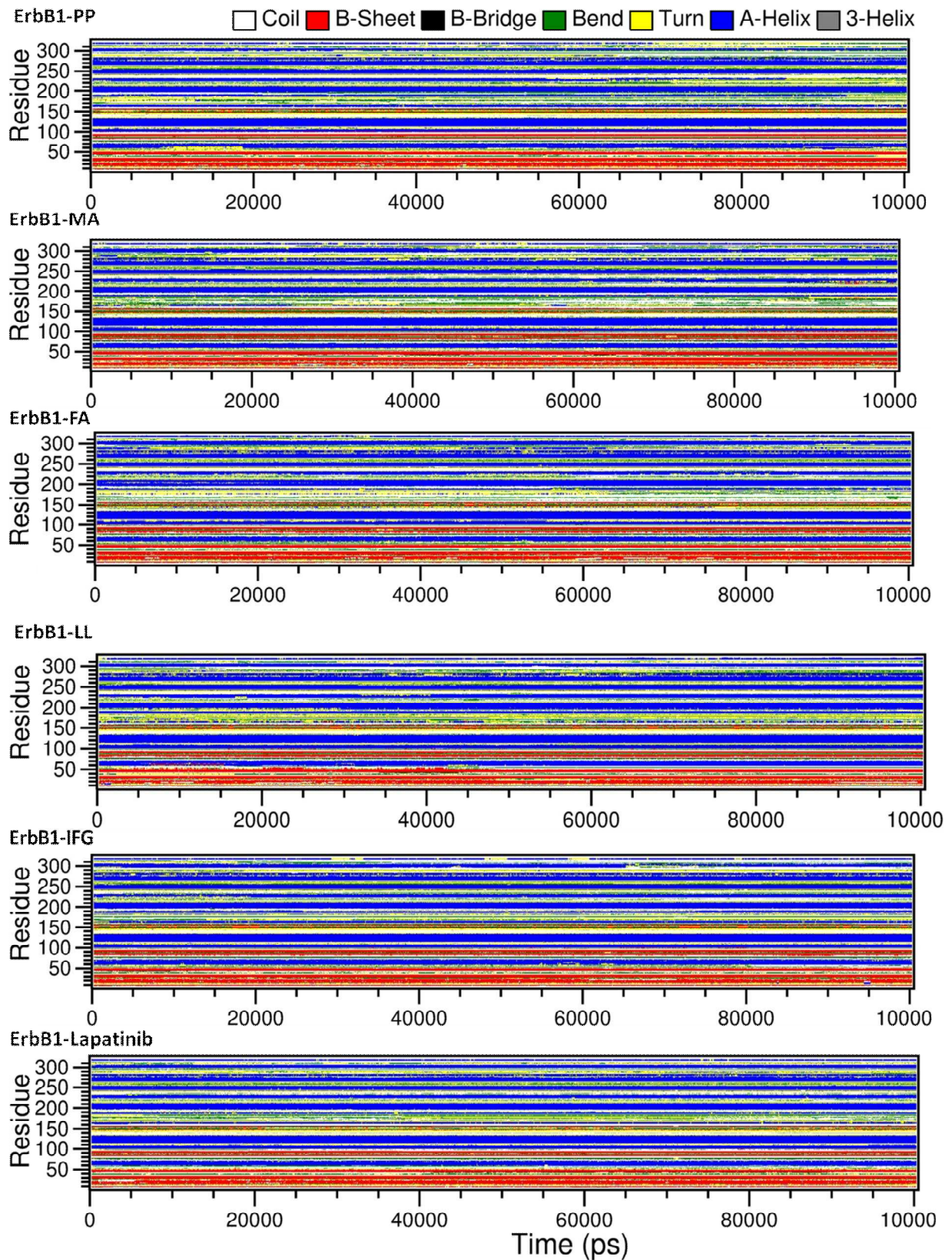
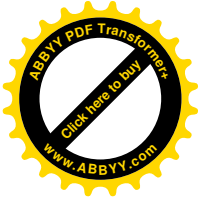
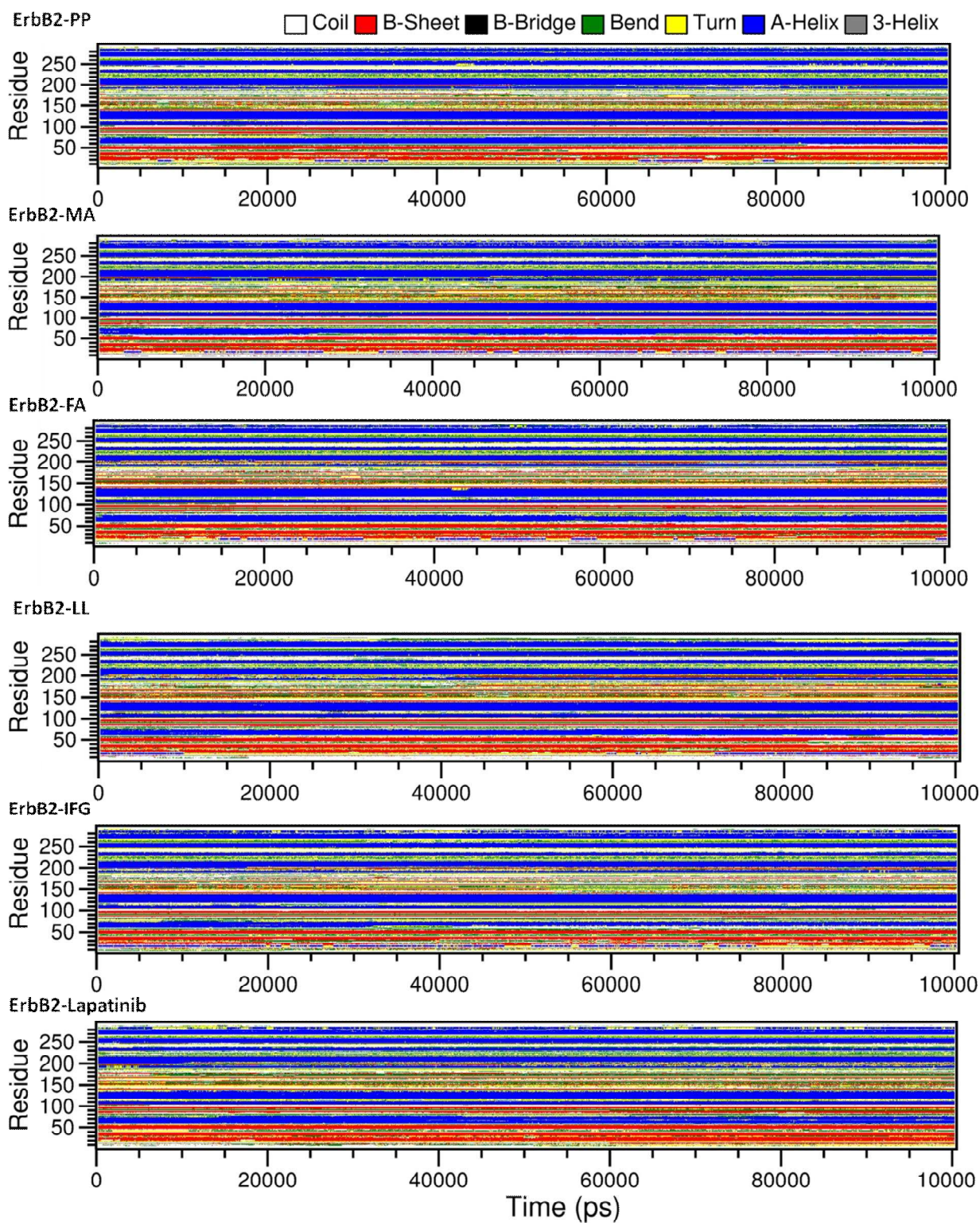


Figure 16a



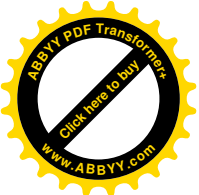


**Figure 16b**

**Figure 16:** Secondary structure analysis of protein-ligand complexes

(16a): ErbB1 (16b): ErbB2

### 3.11. MM-PBSA calculation of binding free energy



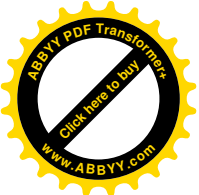
Binding free energy (BFE) calculation is an accurate strategy to prove the binding of ligands with favourable thermodynamics. It is a two-stage end-state process about the relative stability of multiple conformations of noncovalently bound receptor-ligand complexes. The data obtained on BFE of the five ligand-ErbB1 and ligand-ErbB2 complexes are shown in **Table 5**. The data reveal that Lapatinib-ErbB1 and Lapatinib-ErbB2 complexes have a high BFE. Excepting FA-ErbB2 complex all other ligand-ErbB1 and ligand-ErbB2 complexes show reasonably good BFE thus indicating good binding of ligands to the proteins. The dissociation constant  $K_d$  for the five peptide-ErbB1 and peptide-ErbB2 complexes are at a range of 1.39 to 9.89  $\mu\text{M}$  and 1.66 to 7.94  $\mu\text{M}$  respectively which is reasonably comparable with the Lapatinib ErbB1 and ErbB2 complexes.

**Table.5.** Binding free energy of selected peptides

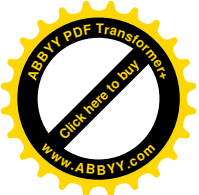
Ligand Name	Binding free energy (kJ/mol)		Dissociation Constant ( $K_d$ ) ( $\mu\text{M}$ )	
	ErbB1	ErbB2	ErbB1	ErbB2
PP	-170.996	-80.355	9.89	7.94
MA	-64.809	-86.817	4.25	5.84
FA	-31.360	-12.236	3.14	7.13
LL	-33.386	-78.533	1.39	1.66
IFG	-162.342	-173.014	3.26	4.38
Lapatinib	-233.212	-136.815	1.20	9.84

#### 4. Conclusion

Targeted chemotherapy and multi-targeting techniques are emerging as powerful techniques to circumvent the drawbacks associated with conventional chemotherapy. Natural peptides have demonstrated selective cytotoxicity to human cancer cells without affecting normal cells. In recent years, therefore, the use of peptides as therapeutic agents to treat cancer is gaining momentum. Despite the presence of certain limitations, the properties of peptides like small size, ease in production, conjugation possibilities and flexibility in their sequences have made peptides a promising drug category for targeting cancer cells. The anticancer effect of the different peptides is ascribed to several mechanisms that limit tumor growth. The advancement in bioinformatic tools and the availability of detailed structural information of ErbB1 and ErbB2 target proteins, are expected to help the discovery of multi-targeting anticancer peptides. Previous studies have not established peptides as potential



therapeutic anticancer agents against ErbB1 and ErbB2. The various peptide databases were considered to build a library with 5465 peptides. The ErbB1 and ErbB2 structures were evaluated and validated . HTVS was performed to identify the dual binders to ErbB1 and ErbB2 receptors. The study identified the 132 peptides were able to bind to both ErbB1 and ErbB2. The ADME potential of each peptide was analyzed and 30 peptides were selected for TOPKAT toxicity studies that resulted in 25 peptides. When screened for physicochemical properties 23 peptides were obtained. The binding free energy calculation of the peptide-protein complexes reveal that three peptides , namely PP , MA & IFG show binding free energies comparable to Lapatanib-protein complex. These three peptides will be taken up for further *in vitro* and *in vivo* studies to exploit them for anticancer chemotherapy.



## **Data availability statement**

All data generated and analyzed during this study are included within this article and supplementary information submitted to the journal.

## **Conflict of Interest**

The authors declare that they have no conflict of interests.

## **Funding Agency**

No funding was provided for the above mentioned research manuscript

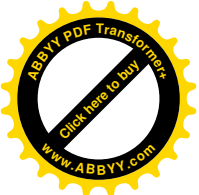
## **Ethical Approval**

Not Required

## **Acknowledgments**

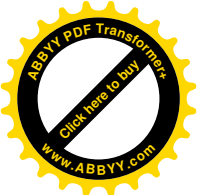
Authors expresses their immense gratitude to JSS College of Pharmacy Ooty, JSS Academy of Higher Education and Research, Mysuru, and School of Life Sciences, JSS Academy of Higher Education & Research (Ooty Campus), Longwood, Mysuru Road, Ooty-643001, Tamilnadu, India and School of Biomedical Sciences, University of Leeds, Leeds LS2 9JT, UK for the facilities offered.

**Author Contributions:** Conceptualization, methodology, software, validation, formal analysis, data curation: **Sunil Kumar Patnaik, Selvaraj Ayyamperumal, Dhananjay Jade;** writing-original draft preparation: **Sunil Kumar Patnaik, Selvaraj Ayyamperumal, Palathoti Nagarjuna, Akey Krishna Swaroop, Jupudi Srikanth;** review, editing and supervision: **Moola Joghee Nanjan, Moola Joghee Nanjan Chandrasekar, Michael A. Harrison,** **Sreenivasan** **Ponnambalam.**

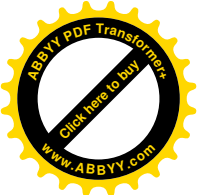


## References

- [1] Cancer n.d. <https://www.who.int/news-room/fact-sheets/detail/cancer> (accessed August 18, 2022).
- [2] Elmetwally SA, Saied KF, Eissa IH, Elkaeed EB. Design, synthesis and anticancer evaluation of thieno [2, 3-d] pyrimidine derivatives as dual EGFR/HER2 inhibitors and apoptosis inducers. *Bioorganic Chemistry* 2019;88:102944.
- [3] Siegel RL, Miller KD, Jemal A. CA: a cancer journal for clinicians. *Cancer Stat* 2016;66:7–30.
- [4] Kang TH, Mao C-P, He L, Tsai Y-C, Liu K, La V, et al. Tumor-targeted delivery of IL-2 by NKG2D leads to accumulation of antigen-specific CD8+ T cells in the tumor loci and enhanced anti-tumor effects. *PLoS One* 2012;7:e35141.
- [5] Xie M, Liu D, Yang Y. Anti-cancer peptides: Classification, mechanism of action, reconstruction and modification. *Open Biology* 2020;10:200004.
- [6] Tyagi A, Kapoor P, Kumar R, Chaudhary K, Gautam A, Raghava GPS. In silico models for designing and discovering novel anticancer peptides. *Scientific Reports* 2013;3:1–8.
- [7] Sharma SV, Bell DW, Settleman J, Haber DA. Epidermal growth factor receptor mutations in lung cancer. *Nature Reviews Cancer* 2007;7:169–81.
- [8] Wee P, Wang Z. Epidermal growth factor receptor cell proliferation signaling pathways. *Cancers* 2017;9:52.
- [9] Roskoski Jr R. The ErbB/HER family of protein-tyrosine kinases and cancer. *Pharmacological Research* 2014;79:34–74.
- [10] Stamos J, Sliwkowski MX, Eigenbrot C. Structure of the epidermal growth factor receptor kinase domain alone and in complex with a 4-anilinoquinazoline inhibitor. *Journal of Biological Chemistry* 2002;277:46265–72.
- [11] Zhang X, Gureasko J, Shen K, Cole PA, Kuriyan J. An allosteric mechanism for activation of the kinase domain of epidermal growth factor receptor. *Cell* 2006;125:1137–49.
- [12] Wang X, Xu L, Lao Y, Zhang H, Xu H. Natural products targeting EGFR signaling pathways as potential anticancer drugs. *Current Protein and Peptide Science* 2018;19:380–8.
- [13] Grunwald V, Hidalgo M. Developing inhibitors of the epidermal growth factor receptor for cancer treatment. *Journal of the National Cancer Institute* 2003;95:851–67.
- [14] Patnaik SK, Chandrasekar MJN, Nagarjuna P, Ramamurthi D, Swaroop AK. Targeting of ErbB1, ErbB2, and their Dual Targeting Using Small Molecules and Natural Peptides: Blocking EGFR Cell Signaling Pathways in Cancer: A Mini Review. *Mini Reviews in Medicinal Chemistry* 2022.
- [15] Woodburn JR. The epidermal growth factor receptor and its inhibition in cancer therapy. *Pharmacology & Therapeutics* 1999;82:241–50.
- [16] Sun M, Jia J, Sun H, Wang F. Design and synthesis of a novel class EGFR/HER2 dual inhibitors containing tricyclic oxazine fused quinazolines scaffold. *Bioorganic & Medicinal Chemistry Letters* 2020;30:127045.
- [17] Normanno N, De Luca A, Bianco C, Strizzi L, Mancino M, Maiello MR, et al. Epidermal growth factor receptor (EGFR) signaling in cancer. *Gene* 2006;366:2–16.
- [18] Tebbutt N, Pedersen MW, Johns TG. Targeting the ERBB family in cancer: couples therapy. *Nature Reviews Cancer* 2013;13:663–73.
- [19] Sever B, Altıntop MD, Radwan MO, Özdemir A, Otsuka M, Fujita M, et al. Design, synthesis and biological evaluation of a new series of thiazolyl-pyrazolines as dual



- EGFR and HER2 inhibitors. *European Journal of Medicinal Chemistry* 2019;182:111648.
- [20] Wang Y. Breast cancer metastasis driven by ErbB2 and 14-3-3 $\xi$ : A division of labor. *Cell Adhesion & Migration* 2010;4:7–9.
- [21] Yang L, Li Y, Bhattacharya A, Zhang Y. Dual inhibition of ErbB1 and ErbB2 in cancer by recombinant human prolidase mutant hPEPD-G278D. *Oncotarget* 2016;7:42340.
- [22] Hu J-B, Dong M-J, Zhang J. A holistic in silico approach to develop novel inhibitors targeting ErbB1 and ErbB2 kinases. *Tropical Journal of Pharmaceutical Research* 2016;15:231–9.
- [23] Deng Y, Li J. Rational Optimization of Tumor Suppressor-Derived Peptide Inhibitor Selectivity between Oncogene Tyrosine Kinases ErbB1 and ErbB2. *Archiv Der Pharmazie* 2017;350:1700181.
- [24] Ryan Q, Ibrahim A, Cohen MH, Johnson J, Ko C, Sridhara R, et al. FDA drug approval summary: lapatinib in combination with capecitabine for previously treated metastatic breast cancer that overexpresses HER-2. *The Oncologist* 2008;13:1114–9.
- [25] Liu L, Greger J, Shi H, Liu Y, Greshock J, Annan R, et al. Novel mechanism of lapatinib resistance in HER2-positive breast tumor cells: activation of AXL. *Cancer Research* 2009;69:6871–8.
- [26] Marqus S, Pirogova E, Piva TJ. Evaluation of the use of therapeutic peptides for cancer treatment. *Journal of Biomedical Science* 2017;24:1–15.
- [27] Lau JL, Dunn MK. Therapeutic peptides: Historical perspectives, current development trends, and future directions. *Bioorganic & Medicinal Chemistry* 2018;26:2700–7.
- [28] Lee S, Xie J, Chen X. Peptides and peptide hormones for molecular imaging and disease diagnosis. *Chemical Reviews* 2010;110:3087–111.
- [29] Chen K, Sun X, Niu G, Ma Y, Yap L-P, Hui X, et al. Evaluation of <sup>64</sup>Cu labeled GX1: a phage display peptide probe for PET imaging of tumor vasculature. *Molecular Imaging and Biology* 2012;14:96–105.
- [30] Ganesan A. The impact of natural products upon modern drug discovery. *Current Opinion in Chemical Biology* 2008;12:306–17.
- [31] Quinn RJ, Carroll AR, Pham NB, Baron P, Palframan ME, Suraweera L, et al. Developing a drug-like natural product library. *Journal of Natural Products* 2008;71:464–8.
- [32] Huan Y, Kong Q, Mou H, Yi H. Antimicrobial peptides: classification, design, application and research progress in multiple fields. *Frontiers in Microbiology* 2020:2559.
- [33] Wu D, Gao Y, Qi Y, Chen L, Ma Y, Li Y. Peptide-based cancer therapy: opportunity and challenge. *Cancer Letters* 2014;351:13–22.
- [34] Farkhani SM, Valizadeh A, Karami H, Mohammadi S, Sohrabi N, Badrzadeh F. Cell penetrating peptides: efficient vectors for delivery of nanoparticles, nanocarriers, therapeutic and diagnostic molecules. *Peptides* 2014;57:78–94.
- [35] Xiao Y-F, Jie M-M, Li B-S, Hu C-J, Xie R, Tang B, et al. Peptide-based treatment: a promising cancer therapy. *Journal of Immunology Research* 2015;2015.
- [36] Guardiola S, Díaz-Lobo M, Seco J, García J, Nevola L, Giralt E. Peptides targeting EGF block the EGF–EGFR interaction. *ChemBioChem* 2016;17:702–11.
- [37] Wood ER, Truesdale AT, McDonald OB, Yuan D, Hassell A, Dickerson SH, et al. A unique structure for epidermal growth factor receptor bound to GW572016 (Lapatinib): relationships among protein conformation, inhibitor off-rate, and receptor activity in tumor cells. *Cancer Res* 2004;64:6652–9. <https://doi.org/10.1158/0008-5472.CAN-04-1168>.



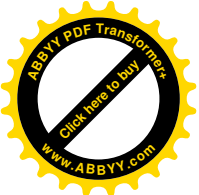
- [38] Aertgeerts K, Skene R, Yano J, Sang B-C, Zou H, Snell G, et al. Structural analysis of the mechanism of inhibition and allosteric activation of the kinase domain of HER2 protein. *Journal of Biological Chemistry* 2011;286:18756–65.
- [39] Vanommeslaeghe K, Hatcher E, Acharya C, Kundu S, Zhong S, Shim J, et al. CHARMM general force field: A force field for drug-like molecules compatible with the CHARMM all-atom additive biological force fields. *Journal of Computational Chemistry* 2010;31:671–90.
- [40] Prilusky J, Felder CE, Zeev-Ben-Mordehai T, Rydberg EH, Man O, Beckmann JS, et al. FoldIndex\copyright: a simple tool to predict whether a given protein sequence is intrinsically unfolded. *Bioinformatics* 2005;21:3435–8.
- [41] Shi G, Kang X, Dong F, Liu Y, Zhu N, Hu Y, et al. DRAMP 3.0: an enhanced comprehensive data repository of antimicrobial peptides. *Nucleic Acids Research* 2022;50:D488–96.
- [42] Tyagi A, Tuknait A, Anand P, Gupta S, Sharma M, Mathur D, et al. CancerPPD: a database of anticancer peptides and proteins. *Nucleic Acids Research* 2015;43:D837–43.
- [43] Minkiewicz P, Dziuba J, Iwaniak A, Dziuba M, Darewicz M. BIOPEP database and other programs for processing bioactive peptide sequences. *Journal of AOAC International* 2008;91:965–80.
- [44] Wang J, Yin T, Xiao X, He D, Xue Z, Jiang X, et al. StraPep: a structure database of bioactive peptides. *Database* 2018;2018.
- [45] Kapoor P, Singh H, Gautam A, Chaudhary K, Kumar R, Raghava GP. TumorHoPe: a database of tumor homing peptides. *PLoS One* 2012;7:e35187.
- [46] Singh S, Chaudhary K, Dhanda SK, Bhalla S, Usmani SS, Gautam A, et al. SATPdb: a database of structurally annotated therapeutic peptides. *Nucleic Acids Research* 2016;44:D1119–26.
- [47] Agrawal P, Bhalla S, Usmani SS, Singh S, Chaudhary K, Raghava GP, et al. CPPsite 2.0: a repository of experimentally validated cell-penetrating peptides. *Nucleic Acids Research* 2016;44:D1098–103.
- [48] Gautam A, Singh H, Tyagi A, Chaudhary K, Kumar R, Kapoor P, et al. CPPsite: a curated database of cell penetrating peptides. *Database* 2012;2012.
- [49] Ayyamperumal S, Jade D, Tallapaneni V, Mohan S, Barge S, Moola Joghee N, et al. Structural and functional analysis of Chitinase-IV of *Brassica juncea*: molecular modeling and dynamic simulation study. *Journal of Biomolecular Structure and Dynamics* 2022;40:1830–42.
- [50] Kumar R, Jade D, Gupta D. A novel identification approach for discovery of 5-HydroxyTryptamine 2A antagonists: combination of 2D/3D similarity screening, molecular docking and molecular dynamics. *Journal of Biomolecular Structure and Dynamics* 2019;37:931–43.
- [51] Rao SN, Head MS, Kulkarni A, LaLonde JM. Validation studies of the site-directed docking program LibDock. *Journal of Chemical Information and Modeling* 2007;47:2159–71.
- [52] Hodgson J. ADMET—turning chemicals into drugs. *Nature Biotechnology* 2001;19:722–6.
- [53] Egan WJ, Merz KM, Baldwin JJ. Prediction of drug absorption using multivariate statistics. *Journal of Medicinal Chemistry* 2000;43:3867–77.
- [54] Cheng A, Merz KM. Prediction of aqueous solubility of a diverse set of compounds using quantitative structure- property relationships. *Journal of Medicinal Chemistry* 2003;46:3572–80.



- [55] Susnow RG, Dixon SL. Use of robust classification techniques for the prediction of human cytochrome P450 2D6 inhibition. *Journal of Chemical Information and Computer Sciences* 2003;43:1308–15.
- [56] Cheng A, Dixon SL. In silico models for the prediction of dose-dependent human hepatotoxicity. *Journal of Computer-Aided Molecular Design* 2003;17:811–23.
- [57] Dixon SL, Merz KM. One-dimensional molecular representations and similarity calculations: methodology and validation. *Journal of Medicinal Chemistry* 2001;44:3795–809.
- [58] Lipinski CA, Lombardo F, Dominy BW, Feeney PJ. Experimental and computational approaches to estimate solubility and permeability in drug discovery and development settings. *Advanced Drug Delivery Reviews* 2012;64:4–17.
- [59] Jhoti H, Williams G, Rees DC, Murray CW. The 'rule of three' for fragment-based drug discovery: where are we now? *Nature Reviews Drug Discovery* 2013;12:644–644.
- [60] Abraham MJ, Murtola T, Schulz R, Páll S, Smith JC, Hess B, et al. GROMACS: High performance molecular simulations through multi-level parallelism from laptops to supercomputers. *SoftwareX* 2015;1:19–25.
- [61] Schmid N, Eichenberger AP, Choutko A, Riniker S, Winger M, Mark AE, et al. Definition and testing of the GROMOS force-field versions 54A7 and 54B7. *European Biophysics Journal* 2011;40:843–56.
- [62] Schüttelkopf AW, Van Aalten DM. PRODRG: a tool for high-throughput crystallography of protein–ligand complexes. *Acta Crystallographica Section D: Biological Crystallography* 2004;60:1355–63.
- [63] Ayyamperumal S, Jade D, Tallapaneni V, Chandrasekar MJN, Nanjan MJ. In silico screening of FDA approved drugs against ACE2 receptor: potential therapeutics to inhibit the entry of SARS-CoV-2 to human cells. *Journal of Biomolecular Structure and Dynamics* 2021:1–12.
- [64] Jade DD, Pandey R, Kumar R, Gupta D. Ligand-based pharmacophore modeling of TNF- $\alpha$  to design novel inhibitors using virtual screening and molecular dynamics. *Journal of Biomolecular Structure and Dynamics* 2022;40:1702–18.
- [65] Barge S, Jade D, Ayyamperumal S, Manna P, Borah J, Nanjan CMJ, et al. Potential inhibitors for FKBP51: an in silico study using virtual screening, molecular docking and molecular dynamics simulation. *Journal of Biomolecular Structure and Dynamics* 2022;40:13799–811.
- [66] Jade D, Ayyamperumal S, Tallapaneni V, Nanjan CMJ, Barge S, Mohan S, et al. Virtual high throughput screening: Potential inhibitors for SARS-CoV-2 PLPRO and 3CLPRO proteases. *European Journal of Pharmacology* 2021;901:174082.
- [67] Genheden S, Ryde U. The MM/PBSA and MM/GBSA methods to estimate ligand-binding affinities. *Expert Opinion on Drug Discovery* 2015;10:449–61.
- [68] Kumari R, Kumar R, Consortium OSDD, Lynn A. g\_mmpbsa □ A GROMACS tool for high-throughput MM-PBSA calculations. *Journal of Chemical Information and Modeling* 2014;54:1951–62.
- [69] Mohan S, Jade D, Gupta S, Ayyamperumal S, Chandrasekar MN, Nanjan MJ. Virtual high-throughput screening: potential inhibitors for the mycobacterial  $\alpha$ -subunit of tryptophan synthase. *Molecular Simulation* 2022;48:342–53.
- [70] Schrödinger, R. (2019). Release 2019-4: LigPrep. Schrödinger, LLC.
- [71] Chen K, Conti PS. Target-specific delivery of peptide-based probes for PET imaging. *Advanced Drug Delivery Reviews* 2010;62:1005–22.
- [72] Buonfiglio R, Recanatini M, Masetti M. Protein flexibility in drug discovery: from theory to computation. *ChemMedChem* 2015;10:1141–8.







## Virtual high throughput screening of natural peptides against ErbB1 and ErbB2 to identify potential inhibitors for cancer chemotherapy

Sunil Kumar Patnaik<sup>1</sup>, Selvaraj Ayyamperumal<sup>1,7</sup>, Dhananjay Jade<sup>2</sup>, Nagarjuna Palathoti<sup>1</sup>,  
Krishna Swaroop Akey<sup>1</sup>, Srikanth Jupudi<sup>1</sup>, Michael A. Harrison<sup>2</sup>, Sreenivasan  
Ponnambalam<sup>3</sup>, MJ Nanjan MJ<sup>5,6</sup>, MJN Chandrasekar<sup>\*1,4</sup>

<sup>1</sup>Department of Pharmaceutical Chemistry, JSS College of Pharmacy, JSS Academy of Higher Education and Research, Ooty, 643001, Tamilnadu, India.

<sup>2</sup>School of Biomedical Sciences, University of Leeds, Leeds LS2 9JT, UK.

<sup>3</sup>School of Molecular & Cellular Biology, University of Leeds, UK

<sup>4</sup>School of Life Sciences, JSS Academy of Higher Education & Research (Ooty Campus), Longwood, Mysuru Road, Ooty-643001, Tamilnadu, India

<sup>5</sup>Research Director(Retd.), JSS College of Pharmacy, JSS Academy of Higher Education and Research, Ooty, 643001, Tamilnadu, India.

<sup>6</sup>Present Address: Masi Educational Consultants, 128, Vijayanagar Palace Road, Ooty-643001, The Nilgiris, Tamilnadu, India

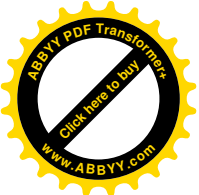
<sup>7</sup>Present Address: IMol Polish Academy of Sciences, M. Flisa 6, 02-247 Warsaw, Poland

### Corresponding Authors:

Prof. MJN Chandrasekar, Ph.D

Email: [ncsekar@jssuni.edu.in](mailto:ncsekar@jssuni.edu.in)

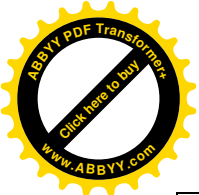
ORCID ID- 0000-0001-6420-9119



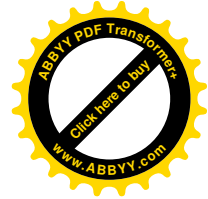
### Supplementary Information

**Supplementary Table 1: ADME properties for the 30 peptides**

S.No	Compound	Amino acid sequence	Solubility Level	EXT CYP2D6 Prediction	EXT Hepatotoxic Prediction	Absorption Level	ADME EXT PPB Prediction	AlogPP98
1.	<b>C15H27N3O4S</b>	<b>VMP</b>	Optimal	FALSE	FALSE	Good	FALSE	-0.106
2.	<b>C16H27N3O4</b>	<b>PLP</b>	Optimal	FALSE	FALSE	Good	FALSE	0.499
3.	<b>C17H25N3O4</b>	<b>GLF</b>	Optimal	FALSE	FALSE	Good	FALSE	0.709
4.	<b>C17H25N3O4</b>	<b>GFL</b>	Optimal	FALSE	FALSE	Good	FALSE	0.709
5.	<b>C7H12N2O3</b>	<b>GP</b>	Too Soluble	FALSE	FALSE	Good	FALSE	-1.079
6.	<b>C12H19N3O4</b>	<b>PGP</b>	Optimal	FALSE	FALSE	Moderate	FALSE	-1.217
7.	<b>C13H18N2O4</b>	<b>FT</b>	Optimal	FALSE	FALSE	Good	FALSE	-0.093
8.	<b>C11H14N2O4</b>	<b>YG</b>	Optimal	FALSE	FALSE	Good	FALSE	-0.309
9.	<b>C13H23N3O4</b>	<b>PLG</b>	Optimal	FALSE	FALSE	Good	FALSE	-0.303
10.	<b>C20H30N4O5</b>	<b>PYK</b>	Optimal	FALSE	FALSE	Good	FALSE	-0.552
11.	<b>C10H16N2O3</b>	<b>PP</b>	Optimal	FALSE	FALSE	Good	FALSE	-0.276
12.	<b>C10H18N2O3S</b>	<b>MP</b>	Optimal	FALSE	FALSE	Good	FALSE	-0.493
13.	<b>C8H16N2O3</b>	<b>VA</b>	Optimal	FALSE	FALSE	Good	FALSE	-0.295
14.	<b>C8H16N2O3S</b>	<b>MA</b>	Too Soluble	FALSE	FALSE	Good	FALSE	-0.811
15.	<b>C9H19N3O3</b>	<b>KA</b>	Too Soluble	FALSE	FALSE	Moderate	FALSE	-1.218
16.	<b>C9H18N2O3</b>	<b>LA</b>	Optimal	FALSE	FALSE	Good	FALSE	0.093
17.	<b>C12H16N2O3</b>	<b>FA</b>	Optimal	FALSE	FALSE	Good	FALSE	0.417
18.	<b>C8H14N2O3</b>	<b>PA</b>	Optimal	FALSE	FALSE	Good	FALSE	-0.82
19.	<b>C8H14N2O3</b>	<b>AP</b>	Optimal	FALSE	FALSE	Good	FALSE	-0.594
20.	<b>C11H20N2O3</b>	<b>LP</b>	Optimal	FALSE	FALSE	Good	FALSE	0.411
21.	<b>C10H18N2O3</b>	<b>VP</b>	Optimal	FALSE	FALSE	Good	FALSE	0.023
22.	<b>C12H24N2O3</b>	<b>LL</b>	Optimal	FALSE	FALSE	Good	FALSE	1.325
23.	<b>C10H20N2O3</b>	<b>VV</b>	Optimal	FALSE	FALSE	Good	FALSE	0.548

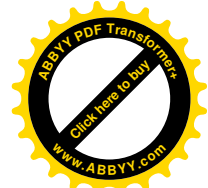


24.	<b>satpdb10938</b>	<b>YGL</b>	Optimal	FALSE	FALSE	Moderate	FALSE	-0.516
25.	<b>satpdb11295</b>	<b>IVF</b>	Optimal	FALSE	FALSE	Good	FALSE	1.121
26.	<b>satpdb13141</b>	<b>FG</b>	Too Soluble	FALSE	FALSE	Good	FALSE	-1.05
27.	<b>satpdb13181</b>	<b>LY</b>	Optimal	FALSE	FALSE	Good	FALSE	0.424
28.	<b>satpdb14624</b>	<b>IPF</b>	Optimal	FALSE	FALSE	Good	FALSE	0.574
29.	<b>satpdb20875</b>	<b>IFG</b>	Optimal	FALSE	FALSE	Good	FALSE	-0.206
30.	<b>satpdb22674</b>	<b>FL</b>	Optimal	FALSE	FALSE	Good	FALSE	0.571

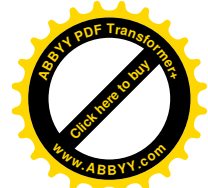


**Supplementary Table 2: TOPKAT properties for the 25 peptides**

S.No	Peptides	Mouse Male	Mouse Female	Rat Male	Rat Female	FDA mouse Female	FDA Mouse Male	FDA Rat Female	FDA Rat Male	Carcinogenic TD50 Mouse (mg/kg_body_weight/day)	Carcinogenic TD50 Rat (mg/kg_body_weight/day)	DTP
1.	<b>VMP</b>	Non-Carcinogen	Non-Carcinogen	Non-Carcinogen	Non-Carcinogen	Non-Carcinogen	Non-Carcinogen	Non-Carcinogen	Non-Carcinogen	65.1778	0.632054	Non-Toxic
2.	<b>PLP</b>	Non-Carcinogen	Non-Carcinogen	Non-Carcinogen	Non-Carcinogen	Non-Carcinogen	Non-Carcinogen	Non-Carcinogen	Non-Carcinogen	40.4326	1.82649	Non-Toxic
3.	<b>GLF</b>	Non-Carcinogen	Non-Carcinogen	Non-Carcinogen	Non-Carcinogen	Non-Carcinogen	Non-Carcinogen	Non-Carcinogen	Non-Carcinogen	339.021	207.253	Non-Toxic
4.	<b>GFL</b>	Non-Carcinogen	Non-Carcinogen	Non-Carcinogen	Non-Carcinogen	Non-Carcinogen	Non-Carcinogen	Non-Carcinogen	Non-Carcinogen	339.021	207.253	Non-Toxic
5.	<b>PGP</b>	Non-Carcinogen	Non-Carcinogen	Non-Carcinogen	Non-Carcinogen	Non-Carcinogen	Non-Carcinogen	Non-Carcinogen	Non-Carcinogen	60.5667	1.99387	Non-Toxic
6.	<b>FT</b>	Non-Carcinogen	Non-Carcinogen	Non-Carcinogen	Non-Carcinogen	Non-Carcinogen	Non-Carcinogen	Non-Carcinogen	Non-Carcinogen	275.928	52.4926	Non-Toxic
7.	<b>PLG</b>	Non-Carcinogen	Non-Carcinogen	Non-Carcinogen	Non-Carcinogen	Non-Carcinogen	Single-Carcinogen	Non-Carcinogen	Non-Carcinogen	86.5962	11.7618	Non-Toxic
8.	<b>PYK</b>	Non-Carcinogen	Non-Carcinogen	Non-Carcinogen	Non-Carcinogen	Non-Carcinogen	Non-Carcinogen	Non-Carcinogen	Non-Carcinogen	25.5396	0.35835	Non-Toxic
9.	<b>PP</b>	Non-Carcinogen	Non-Carcinogen	Non-Carcinogen	Non-Carcinogen	Non-Carcinogen	Non-Carcinogen	Non-Carcinogen	Non-Carcinogen	86.1911	0.902526	Non-Toxic



10.	<b>MP</b>	Non-Carcinogen	Non-Carcinogen	Non-Carcinogen	Non-Carcinogen	Non-Carcinogen	Non-Carcinogen	Single-Carcinogen	Non-Carcinogen	80.7153	0.569773	Non-Toxic
11.	<b>VA</b>	Non-Carcinogen	Non-Carcinogen	Non-Carcinogen	Non-Carcinogen	Non-Carcinogen	Multi-Carcinogen	Non-Carcinogen	Non-Carcinogen	120.901	8.77892	Non-Toxic
12.	<b>MA</b>	Non-Carcinogen	Non-Carcinogen	Non-Carcinogen	Non-Carcinogen	Non-Carcinogen	Single-Carcinogen	Non-Carcinogen	Non-Carcinogen	120.123	1.9077	Non-Toxic
13.	<b>KA</b>	Non-Carcinogen	Non-Carcinogen	Non-Carcinogen	Non-Carcinogen	Non-Carcinogen	Single-Carcinogen	Single-Carcinogen	Non-Carcinogen	123.011	107.022	Non-Toxic
14.	<b>LA</b>	Non-Carcinogen	Non-Carcinogen	Non-Carcinogen	Non-Carcinogen	Non-Carcinogen	Multi-Carcinogen	Single-Carcinogen	Non-Carcinogen	81.1875	7.21302	Non-Toxic
15.	<b>FA</b>	Non-Carcinogen	Non-Carcinogen	Non-Carcinogen	Non-Carcinogen	Non-Carcinogen	Non-Carcinogen	Non-Carcinogen	Non-Carcinogen	300.373	49.1748	Non-Toxic
16.	<b>PA</b>	Non-Carcinogen	Non-Carcinogen	Non-Carcinogen	Non-Carcinogen	Non-Carcinogen	Non-Carcinogen	Single-Carcinogen	Non-Carcinogen	78.3312	1.13421	Non-Toxic
17.	<b>AP</b>	Non-Carcinogen	Non-Carcinogen	Non-Carcinogen	Non-Carcinogen	Non-Carcinogen	Single-Carcinogen	Non-Carcinogen	Non-Carcinogen	113.517	6.73669	Non-Toxic
18.	<b>LP</b>	Non-Carcinogen	Non-Carcinogen	Non-Carcinogen	Non-Carcinogen	Non-Carcinogen	Non-Carcinogen	Single-Carcinogen	Non-Carcinogen	50.6097	1.38212	Non-Toxic
19.	<b>VP</b>	Non-Carcinogen	Non-Carcinogen	Non-Carcinogen	Non-Carcinogen	Non-Carcinogen	Non-Carcinogen	Single-Carcinogen	Non-Carcinogen	76.0235	1.31779	Non-Toxic
20.	<b>LL</b>	Non-Carcinogen	Non-Carcinogen	Non-Carcinogen	Carcinogen	Non-Carcinogen	Single-Carcinogen	Non-Carcinogen	Non-Carcinogen	82.5517	7.60163	Non-Toxic
21.	<b>VV</b>	Non-Carcinogen	Non-Carcinogen	Non-Carcinogen	Non-Carcinogen	Non-Carcinogen	Multi-Carcinogen	Non-Carcinogen	Non-Carcinogen	117.175	8.93959	Non-Toxic



22.	<b>IVF</b>	Non-Carcinogen	Non-Carcinogen	Non-Carcinogen	Non-Carcinogen	Non-Carcinogen	Non-Carcinogen	Non-Carcinogen	Non-Carcinogen	114.068	29.7278	Non-Toxic
23.	<b>IPF</b>	Non-Carcinogen	Non-Carcinogen	Non-Carcinogen	Non-Carcinogen	Non-Carcinogen	Non-Carcinogen	Non-Carcinogen	Non-Carcinogen	177.702	5.3485	Non-Toxic
24.	<b>IFG</b>	Non-Carcinogen	Non-Carcinogen	Non-Carcinogen	Non-Carcinogen	Non-Carcinogen	Non-Carcinogen	Non-Carcinogen	Non-Carcinogen	142.385	111.145	Non-Toxic
25.	<b>FL</b>	Non-Carcinogen	Non-Carcinogen	Non-Carcinogen	Carcinogen	Non-Carcinogen	Multi-Carcinogen	Single-Carcinogen	Non-Carcinogen	10.9006	2.74343	Non-Toxic

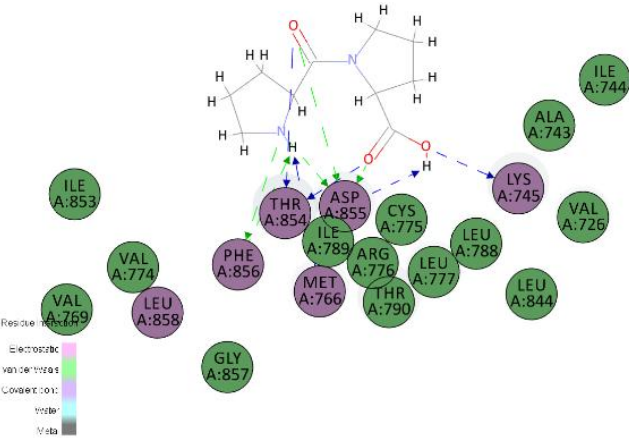
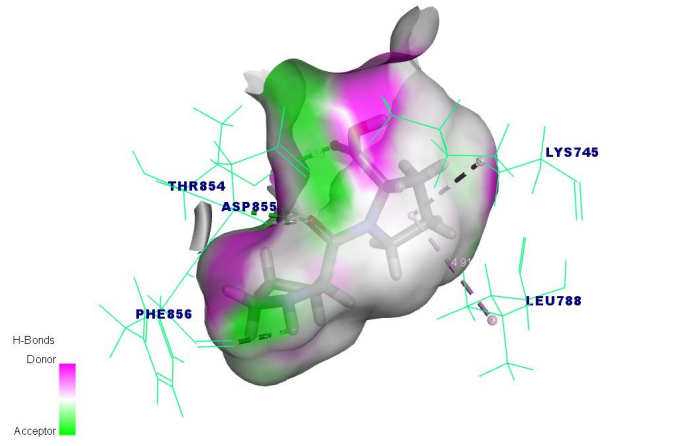
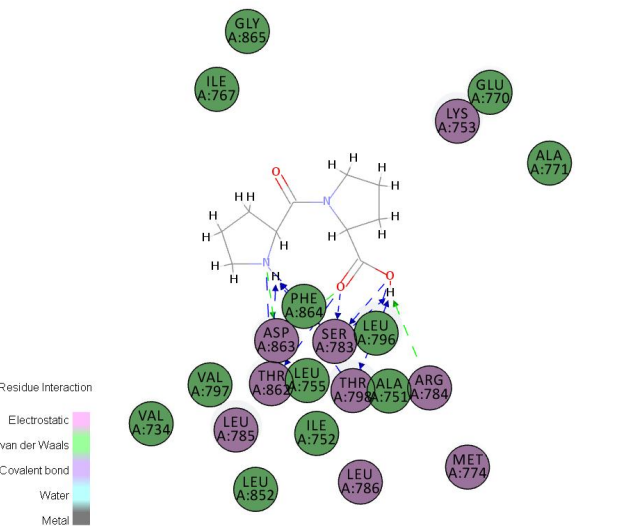
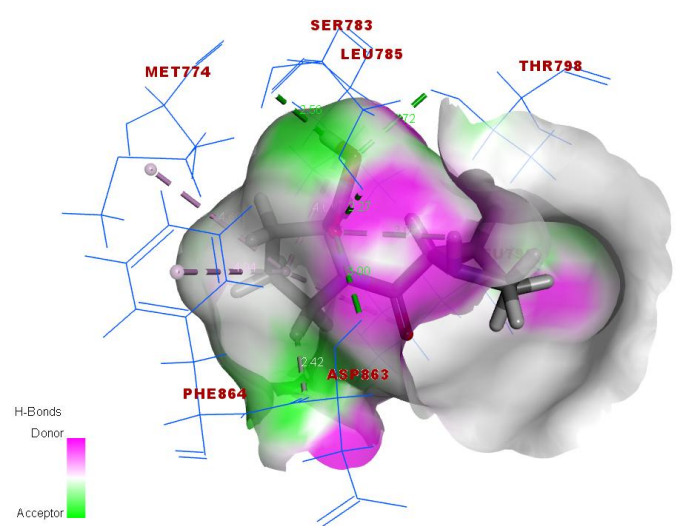


**Supplementary Table 3: CDocker Results of 5 peptides**

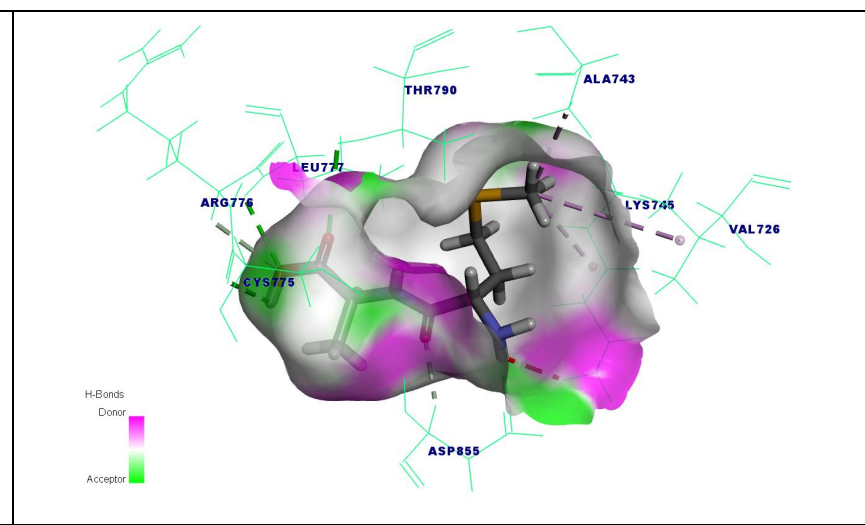
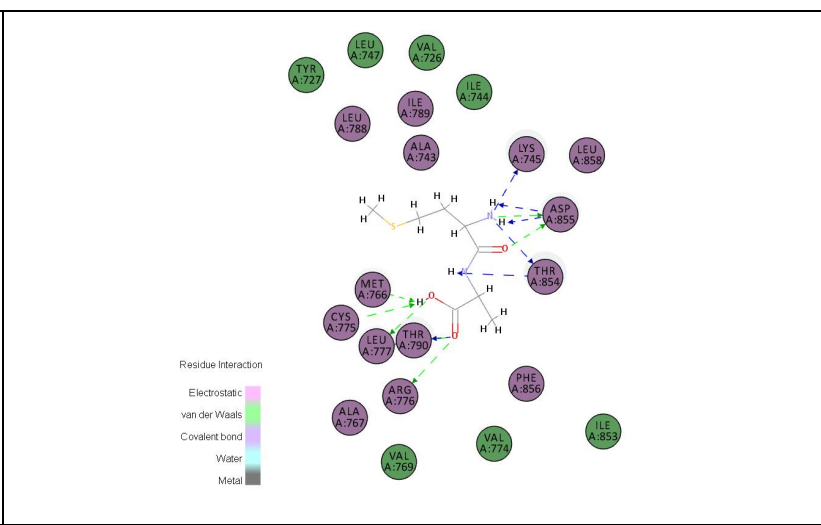
Peptide Formula	ErbB1		ErbB2	
	Cdocker Energy	Cdocker Interaction Energy	Cdocker Energy	Cdocker Interaction Energy
<b>PP</b>	-17.7366	-43.1645	-19.2646	-41.3002
<b>MA</b>	-19.5458	-42.6949	-19.8741	-41.2623
<b>FA</b>	-16.6988	-40.9873	-18.8664	-42.4852
<b>LL</b>	-10.5399	-40.2656	-16.1605	-41.9071
<b>IFG</b>	-15.2057	-40.1004	-24.8334	-47.5134
<b>Lapatanib</b>	-14.8874	-40.6599	-15.7765	-46.4389



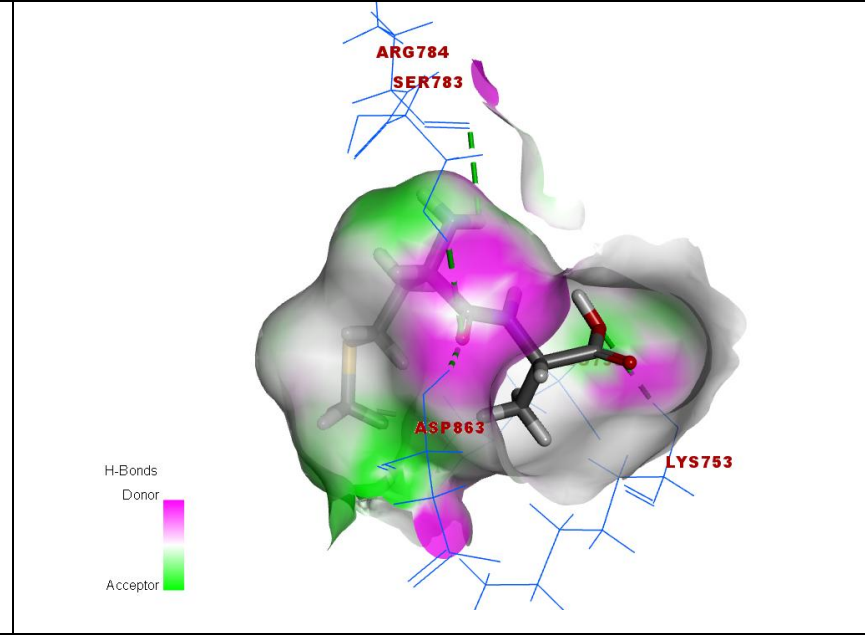
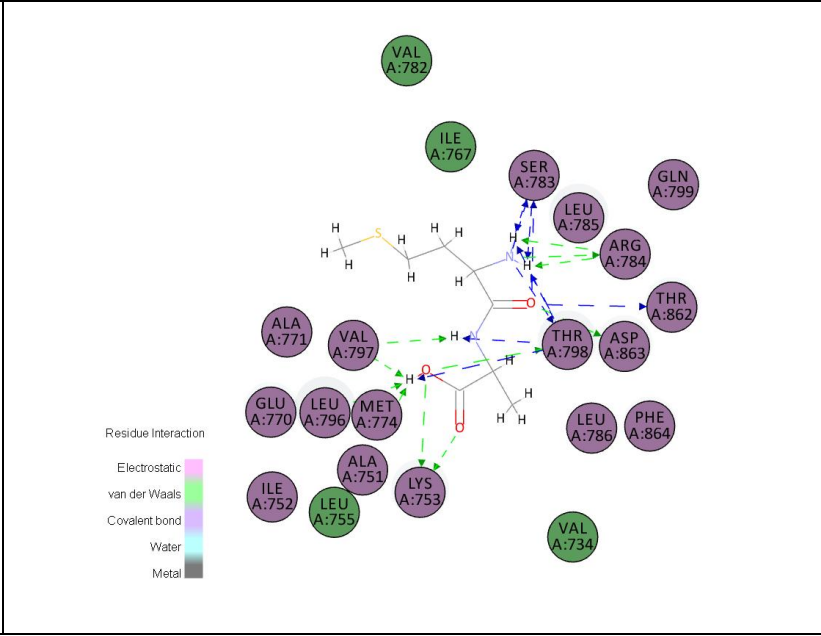
Supplementary Table 4: Molecular Interactions along with non-bond interactions

Peptides	2D-Interactions	Hydrogen Bond Donor-Acceptor Regions with Interactions
<p><b>PP-ErbB1</b></p>		
<p><b>PP -ErbB2</b></p>		

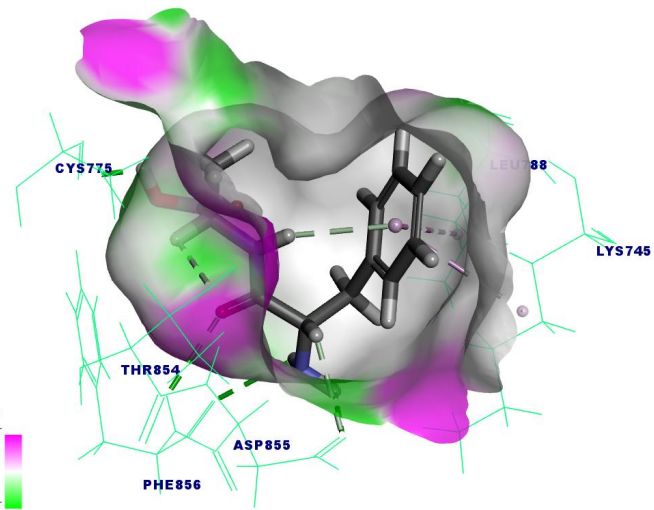
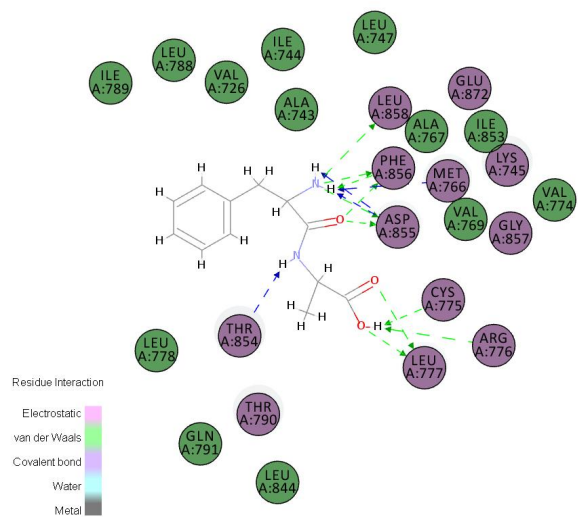
**MA-ErbB1**



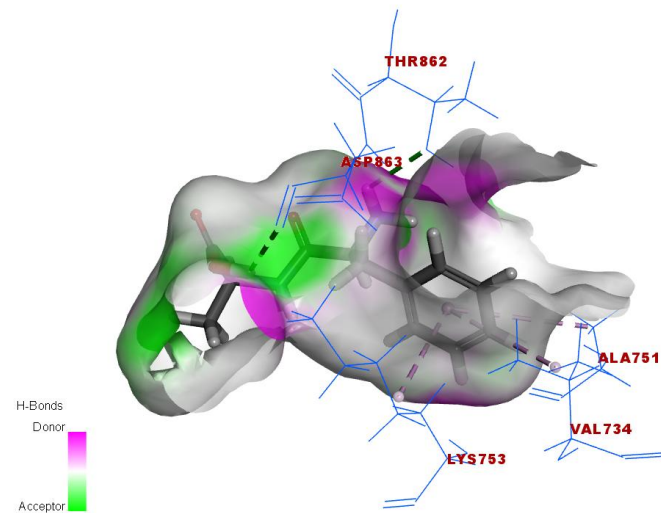
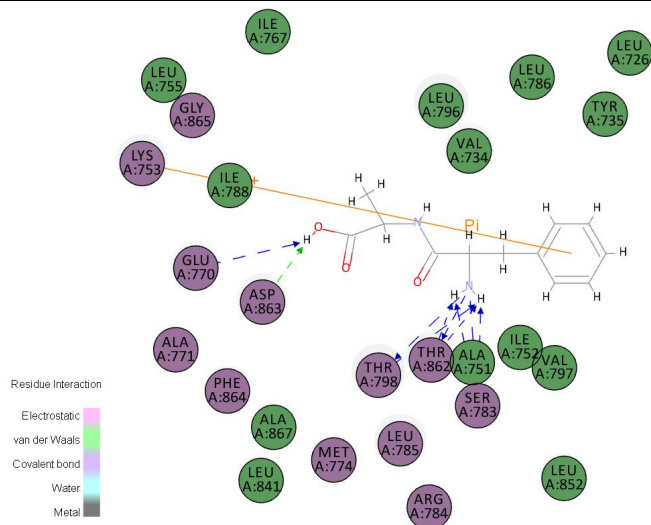
**MA -ErbB2**



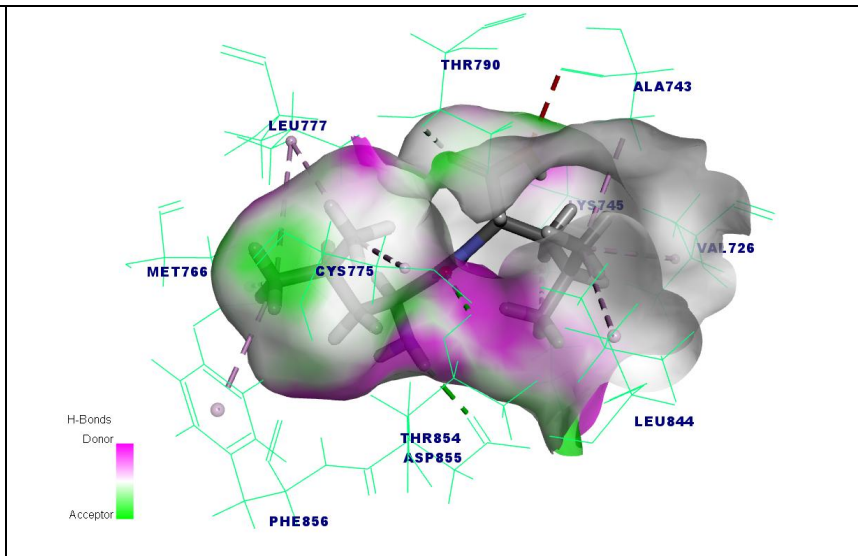
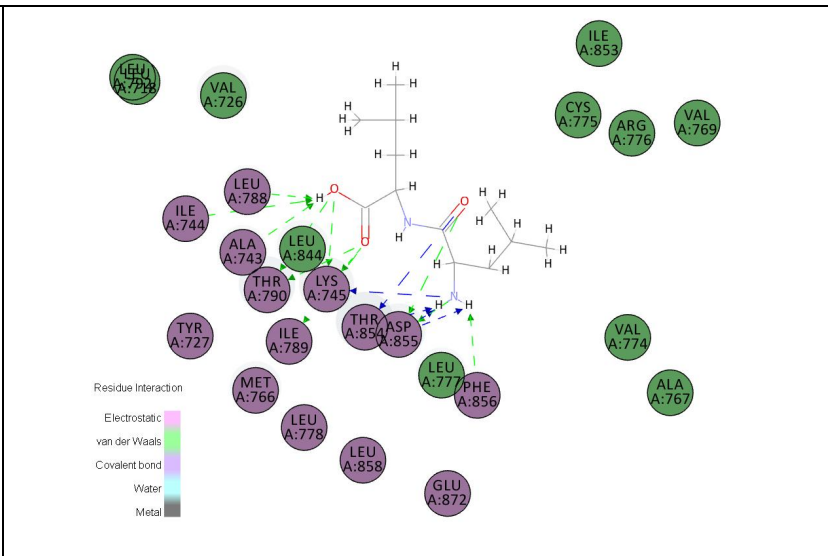
**FA-ErbB1**



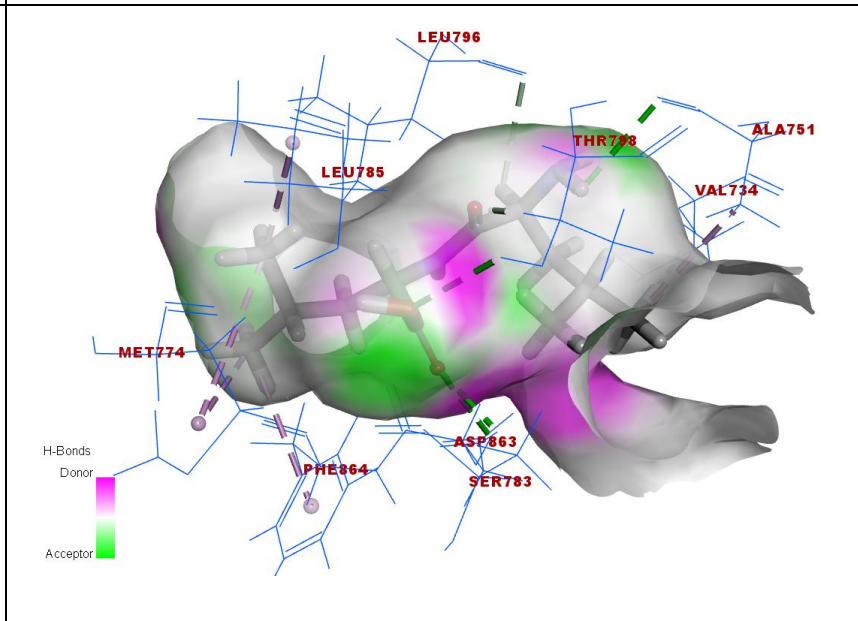
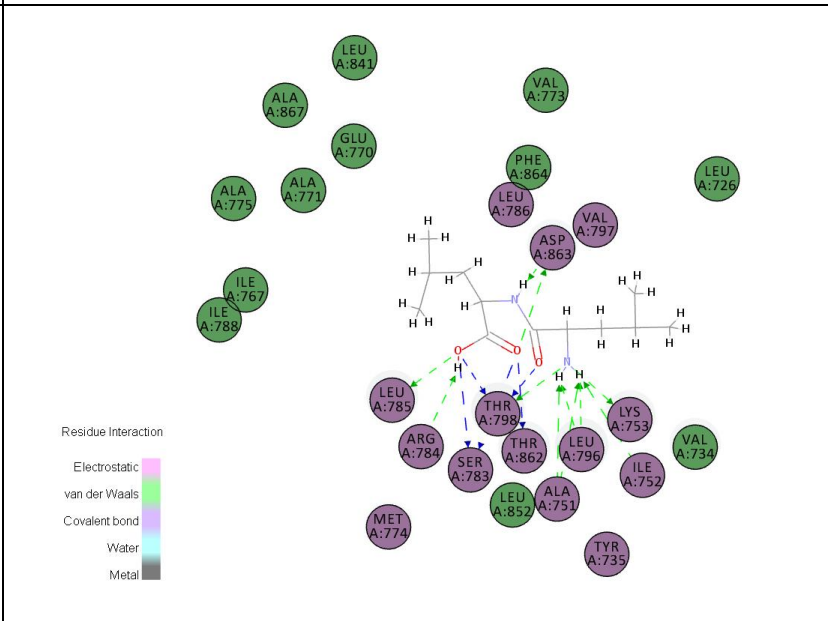
**FA -ErbB2**



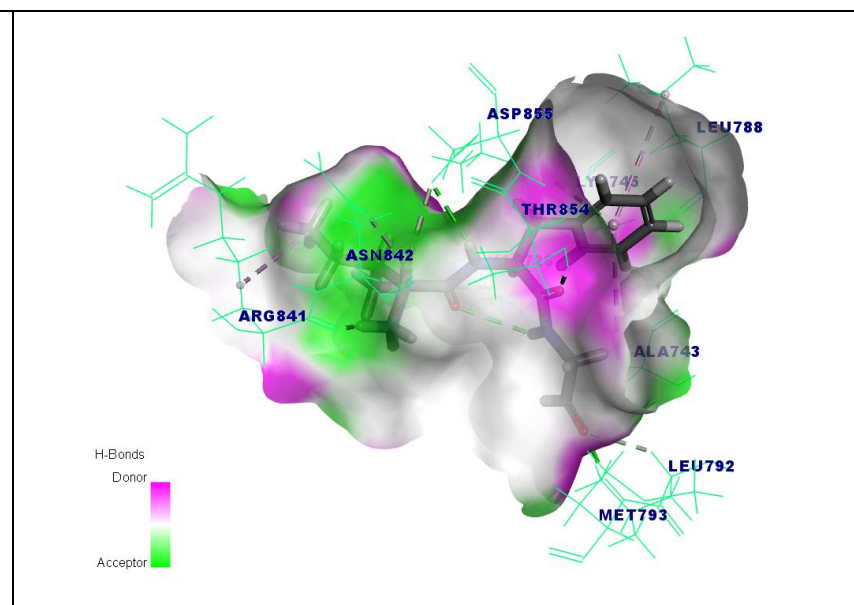
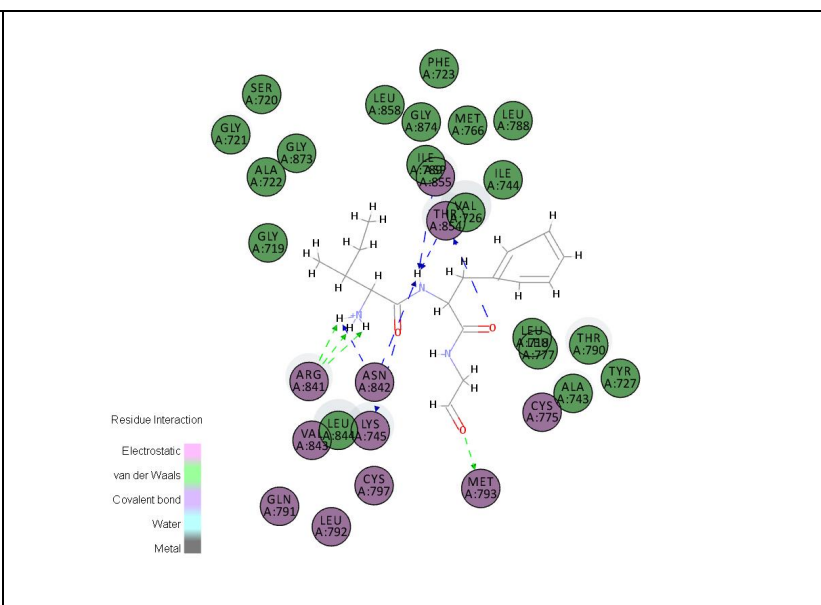
**LL-ErbB1**



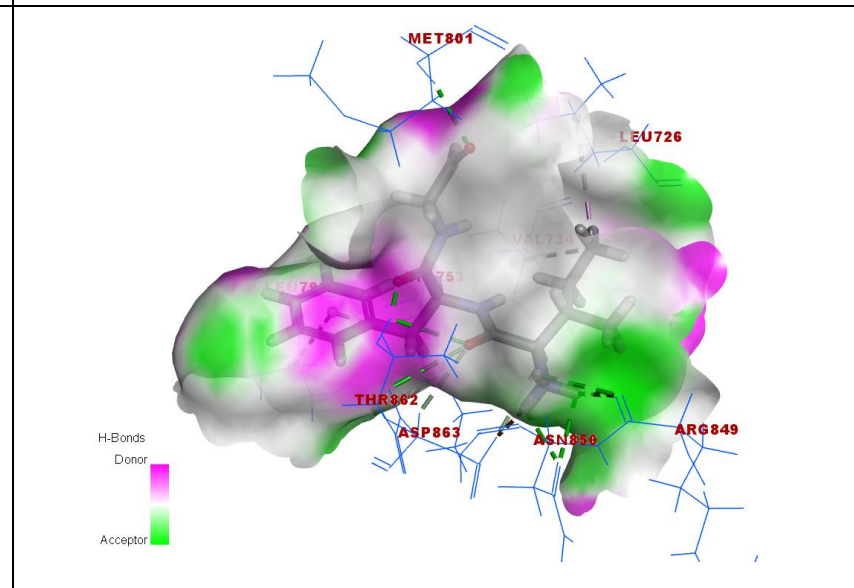
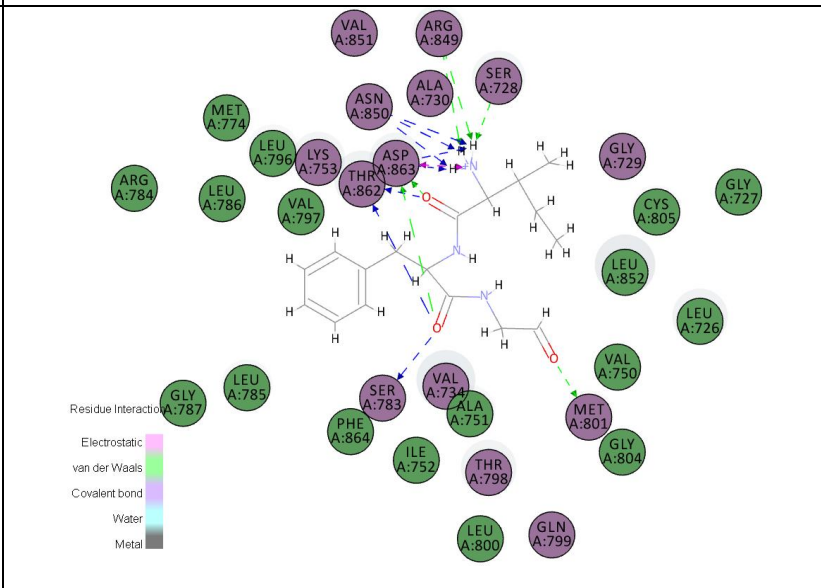
**LL -ErbB2**



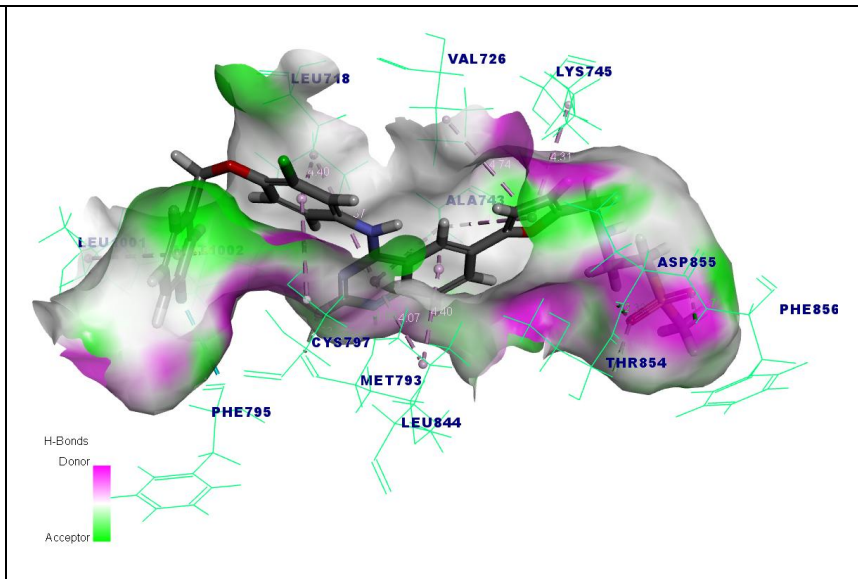
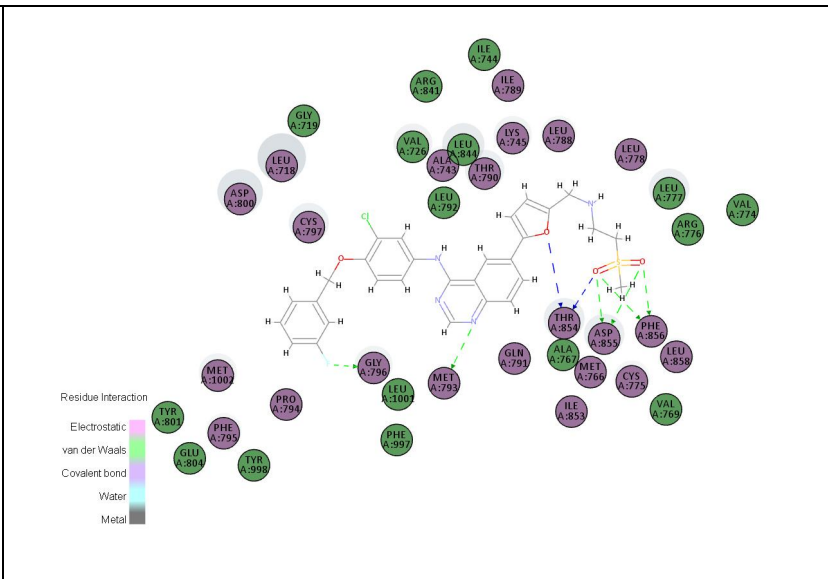
**IFG-ErbB1**



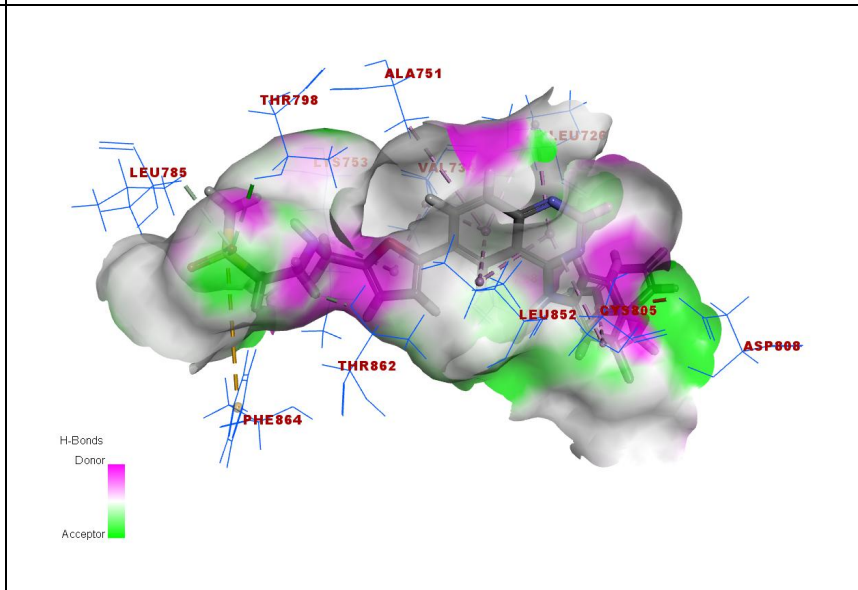
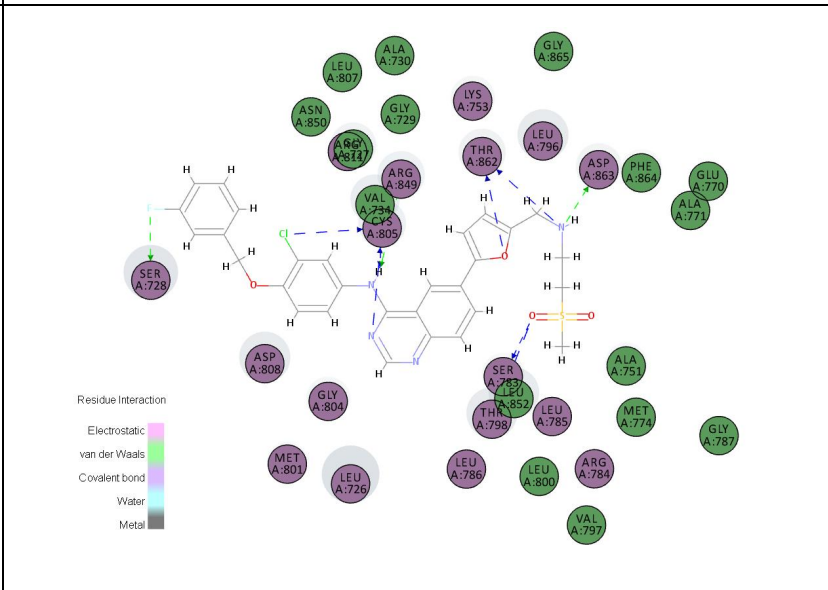
**IFG -ErbB2**

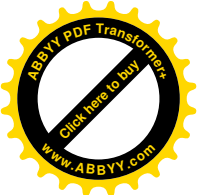


**Lapatanib-  
ErbB1**



**Lapatanib-  
ErbB2**





# 1 Supplementary Table 5: Detailed information of the Interactions:

Name	Distance	Category	Types	From	From Chemistry	To	To Chemistry	Angle DHA	Angle HAY
<b>ErbB1-C10H16N2O3</b>									
A:THR854:HG1 - C10H16N2O3:O14	2.34819	Hydrogen Bond	Conventional Hydrogen Bond	A:THR854:HG1	H-Donor	C10H16N2O3:O14	H-Acceptor	131.418	131.353
A:ASP855:HN - C10H16N2O3:O7	2.15973	Hydrogen Bond	Conventional Hydrogen Bond	A:ASP855:HN	H-Donor	C10H16N2O3:O7	H-Acceptor	124.575	127.651
C10H16N2O3:H16 - A:PHE856:O	2.89006	Hydrogen Bond	Conventional Hydrogen Bond	C10H16N2O3:H16	H-Donor	A:PHE856:O	H-Acceptor	108.459	159.485
A:ASP855:HA - C10H16N2O3:O7	2.21903	Hydrogen Bond	Carbon Hydrogen Bond	A:ASP855:HA	H-Donor	C10H16N2O3:O7	H-Acceptor	128.672	141.835
A:LYS745 - C10H16N2O3	4.3553	Hydrophobic	Alkyl	A:LYS745	Alkyl	C10H16N2O3	Alkyl		
C10H16N2O3 - A:LEU788	4.90757	Hydrophobic	Alkyl	C10H16N2O3	Alkyl	A:LEU788	Alkyl		
<b>ErbB1-C8H16N2O3S:</b>									
A:LEU777:HN - C8H16N2O3S:O14	2.73403	Hydrogen Bond	Conventional Hydrogen Bond	A:LEU777:HN	H-Donor	C8H16N2O3S:O14	H-Acceptor	97.892	114.207
A:THR790:HG1 - C8H16N2O3S:O13	2.94729	Hydrogen Bond	Conventional Hydrogen Bond	A:THR790:HG1	H-Donor	C8H16N2O3S:O13	H-Acceptor	108.239	151.806
C8H16N2O3S:H16 - A:ASP855:OD1	1.76209	Hydrogen Bond	Conventional Hydrogen Bond	C8H16N2O3S:H16	H-Donor	A:ASP855:OD1	H-Acceptor	145.29	105.008
C8H16N2O3S:H30 - A:CYS775:O	2.64814	Hydrogen Bond	Conventional Hydrogen Bond	C8H16N2O3S:H30	H-Donor	A:CYS775:O	H-Acceptor	94.415	132.799
A:ARG776:HA - C8H16N2O3S:O14	2.8454	Hydrogen Bond	Carbon Hydrogen Bond	A:ARG776:HA	H-Donor	C8H16N2O3S:O14	H-Acceptor	117.551	101.185
A:ASP855:HA - C8H16N2O3S:O8	2.30102	Hydrogen Bond	Carbon Hydrogen Bond	A:ASP855:HA	H-Donor	C8H16N2O3S:O8	H-Acceptor	152.316	110.253
A:ALA743 - C8H16N2O3S:C6	4.22291	Hydrophobic	Alkyl	A:ALA743	Alkyl	C8H16N2O3S:C6	Alkyl		
C8H16N2O3S:C6 - A:VAL726	4.88645	Hydrophobic	Alkyl	C8H16N2O3S:C6	Alkyl	A:VAL726	Alkyl		
C8H16N2O3S:C6 - A:LYS745	3.88169	Hydrophobic	Alkyl	C8H16N2O3S:C6	Alkyl	A:LYS745	Alkyl		
<b>ErbB1-C12H16N2O3</b>									
A:PHE856:HN - C12H16N2O3:O11	2.67682	Hydrogen Bond	Conventional Hydrogen Bond	A:PHE856:HN	H-Donor	C12H16N2O3:O11	H-Acceptor	131.67	135.438
C12H16N2O3:H18 - A:ASP855:OD1	2.41259	Hydrogen Bond	Conventional Hydrogen Bond	C12H16N2O3:H18	H-Donor	A:ASP855:OD1	H-Acceptor	110.288	143.742
C12H16N2O3:H19 - A:PHE856:O	2.79482	Hydrogen Bond	Conventional Hydrogen Bond	C12H16N2O3:H19	H-Donor	A:PHE856:O	H-Acceptor	112.657	147.323
C12H16N2O3:H33 - A:CYS775:O	1.7852	Hydrogen Bond	Conventional Hydrogen Bond	C12H16N2O3:H33	H-Donor	A:CYS775:O	H-Acceptor	114.176	94.329
C12H16N2O3:H20 - A:ASP855:OD1	2.70781	Hydrogen Bond	Carbon Hydrogen Bond	C12H16N2O3:H20	H-Donor	A:ASP855:OD1	H-Acceptor	115.266	106.873
C12H16N2O3:H29 - A:THR854:OG1	2.81249	Hydrogen Bond	Carbon Hydrogen Bond	C12H16N2O3:H29	H-Donor	A:THR854:OG1	H-Acceptor	102.888	115.557
C12H16N2O3:H28 - C12H16N2O3	2.77539	Hydrogen Bond	Pi-Donor Hydrogen Bond	C12H16N2O3:H28	H-Donor	C12H16N2O3	Pi-Orbitals		
C12H16N2O3 - A:LYS745	3.92458	Hydrophobic	Pi-Alkyl	C12H16N2O3	Pi-Orbitals	A:LYS745	Alkyl		
C12H16N2O3 - A:LEU788	4.98184	Hydrophobic	Pi-Alkyl	C12H16N2O3	Pi-Orbitals	A:LEU788	Alkyl		
<b>ErbB1-C12H24N2O3</b>									
A:THR854:HG1 - C12H24N2O3:O8	2.2878	Hydrogen Bond	Conventional Hydrogen Bond	A:THR854:HG1	H-Donor	C12H24N2O3:O8	H-Acceptor	98.315	147.224

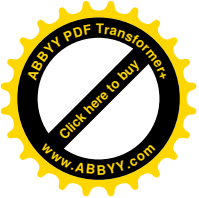


C12H24N2O3:H19 - A:ASP855:OD1	2.32063	Hydrogen Bond	Conventional Hydrogen Bond	C12H24N2O3:H19	H-Donor	A:ASP855:OD1	H-Acceptor	113.445	104.35
A:THR790:HB - C12H24N2O3:O16	2.50182	Hydrogen Bond	Carbon Hydrogen Bond	A:THR790:HB	H-Donor	C12H24N2O3:O16	H-Acceptor	130.663	114.776
A:ALA743 - C12H24N2O3:C13	3.78573	Hydrophobic	Alkyl	A:ALA743	Alkyl	C12H24N2O3:C13	Alkyl		
C12H24N2O3:C5 - A:MET766	3.69607	Hydrophobic	Alkyl	C12H24N2O3:C5	Alkyl	A:MET766	Alkyl		
C12H24N2O3:C5 - A:LEU777	4.92104	Hydrophobic	Alkyl	C12H24N2O3:C5	Alkyl	A:LEU777	Alkyl		
C12H24N2O3:C6 - A:CYS775	4.52527	Hydrophobic	Alkyl	C12H24N2O3:C6	Alkyl	A:CYS775	Alkyl		
C12H24N2O3:C6 - A:LEU777	4.91068	Hydrophobic	Alkyl	C12H24N2O3:C6	Alkyl	A:LEU777	Alkyl		
C12H24N2O3:C13 - A:VAL726	4.57749	Hydrophobic	Alkyl	C12H24N2O3:C13	Alkyl	A:VAL726	Alkyl		
C12H24N2O3:C13 - A:LEU844	5.46192	Hydrophobic	Alkyl	C12H24N2O3:C13	Alkyl	A:LEU844	Alkyl		
C12H24N2O3:C14 - A:LYS745	4.70837	Hydrophobic	Alkyl	C12H24N2O3:C14	Alkyl	A:LYS745	Alkyl		
A:PHE856 - C12H24N2O3:C5	3.91217	Hydrophobic	Pi-Alkyl	A:PHE856	Pi-Orbitals	C12H24N2O3:C5	Alkyl		
<b>ErbB1-satpdb20875</b>									
satpdb20875:N1 - A:ASP855:OD2	4.9506	Electrostatic	Attractive Charge	satpdb20875:N1	Positive	A:ASP855:OD2	Negative		
A:MET793:HN - satpdb20875:O23	1.75503	Hydrogen Bond	Conventional Hydrogen Bond	A:MET793:HN	H-Donor	satpdb20875:O23	H-Acceptor	155.976	172.431
A:THR854:HG1 - satpdb20875:O12	1.73305	Hydrogen Bond	Conventional Hydrogen Bond	A:THR854:HG1	H-Donor	satpdb20875:O12	H-Acceptor	160.29	155.282
satpdb20875:H26 - A:ARG841:O	1.72715	Hydrogen Bond	Conventional Hydrogen Bond	satpdb20875:H26	H-Donor	A:ARG841:O	H-Acceptor	134.631	151.185
satpdb20875:H37 - A:ASP855:OD2	2.37454	Hydrogen Bond	Conventional Hydrogen Bond	satpdb20875:H37	H-Donor	A:ASP855:OD2	H-Acceptor	128.181	104.651
satpdb20875:H46 - satpdb20875:O4	2.8215	Hydrogen Bond	Conventional Hydrogen Bond	satpdb20875:H46	H-Donor	satpdb20875:O4	H-Acceptor	110.538	113.328
A:LEU792:HA - satpdb20875:O23	2.62479	Hydrogen Bond	Carbon Hydrogen Bond	A:LEU792:HA	H-Donor	satpdb20875:O23	H-Acceptor	136.875	124.976
satpdb20875:H27 - A:ASN842:OD1	2.52729	Hydrogen Bond	Carbon Hydrogen Bond	satpdb20875:H27	H-Donor	A:ASN842:OD1	H-Acceptor	147.217	151.296
satpdb20875:H27 - A:ASP855:OD2	2.86178	Hydrogen Bond	Carbon Hydrogen Bond	satpdb20875:H27	H-Donor	A:ASP855:OD2	H-Acceptor	125.015	143.942
satpdb20875:C7 - A:VAL726	5.03109	Hydrophobic	Alkyl	satpdb20875:C7	Alkyl	A:VAL726	Alkyl		
satpdb20875:C8 - A:ARG841	4.37745	Hydrophobic	Alkyl	satpdb20875:C8	Alkyl	A:ARG841	Alkyl		
satpdb20875 - A:ALA743	5.20917	Hydrophobic	Pi-Alkyl	satpdb20875	Pi-Orbitals	A:ALA743	Alkyl		
satpdb20875 - A:LYS745	3.98847	Hydrophobic	Pi-Alkyl	satpdb20875	Pi-Orbitals	A:LYS745	Alkyl		
satpdb20875 - A:LEU788	5.22293	Hydrophobic	Pi-Alkyl	satpdb20875	Pi-Orbitals	A:LEU788	Alkyl		
<b>ErbB1-Lapatanib</b>									
A:MET793:HN - Lapatanib:N10	1.94983	Hydrogen Bond	Conventional Hydrogen Bond	A:MET793:HN	H-Donor	Lapatanib:N10	H-Acceptor	152.157	114.531
A:ASP855:HN - Lapatanib:O6	2.33155	Hydrogen Bond	Conventional Hydrogen Bond	A:ASP855:HN	H-Donor	Lapatanib:O6	H-Acceptor	145.081	110.913
A:PHE856:HN - Lapatanib:O5	2.87449	Hydrogen Bond	Conventional Hydrogen Bond	A:PHE856:HN	H-Donor	Lapatanib:O5	H-Acceptor	124.754	125.583
A:THR854:HA - Lapatanib:O6	3.02785	Hydrogen Bond	Carbon Hydrogen Bond	A:THR854:HA	H-Donor	Lapatanib:O6	H-Acceptor	114.702	138.526
Lapatanib:H57 - A:MET793:O	2.01697	Hydrogen Bond	Carbon Hydrogen Bond	Lapatanib:H57	H-Donor	A:MET793:O	H-Acceptor	139.737	139.859
A:PHE795:C - Lapatanib:F3	3.53804	Halogen	Halogen (Fluorine)	A:PHE795:C	Halogen Acceptor	Lapatanib:F3	Halogen		

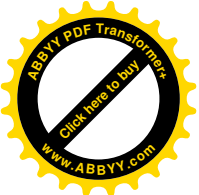




A:MET1002:SD - Lapatanib	5.37749	Other	Pi-Sulfur	A:MET1002:SD	Sulfur	Lapatanib	Pi-Orbitals		
Lapatanib - A:VAL726	4.74174	Hydrophobic	Pi-Alkyl	Lapatanib	Pi-Orbitals	A:VAL726	Alkyl		
Lapatanib - A:ALA743	4.95078	Hydrophobic	Pi-Alkyl	Lapatanib	Pi-Orbitals	A:ALA743	Alkyl		
Lapatanib - A:LYS745	4.30876	Hydrophobic	Pi-Alkyl	Lapatanib	Pi-Orbitals	A:LYS745	Alkyl		
Lapatanib - A:LEU718	5.36627	Hydrophobic	Pi-Alkyl	Lapatanib	Pi-Orbitals	A:LEU718	Alkyl		
Lapatanib - A:ALA743	4.7315	Hydrophobic	Pi-Alkyl	Lapatanib	Pi-Orbitals	A:ALA743	Alkyl		
Lapatanib - A:LEU844	4.07193	Hydrophobic	Pi-Alkyl	Lapatanib	Pi-Orbitals	A:LEU844	Alkyl		
Lapatanib - A:ALA743	3.37439	Hydrophobic	Pi-Alkyl	Lapatanib	Pi-Orbitals	A:ALA743	Alkyl		
Lapatanib - A:LEU844	4.39548	Hydrophobic	Pi-Alkyl	Lapatanib	Pi-Orbitals	A:LEU844	Alkyl		
Lapatanib - A:LEU718	4.39644	Hydrophobic	Pi-Alkyl	Lapatanib	Pi-Orbitals	A:LEU718	Alkyl		
Lapatanib - A:CYS797	4.97019	Hydrophobic	Pi-Alkyl	Lapatanib	Pi-Orbitals	A:CYS797	Alkyl		
Lapatanib - A:LEU1001	5.17837	Hydrophobic	Pi-Alkyl	Lapatanib	Pi-Orbitals	A:LEU1001	Alkyl		
<b>ErbB2-C10H16N2O3</b>									
A:SER783:HG - C10H16N2O3:O14	2.27292	Hydrogen Bond	Conventional Hydrogen Bond	A:SER783:HG	H-Donor	C10H16N2O3:O14	H-Acceptor	100.658	113.466
A:THR798:HG1 - C10H16N2O3:O15	2.71608	Hydrogen Bond	Conventional Hydrogen Bond	A:THR798:HG1	H-Donor	C10H16N2O3:O15	H-Acceptor	106.109	97.965
A:ASP863:HN - C10H16N2O3:O14	3.00174	Hydrogen Bond	Conventional Hydrogen Bond	A:ASP863:HN	H-Donor	C10H16N2O3:O14	H-Acceptor	125.773	158.096
C10H16N2O3:H16 - C10H16N2O3:O14	3.05405	Hydrogen Bond	Conventional Hydrogen Bond	C10H16N2O3:H16	H-Donor	C10H16N2O3:O14	H-Acceptor	91.987	90.6
C10H16N2O3:H31 - A:SER783:O	2.55517	Hydrogen Bond	Conventional Hydrogen Bond	C10H16N2O3:H31	H-Donor	A:SER783:O	H-Acceptor	105.823	101.538
C10H16N2O3:H30 - A:ASP863:O	2.42447	Hydrogen Bond	Carbon Hydrogen Bond	C10H16N2O3:H30	H-Donor	A:ASP863:O	H-Acceptor	152.496	136.389
C10H16N2O3 - A:MET774	4.69461	Hydrophobic	Alkyl	C10H16N2O3	Alkyl	A:MET774	Alkyl		
C10H16N2O3 - A:LEU785	4.61715	Hydrophobic	Alkyl	C10H16N2O3	Alkyl	A:LEU785	Alkyl		
C10H16N2O3 - A:LEU796	4.98087	Hydrophobic	Alkyl	C10H16N2O3	Alkyl	A:LEU796	Alkyl		
A:PHE864 - C10H16N2O3	4.9395	Hydrophobic	Pi-Alkyl	A:PHE864	Pi-Orbitals	C10H16N2O3	Alkyl		
<b>ErbB2-C8H16N2O3S:</b>									
A:LYS753:HN - C8H16N2O3S:O14	2.76021	Hydrogen Bond	Conventional Hydrogen Bond	A:LYS753:HN	H-Donor	C8H16N2O3S:O14	H-Acceptor	137.868	92.535
A:SER783:HG - C8H16N2O3S:O8	2.91352	Hydrogen Bond	Conventional Hydrogen Bond	A:SER783:HG	H-Donor	C8H16N2O3S:O8	H-Acceptor	131.466	90.967
A:ASP863:HN - C8H16N2O3S:O8	2.36847	Hydrogen Bond	Conventional Hydrogen Bond	A:ASP863:HN	H-Donor	C8H16N2O3S:O8	H-Acceptor	139.93	164.331
C8H16N2O3S:H16 - A:ARG784:O	2.72666	Hydrogen Bond	Conventional Hydrogen Bond	C8H16N2O3S:H16	H-Donor	A:ARG784:O	H-Acceptor	98.614	98.733
C8H16N2O3S:C6 - A:LEU796	4.30083	Hydrophobic	Alkyl	C8H16N2O3S:C6	Alkyl	A:LEU796	Alkyl		
<b>ErbB2-C12H16N2O3</b>									
C12H16N2O3:H19 - A:THR862:OG1	2.89999	Hydrogen Bond	Conventional Hydrogen Bond	C12H16N2O3:H19	H-Donor	A:THR862:OG1	H-Acceptor	119.072	109.522
C12H16N2O3:H33 - A:ASP863:O	2.6888	Hydrogen Bond	Conventional Hydrogen Bond	C12H16N2O3:H33	H-Donor	A:ASP863:O	H-Acceptor	112.192	143.647
C12H16N2O3 - A:VAL734	4.87579	Hydrophobic	Pi-Alkyl	C12H16N2O3	Pi-Orbitals	A:VAL734	Alkyl		
C12H16N2O3 - A:ALA751	4.621	Hydrophobic	Pi-Alkyl	C12H16N2O3	Pi-Orbitals	A:ALA751	Alkyl		



C12H16N2O3 - A:LYS753	4.17865	Hydrophobic	Pi-Alkyl	C12H16N2O3	Pi-Orbitals	A:LYS753	Alkyl		
<b>ErbB2-C12H24N2O3</b>									
A:SER783:HG - C12H24N2O3:O16	2.28433	Hydrogen Bond	Conventional Hydrogen Bond	A:SER783:HG	H-Donor	C12H24N2O3:O16	H-Acceptor	106.639	128.051
A:THR798:HG1 - C12H24N2O3:O17	2.95635	Hydrogen Bond	Conventional Hydrogen Bond	A:THR798:HG1	H-Donor	C12H24N2O3:O17	H-Acceptor	111.373	119.224
A:ASP863:HN - C12H24N2O3:O16	2.97299	Hydrogen Bond	Conventional Hydrogen Bond	A:ASP863:HN	H-Donor	C12H24N2O3:O16	H-Acceptor	131.682	154.67
C12H24N2O3:H19 - A:ALA751:O	2.79112	Hydrogen Bond	Conventional Hydrogen Bond	C12H24N2O3:H19	H-Donor	A:ALA751:O	H-Acceptor	94.823	107.612
A:THR798:HB - C12H24N2O3:O8	1.80168	Hydrogen Bond	Carbon Hydrogen Bond	A:THR798:HB	H-Donor	C12H24N2O3:O8	H-Acceptor	170.327	134.589
C12H24N2O3:H20 - A:LEU796:O	3.01374	Hydrogen Bond	Carbon Hydrogen Bond	C12H24N2O3:H20	H-Donor	A:LEU796:O	H-Acceptor	96.795	99.747
A:ALA751 - C12H24N2O3:C6	4.02183	Hydrophobic	Alkyl	A:ALA751	Alkyl	C12H24N2O3:C6	Alkyl		
C12H24N2O3:C6 - A:VAL734	3.99824	Hydrophobic	Alkyl	C12H24N2O3:C6	Alkyl	A:VAL734	Alkyl		
C12H24N2O3:C13 - A:MET774	4.55419	Hydrophobic	Alkyl	C12H24N2O3:C13	Alkyl	A:MET774	Alkyl		
C12H24N2O3:C13 - A:LEU785	3.29547	Hydrophobic	Alkyl	C12H24N2O3:C13	Alkyl	A:LEU785	Alkyl		
C12H24N2O3:C14 - A:MET774	3.695	Hydrophobic	Alkyl	C12H24N2O3:C14	Alkyl	A:MET774	Alkyl		
A:PHE864 - C12H24N2O3:C14	4.11966	Hydrophobic	Pi-Alkyl	A:PHE864	Pi-Orbitals	C12H24N2O3:C14	Alkyl		
<b>ErbB2-satpdb20875</b>									
satpdb20875:H24 - A:ASP863:OD2	2.48789	Hydrogen Bond;Electrostatic	Salt Bridge;Attractive Charge	satpdb20875:H24	H-Donor;Positive	A:ASP863:OD2	H-Acceptor;Negative	138.583	90.568
A:MET801:HN - satpdb20875:O23	2.30382	Hydrogen Bond	Conventional Hydrogen Bond	A:MET801:HN	H-Donor	satpdb20875:O23	H-Acceptor	155.735	108.992
A:THR862:HG1 - satpdb20875:O4	2.83247	Hydrogen Bond	Conventional Hydrogen Bond	A:THR862:HG1	H-Donor	satpdb20875:O4	H-Acceptor	106.443	139.195
A:THR862:HG1 - satpdb20875:O12	1.65791	Hydrogen Bond	Conventional Hydrogen Bond	A:THR862:HG1	H-Donor	satpdb20875:O12	H-Acceptor	153.498	138.027
A:ASP863:HN - satpdb20875:O4	2.95539	Hydrogen Bond	Conventional Hydrogen Bond	A:ASP863:HN	H-Donor	satpdb20875:O4	H-Acceptor	98.154	145.094
satpdb20875:H24 - A:ASN850:OD1	2.36761	Hydrogen Bond	Conventional Hydrogen Bond	satpdb20875:H24	H-Donor	A:ASN850:OD1	H-Acceptor	97.53	143.451
satpdb20875:H25 - A:ARG849:O	2.97414	Hydrogen Bond	Conventional Hydrogen Bond	satpdb20875:H25	H-Donor	A:ARG849:O	H-Acceptor	101.35	132.521
satpdb20875:H26 - A:ARG849:O	2.79229	Hydrogen Bond	Conventional Hydrogen Bond	satpdb20875:H26	H-Donor	A:ARG849:O	H-Acceptor	112.651	141.608
satpdb20875:H26 - A:ASN850:OD1	2.49587	Hydrogen Bond	Conventional Hydrogen Bond	satpdb20875:H26	H-Donor	A:ASN850:OD1	H-Acceptor	90.431	161.383
A:ASP863:HA - satpdb20875:O4	3.02645	Hydrogen Bond	Carbon Hydrogen Bond	A:ASP863:HA	H-Donor	satpdb20875:O4	H-Acceptor	103.894	106.62
satpdb20875:H27 - A:ASP863:OD2	3.02199	Hydrogen Bond	Carbon Hydrogen Bond	satpdb20875:H27	H-Donor	A:ASP863:OD2	H-Acceptor	109.824	139.685
satpdb20875:C8 - A:LEU726	4.55837	Hydrophobic	Alkyl	satpdb20875:C8	Alkyl	A:LEU726	Alkyl		
satpdb20875:C8 - A:VAL734	3.85417	Hydrophobic	Alkyl	satpdb20875:C8	Alkyl	A:VAL734	Alkyl		
satpdb20875 - A:LYS753	4.81934	Hydrophobic	Pi-Alkyl	satpdb20875	Pi-Orbitals	A:LYS753	Alkyl		
satpdb20875 - A:LEU796	4.96345	Hydrophobic	Pi-Alkyl	satpdb20875	Pi-Orbitals	A:LEU796	Alkyl		
<b>ErbB2-Lapatinib</b>									



A:THR798:HG1 - Lapatanib:O6	3.04775	Hydrogen Bond	Conventional Hydrogen Bond	A:THR798:HG1	H-Donor	Lapatanib:O6	H-Acceptor	109.613	128.855
A:SER728:HB2 - Lapatanib:F3	3.00127	Hydrogen Bond	Carbon Hydrogen Bond	A:SER728:HB2	H-Donor	Lapatanib:F3	H-Acceptor	124.159	113.3
A:LEU785:HA - Lapatanib:O6	3.03953	Hydrogen Bond	Carbon Hydrogen Bond	A:LEU785:HA	H-Donor	Lapatanib:O6	H-Acceptor	116.231	97.118
Lapatanib:H43 - A:THR862:OG1	2.01542	Hydrogen Bond	Carbon Hydrogen Bond	Lapatanib:H43	H-Donor	A:THR862:OG1	H-Acceptor	120.851	90.917
A:ASP808:OD2 - Lapatanib	3.66798	Electrostatic	Pi-Anion	A:ASP808:OD2	Negative	Lapatanib	Pi-Orbitals		
Lapatanib:S2 - A:PHE864	5.83336	Other	Pi-Sulfur	Lapatanib:S2	Sulfur	A:PHE864	Pi-Orbitals		
Lapatanib - A:VAL734	4.02364	Hydrophobic	Pi-Alkyl	Lapatanib	Pi-Orbitals	A:VAL734	Alkyl		
Lapatanib - A:LYS753	4.72918	Hydrophobic	Pi-Alkyl	Lapatanib	Pi-Orbitals	A:LYS753	Alkyl		
Lapatanib - A:LEU726	4.63269	Hydrophobic	Pi-Alkyl	Lapatanib	Pi-Orbitals	A:LEU726	Alkyl		
Lapatanib - A:CYS805	4.68789	Hydrophobic	Pi-Alkyl	Lapatanib	Pi-Orbitals	A:CYS805	Alkyl		
Lapatanib - A:LEU852	5.26622	Hydrophobic	Pi-Alkyl	Lapatanib	Pi-Orbitals	A:LEU852	Alkyl		
Lapatanib - A:LEU726	4.93531	Hydrophobic	Pi-Alkyl	Lapatanib	Pi-Orbitals	A:LEU726	Alkyl		
Lapatanib - A:VAL734	4.45869	Hydrophobic	Pi-Alkyl	Lapatanib	Pi-Orbitals	A:VAL734	Alkyl		
Lapatanib - A:ALA751	5.21522	Hydrophobic	Pi-Alkyl	Lapatanib	Pi-Orbitals	A:ALA751	Alkyl		
Lapatanib - A:LEU852	4.50347	Hydrophobic	Pi-Alkyl	Lapatanib	Pi-Orbitals	A:LEU852	Alkyl		
Lapatanib - A:CYS805	4.35805	Hydrophobic	Pi-Alkyl	Lapatanib	Pi-Orbitals	A:CYS805	Alkyl		

2  
3